Supplementary materials

Synthesis of new selective cytotoxic ricinine analogues against oral squamous cell carcinoma

Mai H. El-Naggar[a], Fatma M. Abdel Bar[b,c], Choudhary Harsha[d], Javadi Monisha[d], Kuniyoshi Shimizu[e], Ajaikumar B. Kunnumakkara[d], Farid A. Badria[c*]

[a] Pharmacognosy Department, Faculty of Pharmacy, Kafrelsheikh university, Kafrelsheikh, Egypt.

[b] Pharmacognosy Department, Faculty of Pharmacy, Prince Sattam Bin Abdulaziz University, Al-Kharj 11942, Saudi Arabia

[c] Pharmacognosy Department, Faculty of Pharmacy, Mansoura University, Mansoura 35516 Egypt.

[d] Laboratory of Cancer Biology and DBT-AIST International Laboratory for Advanced Biomedicine, Biosciences and Bioengineering Department, Indian Institute of Technology Guwahati, Assam, India.

[e] Systematic Forest and Forest Products Sciences Division, Agro-Environmental Sciences Department, Bioresource and Bioenvironmental Sciences Graduate School, Kyushu University, Fukuoka, Japan.

***Address Correspondence to:**

Farid A. Badria, email: faridbadria@gmail.com.

Declarations of interest: Authors declare that there are no conflicts of interest.

Abstract

Sixteen new analogues were synthesized from ricinine and tested alongside with seven known analogues for their cytotoxic activity against oral cancer (SAS cells) and normal epithelial cells (L132 cells). In contrast to 5-FU, the synthesized ricinine analogues did not show toxicity to normal cells. However, some of them inhibited the proliferation of oral cancer cells at 25 μM as evident from the MTT assay results. Ricinine analogue (**19**) was shown to be the most active derivative (69.22 % inhibition). Potential targets involved in the oral cancer inhibitory activity of compound **19** were investigated using *in-silico* studies and western blot analysis. PTP1B was predicted to be a target for ricinine using reverse docking approach. This prediction was confirmed by western blot analysis that revealed the downregulation of PTP1B protein by compound **19**. Moreover, it showed downregulation of COX-2 which is also extensively expressed in oral cancer.

Contents

1. Experimental	Page
1.1. General experimental methods.	5
1.2. Virtual screening.	5
1.3. Biological assays.	6
1.4. Detailed procedures of preparation, FT-IR, and ^{1}H-NMR of ricinine derivatives (**5**-**9**).	8
1.5. General method of preparation for compounds **12**-**14**, **16, 17,** and **19**-**22**.	11
2. Spectra (MS & NMR) of new compounds:	
Figure S1: High resolution FAB$^+$ -MS spectra of compound **5**.	17
Figure S2. ^{1}H-NMR spectrum (400 MHz, $CDCl_3$) of compound **5**.	18
Figure S3. Expansion of ^{1}H-NMR spectrum (400 MHz, $CDCl_3$) of compound **5**.	18
Figure S4. APT spectrum (100 MHz, $CDCl_3$) of compound **5**.	19
Figure S5. High resolution FAB$^+$ -MS spectra of compound **6**.	19
Figure S6. ^{1}H-NMR spectrum (400 MHz, $CDCl_3$) of compound **6**.	20
Figure S7. APT spectrum (100 MHz, $CDCl_3$) of compound **6**.	20
Figure S8. High resolution FAB$^+$ -MS spectra of compound **7**.	21
Figure S9. ^{1}H-NMR spectrum (400 MHz, $CDCl_3$) of compound **7**.	21
Figure S10. Expansion of ^{1}H-NMR spectrum (400 MHz, $CDCl_3$) of compound **7**.	22
Figure S11. APT spectrum (100 MHz, $CDCl_3$) of compound **7**.	22
Figure S12. HMBC correlation spectrum of compound **7**.	23
Figure S13. Selected HMBC correlations of compound **7** from δ_H 6-8 ppm, and from δ_C 100-170 ppm.	24
Figure S14. High resolution FAB$^+$ -MS spectra of compound **8**.	25
Figure S15. ^{1}H-NMR spectrum (400 MHz, $(CD_3)_2SO$) of compound **8**.	25
Figure S16. Expansion of ^{1}H-NMR spectrum (400 MHz, $(CD_3)_2SO$) of compound **8**.	26
Figure S17. APT spectrum (100 MHz, $(CD_3)_2SO$) of compound **8**.	26
Figure S18. HMBC correlation spectrum of compound **8**.	27
Figure S19. Selected HMBC correlations of compound **8** from δ_H 5-8.5 ppm, and from δ_C 70-190 ppm.	28
Figure S20. High resolution FAB$^+$ -MS spectra of compound **9**.	29
Figure S21. ^{1}H-NMR spectrum (400 MHz, $CDCl_3$) of compound **9**.	29
Figure S22. Expansion of ^{1}H-NMR spectrum (400 MHz, $CDCl_3$) of compound **9**.	30
Figure S23. APT spectrum (100 MHz, $CDCl_3$) of compound **9**.	30
Figure S24. Expansion of APT spectrum (100 MHz, $CDCl_3$) of compound **9**.	31
Figure S25. HMBC correlation spectrum of compound **9**.	32
Figure S26. Selected HMBC correlations of compound **9** from δ_H 5.5-8.5 ppm and δ_C 90-190 ppm.	33
Figure S27. High resolution FAB$^+$ -MS spectra of compound **12**.	34
Figure S28. ^{1}H-NMR spectrum (400 MHz, $CDCl_3$) of compound **12**.	34
Figure S29. Expansion of ^{1}H-NMR spectrum (400 MHz, $CDCl_3$) of compound **12**.	35
Figure S30. APT spectrum (100 MHz, $CDCl_3$) of compound **12**.	35
Figure S31. High resolution FAB$^+$ -MS spectra of compound **13**.	36
Figure S32. ^{1}H-NMR spectrum (400 MHz, $(CD_3)_2SO$) of compound **13**.	36
Figure S33. Expansion of ^{1}H-NMR spectrum (400 MHz, $(CD_3)_2SO$) of compound **13**.	37
Figure S34. APT spectrum (100 MHz, $(CD_3)_2SO$) of compound **13**.	37
Figure S35. High resolution FAB$^+$ -MS spectra of compound **14**.	38
Figure S36. ^{1}H-NMR spectrum (400 MHz, $(CD_3)_2SO$) of compound **14**.	38
Figure S37. APT spectrum (100 MHz, $(CD_3)_2SO$) of compound **14**.	39
Figure S38. High resolution FAB$^+$ -MS spectra of compound **15**.	39
Figure S39. ^{1}H-NMR spectrum (500 MHz, $CDCl_3$) of compound **15**.	40
Figure S40. Expansion of ^{1}H-NMR spectrum (500 MHz, $CDCl_3$) of compound **15**.	40
Figure S41. APT spectrum (125 MHz, $CDCl_3$) of compound **15**.	41
Figure S42. High resolution FAB$^+$ -MS spectra of compound **16**.	41

Figure S43. ^{1}H-NMR spectrum (400 MHz, $CDCl_3$) of compound **16**.	42
Figure S44. APT spectrum (100 MHz, $CDCl_3$) of compound **16**.	42
Figure S45. High resolution FAB^+ -MS spectra of compound **17**.	43
Figure S46. ^{1}H-NMR spectrum (400 MHz, $CDCl_3$) of compound **17**.	43
Figure S47. Expansion of ^{1}H-NMR spectrum (400 MHz, $CDCl_3$) of compound **17**.	44
Figure S48. APT spectrum (100 MHz, $CDCl_3$) of compound **17**.	44
Figure S49. High resolution FAB^+ -MS spectra of compound **18.**	45
Figure S50. ^{1}H-NMR spectrum (400 MHz, $(CD_3)_2SO$) of compound **18**.	45
Figure S51. Expansion of ^{1}H-NMR spectrum (400 MHz, $(CD_3)_2SO$) of compound **18**.	46
Figure S52. APT spectrum (100 MHz, $(CD_3)_2SO$) of compound **18**.	46
Figure S53. HMBC correlation spectrum of compound **18**.	47
Figure S54. Selected HMBC correlations of compound **18** from δ_H 6.5-9 ppm, and δ_C 100-180 ppm.	48
Figure S55. High resolution FAB^+ -MS spectra of compound **19**.	49
Figure S56. ^{1}H-NMR spectrum (400 MHz, $CDCl_3$) of compound **19**.	49
Figure S57. Expansion ^{1}H-NMR spectrum (400 MHz, $CDCl_3$) of compound **19**.	50
Figure S58. APT spectrum (100 MHz, $CDCl_3$) of compound **19**.	50
Figure S59. Expansion of APT spectrum (100 MHz, $CDCl_3$) of compound **19**.	51
Figure S60. HMBC correlation spectrum of compound **19**.	52
Figure S61. Selected HMBC correlations of compound **19** from δ_H 5-10 ppm, and δ_C 120-170 ppm.	53
Figure S62. High resolution FAB^+ -MS spectra of compound **20.**	54
Figure S63. ^{1}H-NMR spectrum (400 MHz, $(CD_3)_2SO$) of compound **20**.	54
Figure S64. Expansion of ^{1}H-NMR spectrum (400 MHz, $(CD_3)_2SO$) of compound **20**.	55
Figure S65. APT spectrum (100 MHz, $(CD_3)_2SO$) of compound **20**.	55
Figure S66. HMBC correlation spectrum of compound **20**.	56
Figure S67. Selected HMBC correlations of compound **20** from δ_H 7-8.8 ppm, and δ_C 90-180 ppm.	57
Figure S68. High resolution FAB^+ -MS spectra of compound **21**.	58
Figure S69. ^{1}H-NMR spectrum (400 MHz, $(CD_3)_2SO$) of compound **21**.	58
Figure S70. APT spectrum (100 MHz, $(CD_3)_2SO$) of compound **21**.	59
Figure S71. HMBC correlation spectrum of compound **21**.	60
Figure S72. Selected HMBC correlations of compound **21** from δ_H 6.5-9 ppm, and δ_C 90-180 ppm.	61
Figure S73. High resolution FAB^+ -MS spectra of compound **22**	62
Figure S74. ^{1}H-NMR spectrum (400 MHz, $(CD_3)_2SO$) of compound **22**.	62
Figure S75. Expansion of ^{1}H-NMR spectrum (400 MHz, $(CD_3)_2SO$) of compound **22**.	63
Figure S76. APT spectrum (100 MHz, $(CD_3)_2SO$) of compound **22**.	63
Figure S77. HMBC correlation spectrum of compound **22**.	64
Figure S78. Selected HMBC correlations of compound **22** from δ_H 6-8.5 ppm, and δ_C 90-180 ppm.	65
Figure S79. Western blot analysis of Akt1, Akt2, Akt3, PTP1B, Survivin, REDD1, p-STAT3, STAT3, pNF-κB, NF-κB, pS6, S6, β-actin, GAPDH and COX-2 proteins in the cytosolic extract of SAS cells treated with compound **19**.	66
Figure S80. Molecular model of compound **19** binding with; A) PTP1B; B) COX-2 active sites, obtained by AutoDock Vina in PyRx 0.8.	66
Figure S81. Bar graph shows the effect of ricinine derivatives and standard chemotherapeutic agent 5-FU on the proliferation of normal epithelial cells (L132 cells).	67
References	67

1. Experimental

1.1.General experimental methods

Melting points were determined on Stuart® melting point apparatus model SMP10 and are uncorrected. ^{1}H- and ^{13}C-NMR spectra were obtained using $CDCl_3$ or $(CD_3)_2SO$ solvents and TMS as an internal standard at 400 MHz for ^{1}H-NMR and 100 MHz for ^{13}C-NMR on BRUKER Avance III spectrometer (Bruker AG, Switzerland) or Jeol 500 MHz ^{TM}spectrometer. Chemical shifts (δ) are reported in ppm relative to the solvent signal and coupling constants are given in Hz. Mass spectrometry, HR-TOF–MS data were determined using LC–MS–IT–TOF (Shimadzu, Tokyo, Japan). IR spectra were obtained using a Thermo Scientific Nicolet^{TM} iS^{TM}10 FT-IR or BRUKER FT-IR (Alpha platinum-ATR) spectrometer. The progress of reactions and the purity of final products were monitored by thin layer chromatography (TLC) which was performed on precoated silica gel 60 GF_{254} (20 x 20 cm, 0.2 mm thick) on aluminum sheets (Merck, Germany). UV was applied to visualize the spots. Column chromatography was carried out on silica gel G 60-230 mesh (Merck, Germany). Organic solvents were distilled prior use. Chemical reagents were purchased from Sigma-Aldrich or Combi-Blocks and were used without purification.

1.2.Virtual screening

1.2.1. Reverse docking

Reverse docking for the parent compound, ricinine, was done using PharmMapper web server (http://lilab.ecust.edu.cn/pharmmapper/) for its target identification.

1.2.2. Docking study of ricinine and its derivatives against PTP1B and COX-2 proteins

Structure based docking study was accomplished using PyRx 0.8 (http://pyrx.sourceforge.net/). AutoDock Vina (Trott and Olson 2010) was used as the docking software, installed on Dell desktop equipped with 2.20 GHz Intel® Core (TM) i5 processor running windows 8 operating

system. Ricinine and its analogues were drawn using ChemBio3D Ultra 12.0 and saved with SDF file extension. The energy forms of these structures were minimized with the help of uff force field, then they were transformed to pdbqt format. AutoDock Vina implemented in PyRx 0.8 was used as the molecular modeling software. PTP1B (PDB code: 1QXK) and COX-2 (PDB code: 5IKR) crystal structures obtained from RCSB-Protein Data Bank were used in this docking study. The ligands' docking site was located by forming a cube with the dimensions 25x 25x 25 Å covering the binding site of the standard ligand in the used PDB structure. The coordinates X, Y and Z from center grid box were 29.5479, 30.7994 and 19.6718 respectively for PTP1B and 38.9382, 2.9069 and 61.2034 respectively for COX-2. Docking files visualization was performed using PyMol molecular graphics system (www.pymol.org).

1.3.Biological assays

1.3.1. Materials

MTT (3-(4,5-dimethylthiazol-2-yl)-2,5-diphenyltetrazolium bromide) was purchased from Sigma-Aldrich Chemicals, St. Louis, MO, USA. Dimethyl sulfoxide (DMSO) was purchased from Merck Life Science Pvt. Ltd., India. Dulbecco's modified eagle medium (DMEM), fetal bovine serum (FBS), and penicillin/streptomycin were purchased from Gibco. The SAS human oral squamous cell carcinoma cell line was obtained from Rajiv Gandhi Centre for Biotechnology (RGCB), Thiruvananthapuram and normal lung cell L-132 were obtained from NCCS, Pune. The primary antibodies specific for Survivin, COX-2, Akt1, Akt2, Akt-3, PTP1B, β- actin and GAPDH were purchased from Cell Signaling Technology, USA and the primary antibodies for REDD1, S6, pS6, STAT3 and pSTAT3 were purchased from Abcam, UK.

2.3.2. Cytotoxic activity against oral cancer

The cytotoxic activity of ricinine (**1**) and its synthesized derivatives (**2-24**) against oral carcinoma was evaluated in a cell-based assay in comparison to 5- FU as a positive control using SAS cells and MTT colorimetric assay. SAS cells were harvested using 0.05% trypsin-0.02% EDTA solution in DMEM-High glucose medium and seeded at a concentration of 2000 cells/100 µL per well in a flat-bottomed 96-well polystyrene coated plate. After 24 hr. incubation at 37°C in a 5% CO_2 incubator, the compounds (**1-24**) were added to the cells at a concentration of 25 µM each in hexaplates. 10 µL of 5 mg/mL MTT reagent was added to each well at 0^{th} and 72^{th} hr. of drug treatment and the plates were incubated for 2 hr. Formazan crystals formed after 2 hr. in each well were dissolved in 100 µL of DMSO and the absorbance was read after 1 hr. in a microplate reader at 570 nm. Cells treated only with complete medium were used as control. The IC_{50} of the active compound was determined by plotting proliferation versus concentration.

2.3.3. Selectivity study

The effect of ricinine and its synthetic analogues on the proliferation of normal epithelial cells (L132 cells) was determined in comparison to the standard chemotherapeutic agent, 5-FU. L132 cells were seeded in 96 well culture plates at a density of 2000 cells/100µl/well and treated with 0, 25 and 50 µM of the compounds **1-24** and 5-FU for 72hr. The rate of proliferation was estimated by MTT assay.

2.3.4 Western blot analysis and differential expression of PTP1B and other proteins in compound 19 treated SAS cells

SAS cells were seeded in 6-well plates at a concentration of $6x10^5$ cells/2 mL and incubated for 24 hr. in a 37°C CO_2 incubator. After 24 hr., the cells were treated with 0, 5, 10, 25 and 50 µM of the compound **19**. The whole cell lysates were prepared by treating with lysis buffer (20 µM HEPES buffer, 0.5 M EDTA, 1 M NaCl, 1 mg/mL leupeptin, 5mg/ml aprotinin, 100 mM PMSF,

1M DTT, 0.1% (v/v) Triton X-100) at the end of 24 hr. treatment. The protein concentrations were determined using Bradford protein assay using bovine serum albumin as the standard. Equal amounts of protein were loaded onto a 12% sodium dodecyl sulfate (SDS) polyacrylamide gel; electrophoresis was carried out and the proteins were transferred to a nitrocellulose membrane. Successful transfer of protein to the membrane was confirmed by staining with Ponceau-S. The membrane was then blocked with 5% non-fat dry milk in 1X TBST buffer for 2 hr. at room temperature. Following blocking, the blots were incubated overnight at 4°C with an appropriate dilution of the respective antibodies (Akt1, Akt2 and Akt3, PTP1B, Survivin, REDD1, pSTAT3, STAT3, pNF-κB, NF-κB, pS6, S6, β-actin and GAPDH). After around 16-20 hr., the blots were washed with 1X TBST and incubated with HRP conjugated secondary antibodies for 2 hr. Finally, the blots were developed using an Optiblot ECL Detect Kit (Abcam) and ChemiDoc™ XRS System (BioRad). The housekeeping genes GAPDH and β-actin were used as loading control. These results have been analyzed using Image Lab software.

1.4.Detailed experimental procedures of preparation, FT-IR, and ^{1}H-NMR of ricinine derivatives (5-9):

4-(Allyloxy)-1-methyl-2-oxo-1,2-dihydropyridine-3-carbonitrile **(5)**

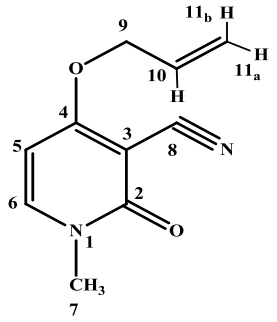

The starting compound, **3** (ricininic acid, 50 mg) was partially dissolved in 10 mL acetone then 43 μL of allyl bromide (1.5 equiv.) and 91 mg of K_2CO_3 (2 equiv.) were added. The reaction mixture was refluxed with stirring at 80ºC for 24 hr. The reaction was stopped by evaporation of acetone and addition of distilled water then extracted with (3x 10 mL) DCM. The DCM extract

was dried over anhydrous sodium sulfate and evaporated under vacuum to afford compound **5** as opaque rhombic crystals (24.5 mg, 38.7 %).

R_f value of 0.61 using DCM- MeOH (9.5:0.5, v/v) as developing system; **m.p.** 164°C; **FT-IR** ν_{max} 3094, 2921, 2851, 2223, 1650, 1596, 1130, 1251 cm^{-1}; **^{1}H-NMR** (400 MHz, $CDCl_3$) δ 7.42 (1H, d, *J*= 4.0 Hz, H-6), 5.96 (1H, br s, H-5), 5.89 (1H, m, H-10), 5.36 (1H, d, *J*=16.0 Hz, H-11_b), 5.28 (1H, d, *J*=12.0 Hz, H-11_a), 4.66 (2H, br s, H-9), 3.46 (3H, s, H-7).

1-Methyl-4-((3-methylbut-2-en-1-yl)oxy)-2-oxo-1,2-dihydropyridine-3-carbonitrile **(6)**

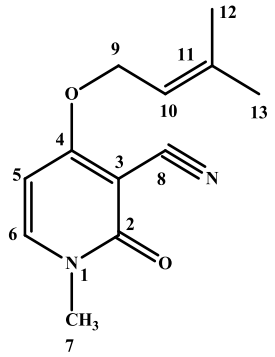

The starting compound, **3** (ricininic acid, 30 mg), after its characterization, was partially dissolved in 7 mL acetone then 28 μL of prenyl bromide (1.2 equiv.) and 55 mg of K_2CO_3 (2 equiv.) were added. The reaction mixture was refluxed with stirring at 80ºC for 4 hrs. The reaction was stopped by evaporation of acetone and addition of distilled water then extracted with (3x 5 mL) DCM. The DCM extract was dried over anhydrous sodium sulfate and evaporated under vacuum to afford compound **6** as pale yellow, very fine, needle like crystals (27 mg, 62 %).

R_f value of 0.65 using DCM- MeOH (9.5:0.5, v/v) as developing system; **m.p.** 115°C; **FT-IR** ν_{max} 3106, 2914, 2853, 2226, 1642, 1589, 1128, 1263cm^{-1}; **^{1}H-NMR** (400 MHz, $CDCl_3$) δ 7.38 (1H, d, *J*=6.8 Hz, H-6), 5.94 (1H,d, *J*=6.8 Hz, H-5), 5.34 (1H, br. s, H-10), and 4.64 (2H, d, *J*=5.2 Hz, H-9), 3.45 (3H, s, H-7), 1.72 (3H, s, H-13), 1.68 (3H, s, H-12).

***3-Cyano-1-methyl-2-oxo-1,2-dihydropyridin-4-yl benzenesulfonate* (7)**

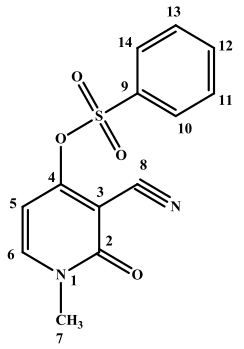

Compound **3** (ricininic acid), 50 mg, was dissolved in 60 mL DCM then 51 μL (1.2 equiv.) of benzene sulfonylchloride and 93 μL (2 equiv.) of triethylamine were added. The reaction mixture was stirred overnight at room temperature, then it was evaporated under vacuum and purified by crystallization to afford compound **7** as white rhombic crystals (55 mg, 57 %).

R_f value of 0.21 using EtOAc- PE (6:4, v/v) as developing system; **m.p.** 126°C; **FT-IR** ν_{max} 3048, 2225, 1649, 1595, 1538, 1366, 1190 cm^{-1}; **^{1}H-NMR** (400 MHz, $CDCl_3$) δ 7.94 (2H, d, *J*=7.8 Hz, H-10/14), 7.68 (1H, dd, *J*=7.6, 7.3 Hz, H-12), 7.54 (2H, dd, *J*=8.1, 7.6 Hz, H-11/13), 7.51 (1H,d, *J*=7.6 Hz, H-6), 6.52 (1H,d, *J*=7.6 Hz, H-5), 3.51 (3H, s, H-7).

***1-Methyl-2-oxo-4-(2-oxo-2-phenylethoxy)-1,2-dihydropyridine-3-carbonitrile* (8)**

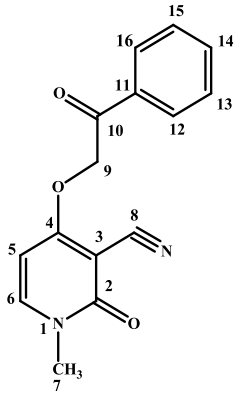

Compound **3** (ricininic acid), 100 mg, was partially dissolved in 50 mL acetone then 159 mg of phenacyl bromide (1.2 equiv.) and 184 mg of K_2CO_3 (2 equiv.) were added. The reaction mixture was refluxed with stirring at 50ºC for 24 hr. The reaction was stopped by evaporation of acetone and addition of distilled water then extracted with (3x 10 mL) DCM. The DCM extract was dried over anhydrous sodium sulfate and evaporated under vacuum to afford compound **8** as granular white powder (94.3 mg, 52.8 %).

R_f value of 0.58 using DCM- MeOH (9.5:0.5, v/v) as developing system; **m.p.** 112°C; **FT-IR** ν_{max} 3064, 3092, 2918, 2937, 2217, 1701, 1639, 1533, 1138, 1235 cm^{-1}; **^{1}H-NMR** (400 MHz, (CD3)2SO) δ 8.03 (3H, d, *J*=7.8 Hz, H-6/12/16), 7.76 (1H, dd, *J*=7.3, 7.4 Hz, H-14), 7.63 (2H, dd, *J*=7.6, 7.6 Hz, H-13/15), 6.41 (1H,d, *J*=7.8 Hz, H-5), 6.01 (2H, br s, H-9), 3.48 (3H, s, H-7).

3-Amino-2-benzoyl-5-methylfuro[3,2-c]pyridin-4(5H)-one **(9)**

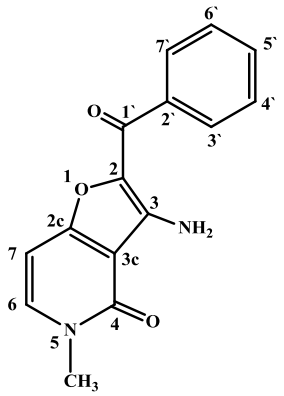

To 70 mg of compound **8**, after its characterization, about 3 mL poly-phosphoric acid (PPA) were added. The reaction mixture was heated at 110ºC for 1.5 hrs. The work up was done in ice bath by addition of distilled water (10 mL) to the reaction mixture and neutralization with aqueous ammonia till pH 6, then extraction with DCM (3 x 10 mL). The obtained DCM extract was dried over anhydrous sodium sulfate and evaporated under vacuum to afford compound **9** as bright yellow flakes (32 mg, 45.7 %).

R_f values of 0.78 using DCM- MeOH (9.5:0.5, v/v) as developing system and 0.30 using EtOAc-PE (6:4, v/v) as developing system, **m.p.** 242°C; **FT-IR** ν_{max} 3425, 3304, 3034, 3058, 2917, 1672, 1567, 1298, 1117 cm^{-1}; **^{1}H-NMR** (400 MHz, $CDCl_3$) δ 8.13 (2H, dd, *J*=8, 1.48 Hz, H-3`/7`), 7.49 (2H, overlapped, H-4`/6`), 7.35 (1H, d, *J*=7.6 Hz, H-6), 6.42 (1H, d, *J*=7.6 Hz, H-7), 3.62 (3H, s, *N*-CH_3).

1.5. Detailed experimental procedures of preparation, FT-IR, and ^{1}H-NMR of ricinine derivatives 12-14, 16, 17, and 19-22 (Thompson and Gaudino, 1984)

They were prepared from bromoricinine analogue (**11**), that was obtained from ricinine as reported by El-Naggar *et al*. (El-Naggar et al. 2019). To a solution of compound **11** (100 mg, 0.4 mM, 1 equiv.) in MeOH (60 mL), were added 114 mg of K_2CO_3 (2 equiv.)**,** 9 mg palladium acetate (10 mol %), and 1.2 equivalent of boronic acid derivative. The reaction mixtures were

refluxed with stirring at 80ºC. scheme 2. Work up was done by filtration of the reaction mixtures over silica gel and evaporation under vacuum. Purification was carried out over silica gel chromatography till purity reached >95% as detected by TLC.

4-Methoxy-1-methyl-2-oxo-5-phenyl-1,2-dihydropyridine-3-carbonitrile **(12)**

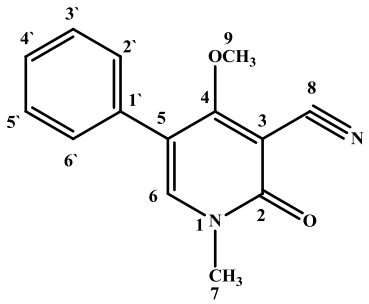

It was purified over silica gel CC. and isocratic elution using DCM- MeOH (9.5:0.5, v/v). Colorless feather-like crystals (15.6 mg, 15.8 % yield), **m.p.** 177°C, $\mathbf{R_f}$ value of 0.41 using EtOAc- PE (6:4, v/v) as developing system. **FT-IR** ν_{max} 3073, 2937, 2858, 2220, 1633, 1520, 1157 & 1350 cm^{-1}; **^{1}H-NMR** (400 MHz, $CDCl_3$) δ 7.40 (3H, dd, *J*=7.1, 7.1 Hz, H-3`/4`/5`), 7.37 (1H, s, H-6), 7.31 (2H, dd, *J*=5.9, 2 Hz, H-2`/6`), 4.24 (3H, s, H-9), 3.59 (3H, s, H-7).

5-(4-Acetylphenyl)-4-methoxy-1-methyl-2-oxo-1,2-dihydropyridine-3-carbonitrile **(13)**

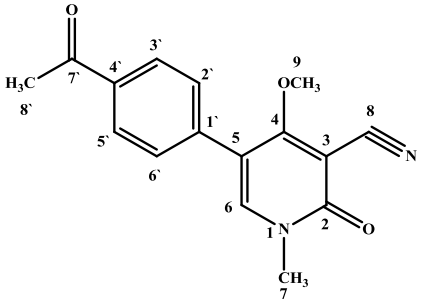

It was purified over silica gel CC. and isocratic elution using PE- EtOAc (1:1, v/v). white powder (37.8 mg, 32.5 %), $\mathbf{R_f}$ values of 0.17 using EtOAc- PE (6:4, v/v) as developing system and 0.76 using DCM-MeOH (9.5:0.5, v/v) as developing system. **FT-IR** ν_{max} 3047, 2928, 2967, 2222, 1647, 1602, 1521, 1188, 1275 cm^{-1}; **^{1}H-NMR** (400 MHz, $(CD_3)_2SO$) δ 8.16 (1H, s, H-6), 7.99 (2H, d, *J*=8 Hz, H-3`/5`), 7.56 (2H, d, *J*=8 Hz, H-2`/6`), 4.11 (3H, s, H-9), 3.50 (3H, s, H-7), 2.61 (3H, s, H-8`).

4-(5-Cyano-4-methoxy-1-methyl-6-oxo-1,6-dihydropyridin-3-yl)benzamide **(14)**

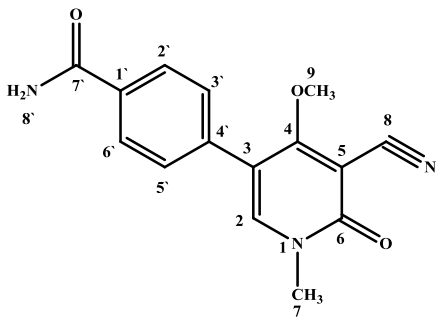

It was purified over MPLC using silica gel (4 g), and DCM- MeOH (gradient elution). Fractions (5 mL) were collected to afford compound **14** that was eluted with DCM- MeOH (8.5:1.5, v/v) as white powder (20 mg, 17 % yield), $\mathbf{R}_f$ values of 0.27 using DCM- MeOH (9.5:0.5, v/v) as developing system. **FT-IR** ν_{max} 3449, 3152, 3049, 2927, 2219, 1697, 1642, 1522, 1143 cm^{-1}; **^{1}H-NMR** (400 MHz, $(CD_3)_2SO$) δ 8.13 (1H, s, H-2), 7.92 (2H, d, *J*=8 Hz, H-2`/6`), 7.48 (2H, d, *J*=8 Hz, H-3`/5`), 4.10 (3H, s, H-9), 3.50 (3H, s, H-7).

***5-(Benzo[d][1,3]dioxol-5-yl)-4-methoxy-1-methyl-2-oxo-1,2-dihydropyridine-3-carbonitrile* (16)**

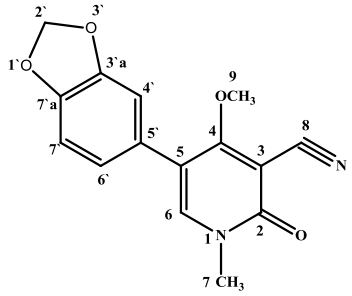

It was purified by crystallization. colorless prisms (67.8, 58 %), **m.p.** 252°C**,** $\mathbf{R}_f$ value of 0.36 using EtOAc- PE (6:4, v/v) as developing system. **FT-IR** ν_{max} 3039, 2862, 2918, 2213, 1645, 1527, 1235, 1137 cm^{-1}; **^{1}H-NMR** (400 MHz, $CDCl_3$) δ 7.33 (1H, s, H-6), 6.85 (1H, d, *J*=8.2 Hz, H-7`), 6.80 (1H, d, *J*=1.2 Hz, H-4`), 6.73 (1H, dd, *J*=8, 1.4 Hz, H-6`), 6.03 (2H, s, H-2`), 4.26 (3H, s, H-9), 3.58 (3H, s, H-7).

***4-methoxy-1-methyl-2-oxo-5-(4-phenoxyphenyl)-1,2-dihydropyridine-3-carbonitrile* (17)**

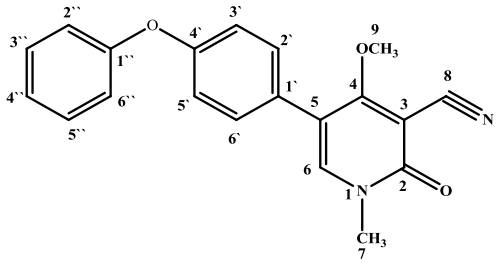

It was purified over silica gel (4 g) CC. and isocratic elution using 100% DCM. white Feather-like crystals (60.8 mg, 44.5 % yield), **m.p.** 244°C, $\mathbf{R}_f$ value of 0.48 using EtOAc- PE (6:4, v/v) as developing system. **FT-IR** ν_{max} 3048, 2928, 2881, 2218, 1648, 1516, 1231, 1165 cm^{-1}; **^{1}H-NMR** (400 MHz, $CDCl_3$) δ 7.38 (2H, dd, *J*=7.5, 7.8 Hz, H-3``/5``), 7.36 (1H, s, H-6), 7.25 (2H, d, *J*=8.3 Hz, H-2`/6`), 7.16 (1H, dd, *J*=7.4, 7.4 Hz, H-4``), 7.07 (2H, d, *J*=8.3 Hz, H-2``/6``), 7.03 (2H, d, *J*=8.3 Hz, H-3`/5`), 4.28 (3H, s, H-9), 3.59 (3H, s, H-7).

5-([1,1'-Biphenyl]-4-yl)-4-methoxy-1-methyl-2-oxo-1,2-dihydropyridine-3-carbonitrile **(19)**

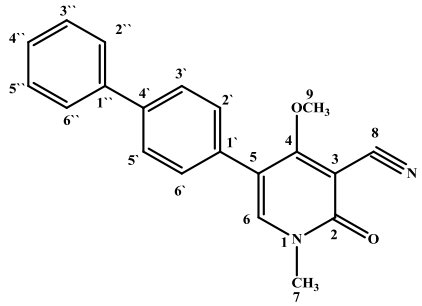

It was purified over silica gel (3 g) CC. and isocratic elution using PE- EtOAc (1:1, v/v). Amorphous white powder (60 mg, 46.6% yield). $\mathbf{R}_f$ value of 0.45 using EtOAc- PE (6:4, v/v) as developing system. **FT-IR** ν_{max} 3060, 2859, 2928, 2215, 1637, 1522, 1163, 1288 cm^{-1}; **^{1}H-NMR** (400 MHz, $CDCl_3$) δ 7.65 (2H, d, *J*=8.6, H-3`/5`), 7.63 (2H, d, J=8.8, H-2``/6``), 7.47 (2H, dd, *J*=7.3, 7.3 Hz, H-3``/5``), 7.39 (4H, overlapped, H-6/2`/6`, 4``), 4.29 (3H, s, H-9), 3.61 (3H, s, H-7).

4-Methoxy-1-methyl-2-oxo-5-(thiophen-3-yl)-1,2-dihydropyridine-3-carbonitrile **(20)**

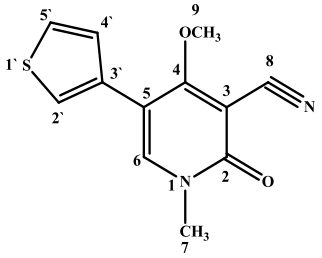

It was purified over silica gel (3 g) CC. and isocratic elution using PE- EtOAc (1:1, v/v). Amorphous white powder (13.8 mg, 13.6 % yield) with $\mathbf{R}_f$ values of 0.39 using EtOAc- PE (6:4, v/v) as developing system. **FT-IR** ν_{max} 3101, 2932, 2219, 1634, 1523, 1155, 1204 cm^{-1}; **^{1}H-NMR** (400 MHz, $(CD_3)_2SO$) δ 8.27 (1H, s, H-6), 7.67 (1H, s, H-2`), 7.66 (1H, overlapped d, *J*=4.9 Hz, H-5`), 7.34 (1H, d, *J*=4.4 Hz, H-4`), 4.21 (3H, s, H-9), 3.53 (3H, s, H-7).

***5-(Furan-3-yl)-4-methoxy-1-methyl-2-oxo-1,2-dihydropyridine-3-carbonitrile* (21)**

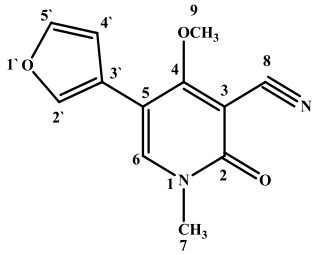

It was purified over MPLC using silica gel (4 g) CC. and isocratic elution using petr. ether-EtOAc (1:1, v/v). Amorphous white powder (10 mg, 10.5 % yield), $\mathbf{R}_f$ values of 0.32 using EtOAc- PE (6:4, v/v) as developing system. **FT-IR** ν_{max} 3015, 3078, 2962, 2215, 1642, 1607, 1364, 1180 cm^{-1}; **^{1}H-NMR** (400 MHz, $(CD_3)_2SO$) δ 8.35 (1H, s, H-6), 7.99 (1H, br s, H-2`), 7.77 (1H, br s, H-5`), 6.90 (1H, br s, H-4`), 4.36 (3H, s, H-9), 3.54 (3H, s, H-7).

***5-(1H-indol-5-yl)-4-methoxy-1-methyl-2-oxo-1,2-dihydropyridine-3-carbonitrile* (22)**

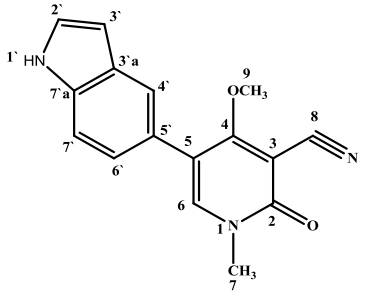

It was purified over silica gel (3 g) CC. and isocratic elution using PE- EtOAc (1:1, v/v). Amorphous white powder (30 mg, 26 % yield) with $\mathbf{R}_f$ values of 0.32 using EtOAc- PE (6:4, v/v) as developing system. **FT-IR** ν_{max} 3233, 3061, 2958, 2217, 1642, 1603, 1528, 1147, 1196 cm^{-1}; **^{1}H-NMR** (400 MHz, $(CD_3)_2SO$) δ 11.15 (1H, br s, 1`-NH), 8.04 (1H, s, H-6), 7.55 (1H, s, H-5`), 7.43 (1H, d, *J*=8.3 Hz, H-7`), 7.39 (1H, br s, H-2`), 7.09 (1H, d, *J*=8.6 Hz, H-6`), 6.46 (1H, br s, H-3`), 3.94 (3H, s, H-9), 3.50 (3H, s, H-7).

***4-Methoxy-5-(4-methoxyphenyl)-1-methyl-2-oxo-1,2-dihydropyridine-3-carbonitrile* (15)**

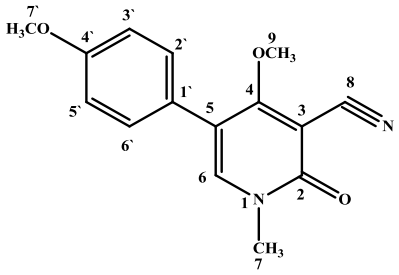

To a solution of bromoricinine **(11),** (50 mg, 0.2 mM, 1 equiv.) in MeOH (30 mL), 56 mg of K_2CO_3 (2 equiv.), 4.5 mg palladium acetate (10 mol %), and 31 mg of 4-methoxyphenylboronic acid (1 equiv.) were added. The reaction mixture was refluxed with stirring at 80ºC for 16 hrs. Work up was done by its evaporation under vacuum, addition of water (10 mL) and fractionation with EtOAc (3x10 mL) as shown in scheme 2. The EtOAc extract was dried over anhydrous sodium sulfate and evaporated under vacuum.

It was purified by column chromatography using 1.5 g silica gel and isocratic elution with 100% DCM. Needle-like crystals (45.3 mg, 81.5% yield) with $\mathbf{R}_f$ value of 0.32 using EtOAc- PE (6:4, v/v) as developing system; **m.p.** 200°C; **FT-IR** ν_{max} 3049, 2927, 2857, 1649, 1517, 2221, 1246, 1120 cm^{-1}; **^{1}H-NMR** (500 MHz, $CDCl_3$) δ 7.30 (1H, s, H-6), 7.19 (2H, d, *J*=8.5 Hz, H-2`/6`), 6.91 (1H, d, *J*=8.5 Hz, H-3`/5`), 4.21 (3H, s, H-9), 3.82 (3H, s, H-7`), 3.54 (3H, s, H-7).

4-(5-Cyano-4-methoxy-1-methyl-6-oxo-1,6-dihydropyridin-3-yl)phenyl benzenesulfonate **(18)**

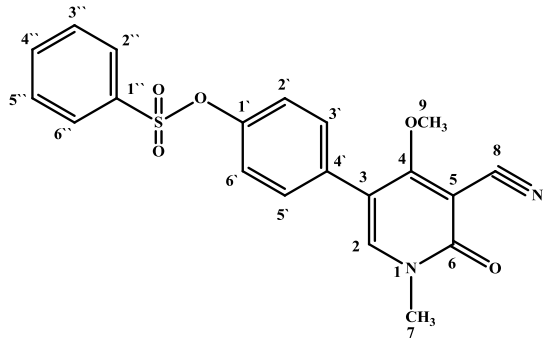

To a solution of bromoricinine **(11)** (50 mg, 0.2 mM, 1 equiv.) in MeOH (30 mL) 56 mg of K_2CO_3 (2 equiv.), 4.5 mg palladium acetate (10 mol %), and 34 mg of 4-hydroxyphenylboronic acid (1.2 equiv.) were added. The reaction mixture was refluxed with stirring at 80ºC for 5 hrs. When the reaction was complete, the reaction mixture was filtered over silica gel and evaporated under vacuum. The crude reaction residue was dissolved in 30 mL of DCM, then 31 µL of benzene sulfonylchloride (1.2 equiv.) and 41 µL of triethylamine (2 equiv.) were added. The reaction mixture was stirred at room temperature for 18 hr., then it was evaporated under vacuum.

It was purified over silica gel (3 g) CC. and isocratic elution using PE- EtOAc (1:1, v/v). white powder (20 mg, 24.5% yield) with $\mathbf{R_f}$ value of 0.63 using DCM- MeOH (9.5:0.5, v/v) as developing system. **FT-IR** ν_{max} 3034, 2957, 2228, 1650, 1521, 1371, 1182, 1156 cm^{-1}; **^{1}H-NMR** (400 MHz, $(CD_3)_2SO$) δ 8.07 (1H, s, H-2), 7.90 (2H, d, *J*=7.6 Hz), H-2``/6``), 7.83 (1H, dd, *J*=7.6, 7.6 Hz, H-4``), 7.68 (2H, dd, *J*=7.8, 7.8 Hz, H-3``/5``), 7.40 (2H, d, *J*=8.6 Hz, H-3`/5`), 7.09 (2H, d, *J*=8.6 Hz, H-2`/6`), 4.06 (3H, s, H-9), 3.46 (3H, s, H-7).

2. Spectra (mass & NMR) of new compounds

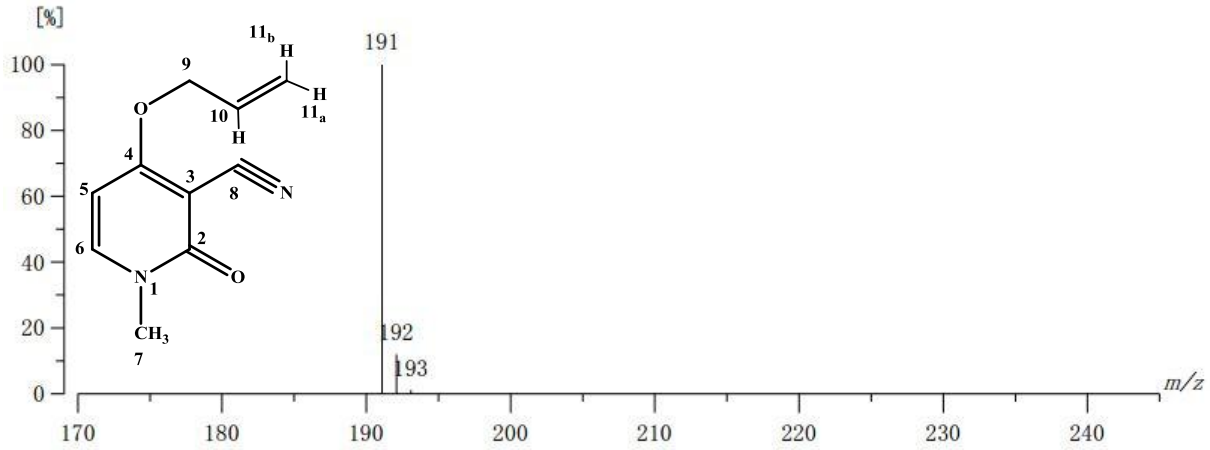

Figure S1. High resolution FAB^+-MS spectra of compound **5**, showing $[M+H]^+$ ion peak at *m/z* 191.0820 (calcd.. for $C_{10}H_{11}N_2O_2$, 191.0821).

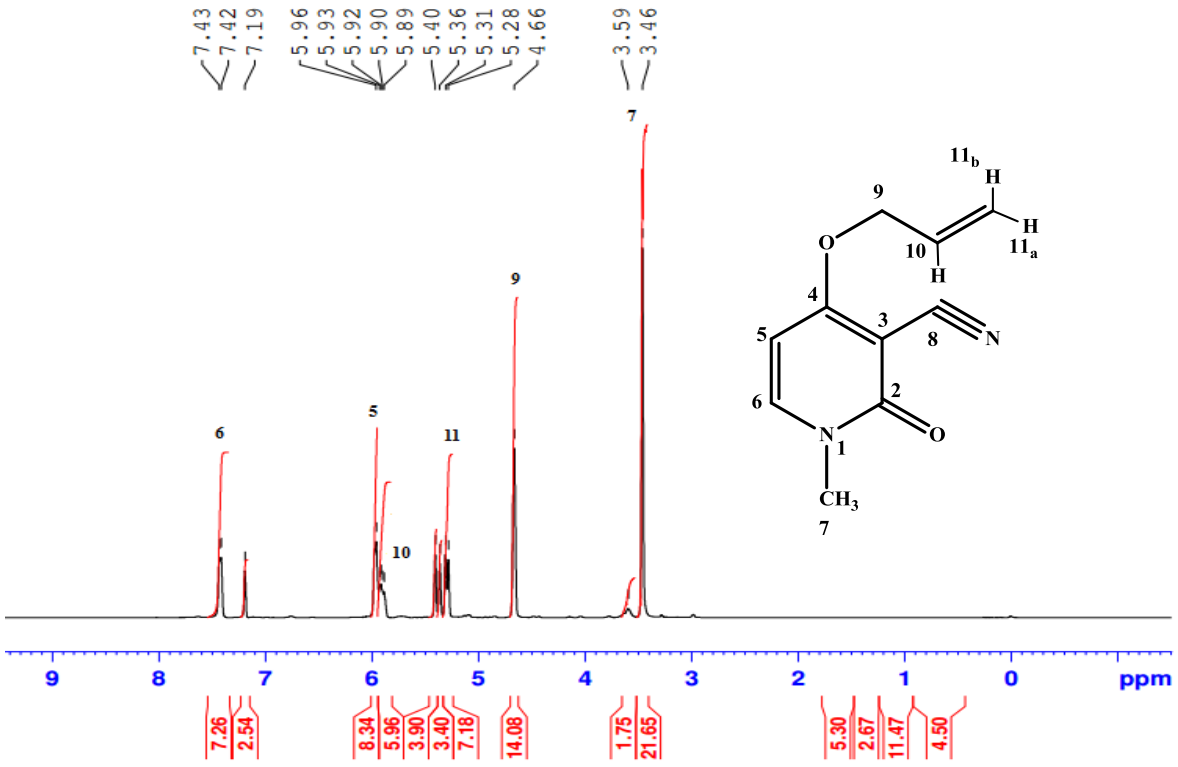

Figure S2. ^{1}H-NMR spectrum (400 MHz, $CDCl_3$) of compound **5**.

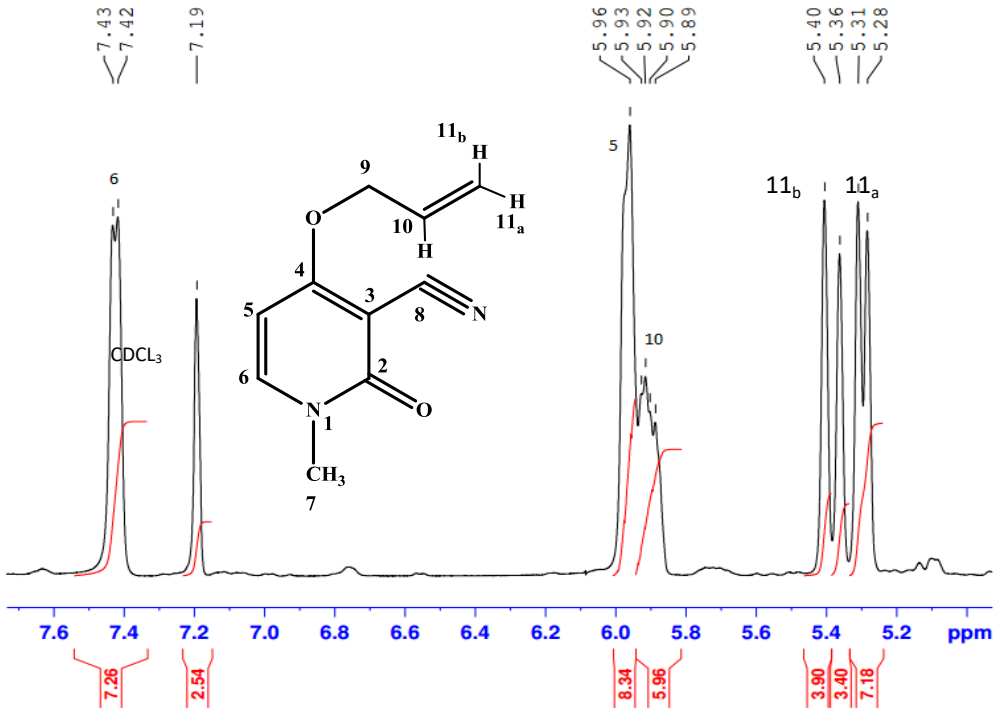

Figure S3. Expansion of ^{1}H-NMR spectrum (400 MHz, $CDCl_3$) of compound **5**.

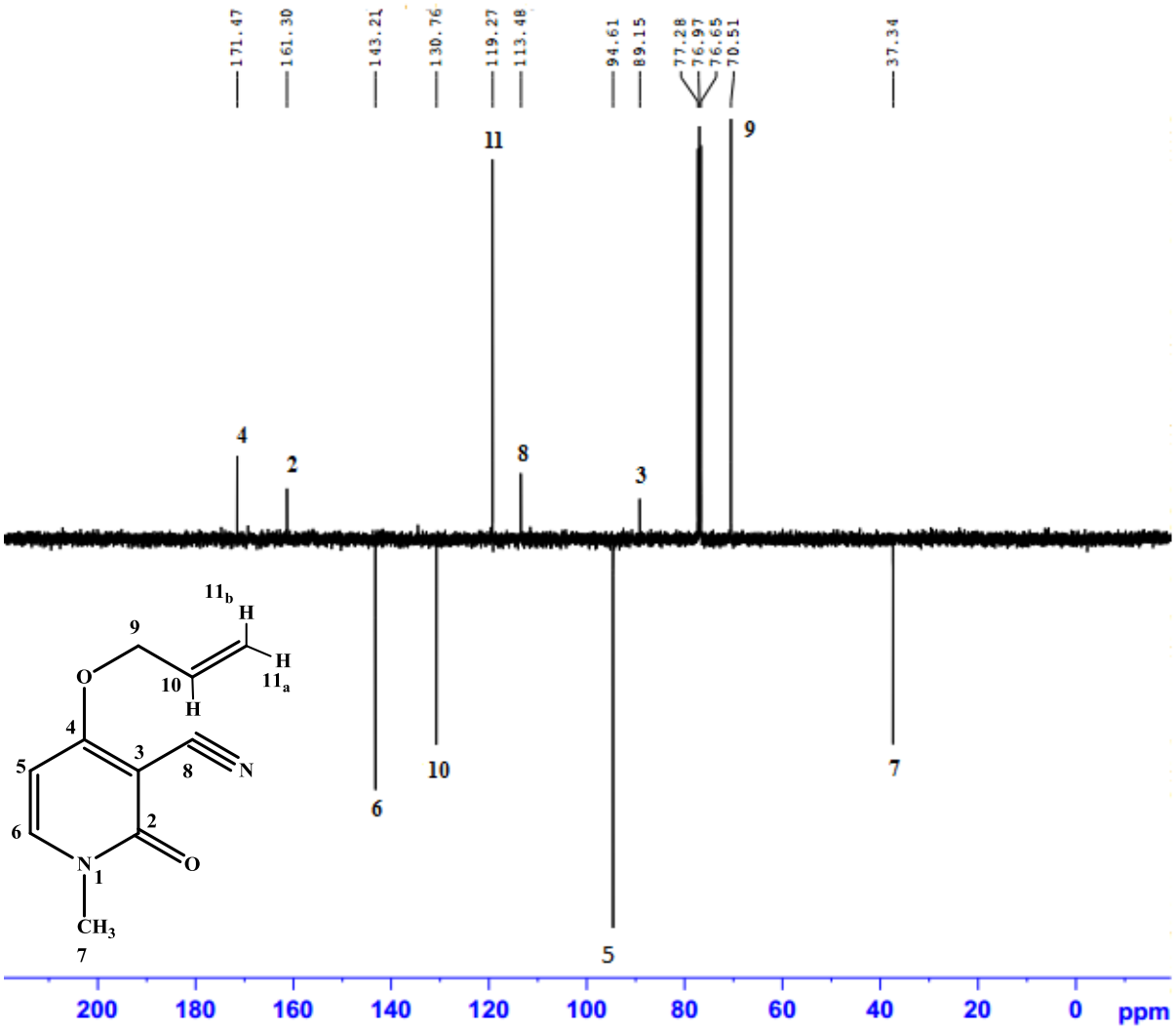

Figure S4. APT spectrum (100 MHz, $CDCl_3$) of compound **5**.

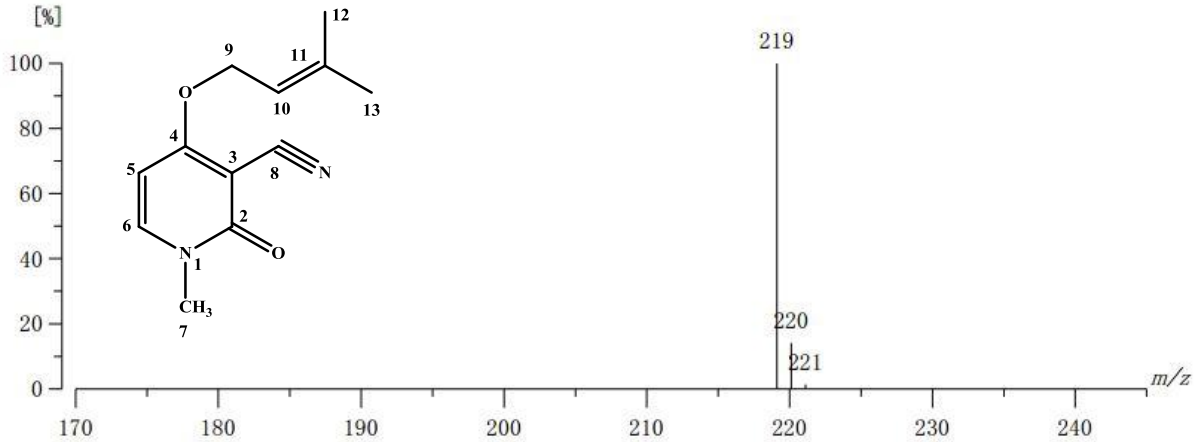

Figure S5. High resolution FAB^+-MS spectra of compound **6**, showing $[M+H]^+$ ion peak at *m/z* 219.1135 (calcd. for $C_{12}H_{15}N_2O_2$, 219.1134).

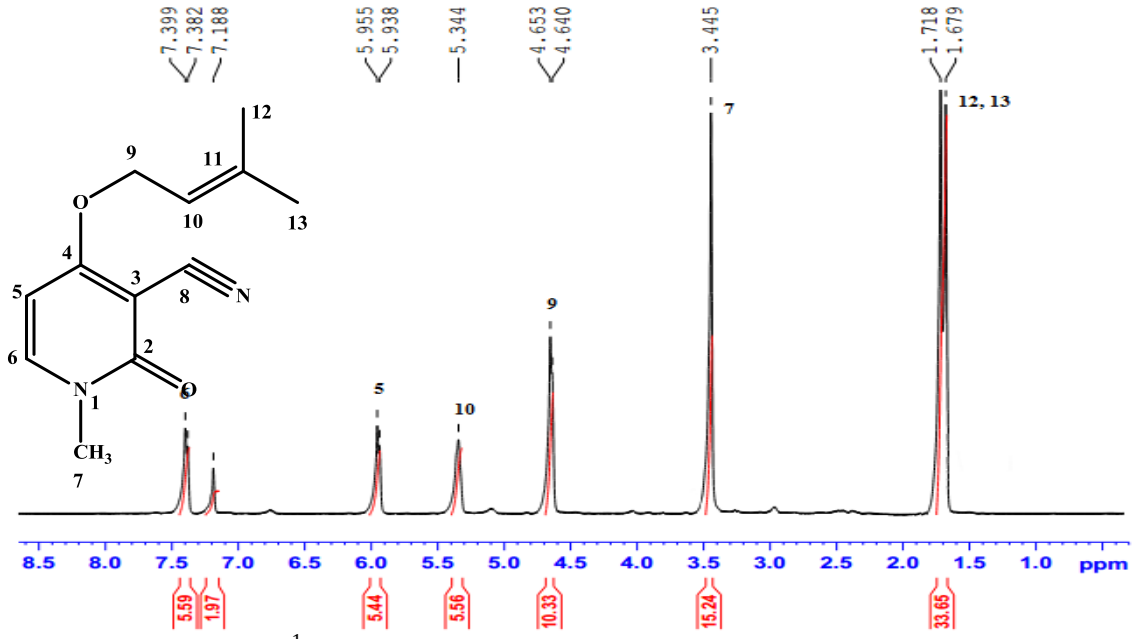

Figure S6. ^{1}H-NMR spectrum (400 MHz, $CDCl_3$) of compound **6**.

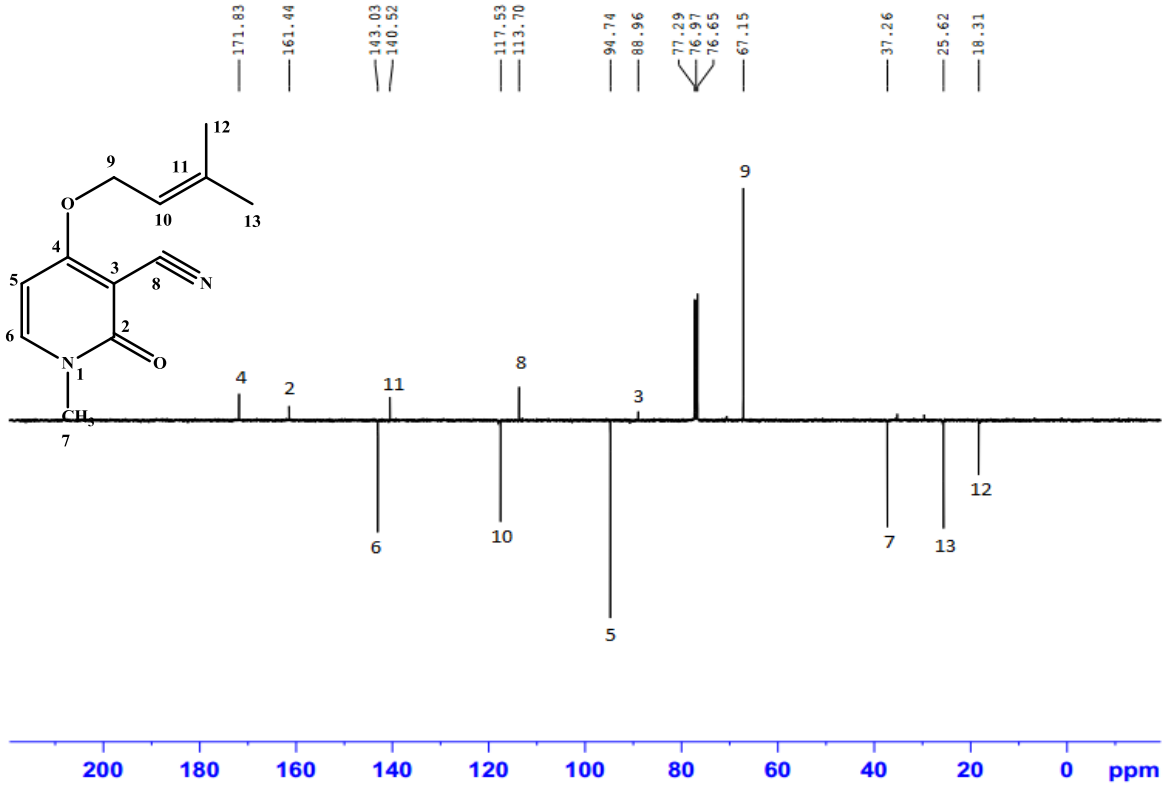

Figure S7. APT spectrum (100 MHz, $CDCl_3$) of compound **6**.

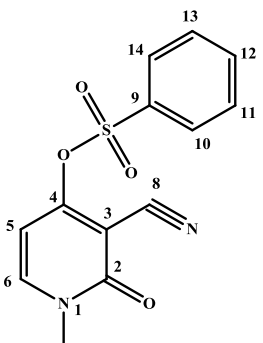

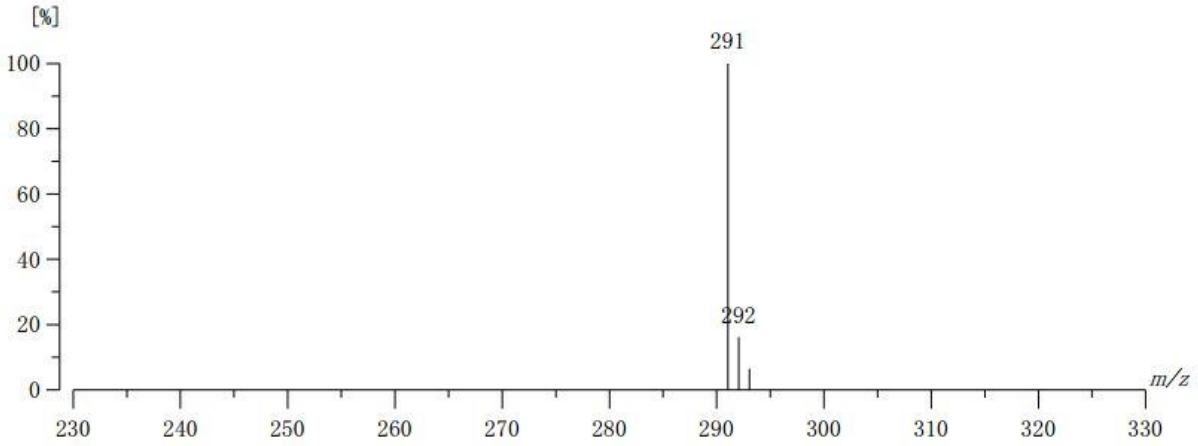

Figure S8. High resolution FAB$^+$ -MS spectra of compound **7**, showing $[M+H]^+$ ion peak at *m/z* 291.0442 (calcd. for $C_{13}H_{11}N_2O_4S$, 291.0440).

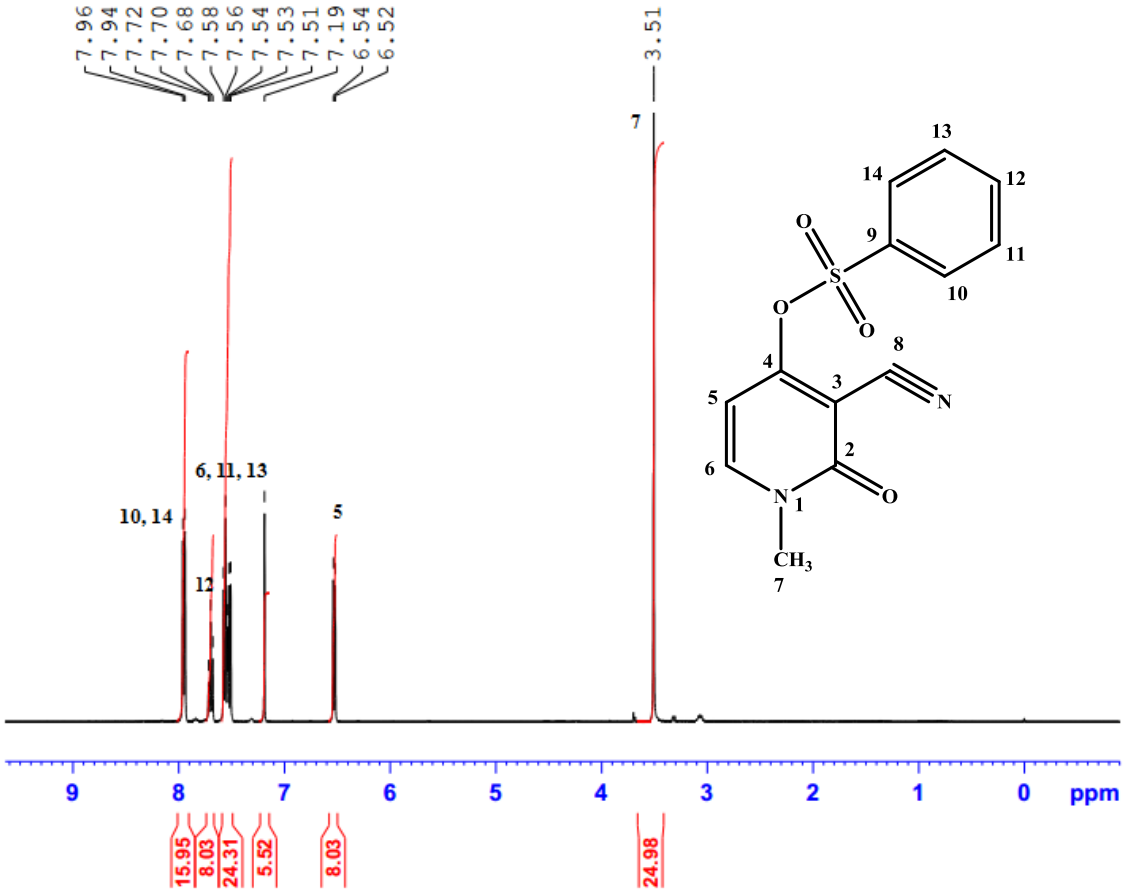

Figure S9. ^{1}H-NMR spectrum (400 MHz, $CDCl_3$) of compound **7**.

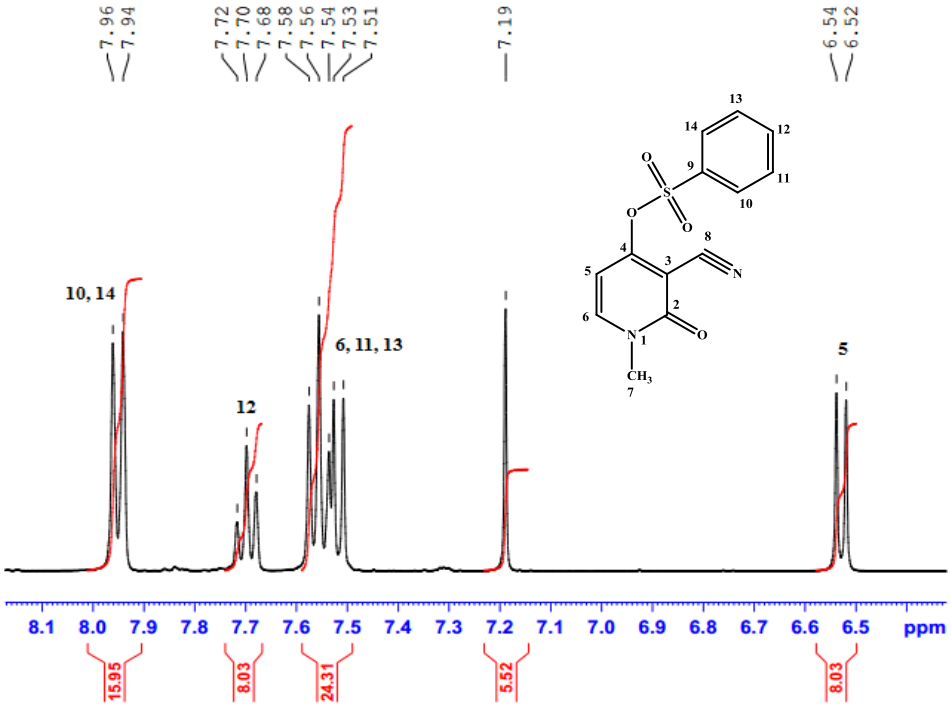

Figure S10. Expansion of ^{1}H-NMR spectrum (400 MHz, $CDCl_3$) of compound **7**.

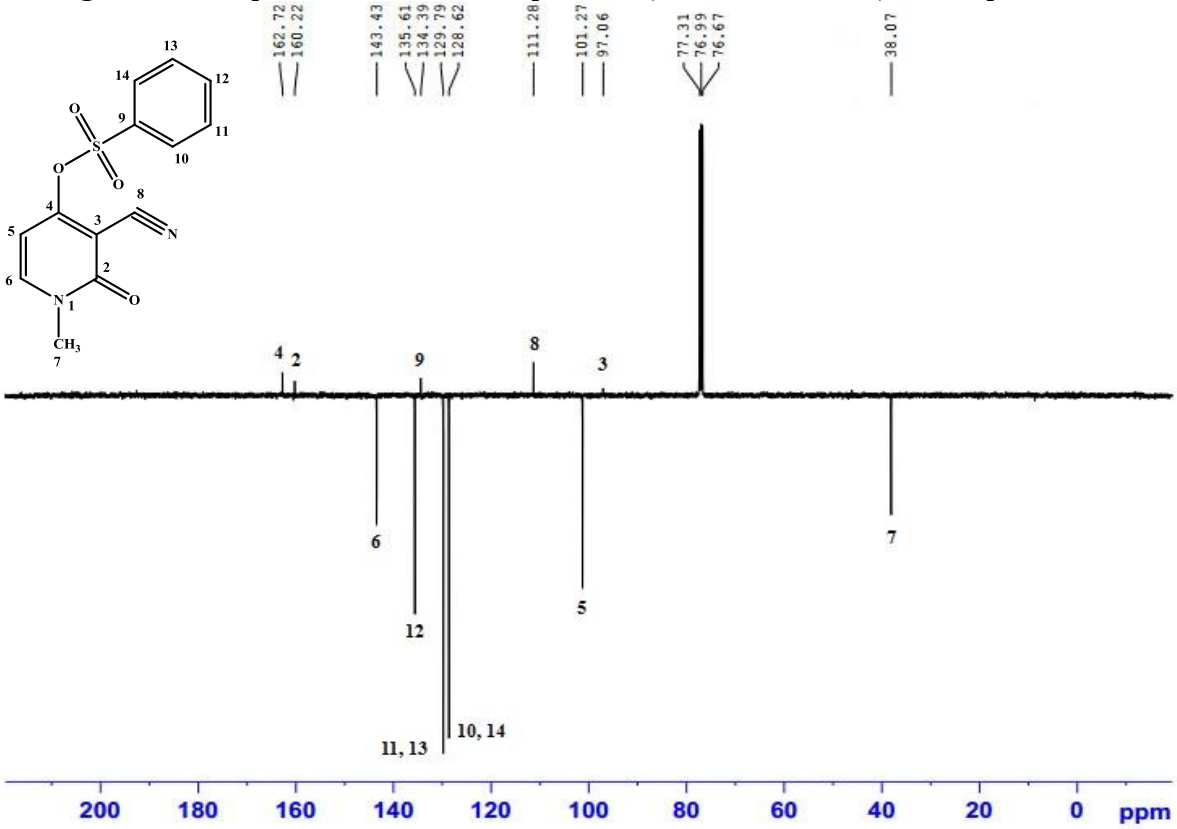

Figure S11. APT spectrum (100 MHz, $CDCl_3$) of compound **7**.

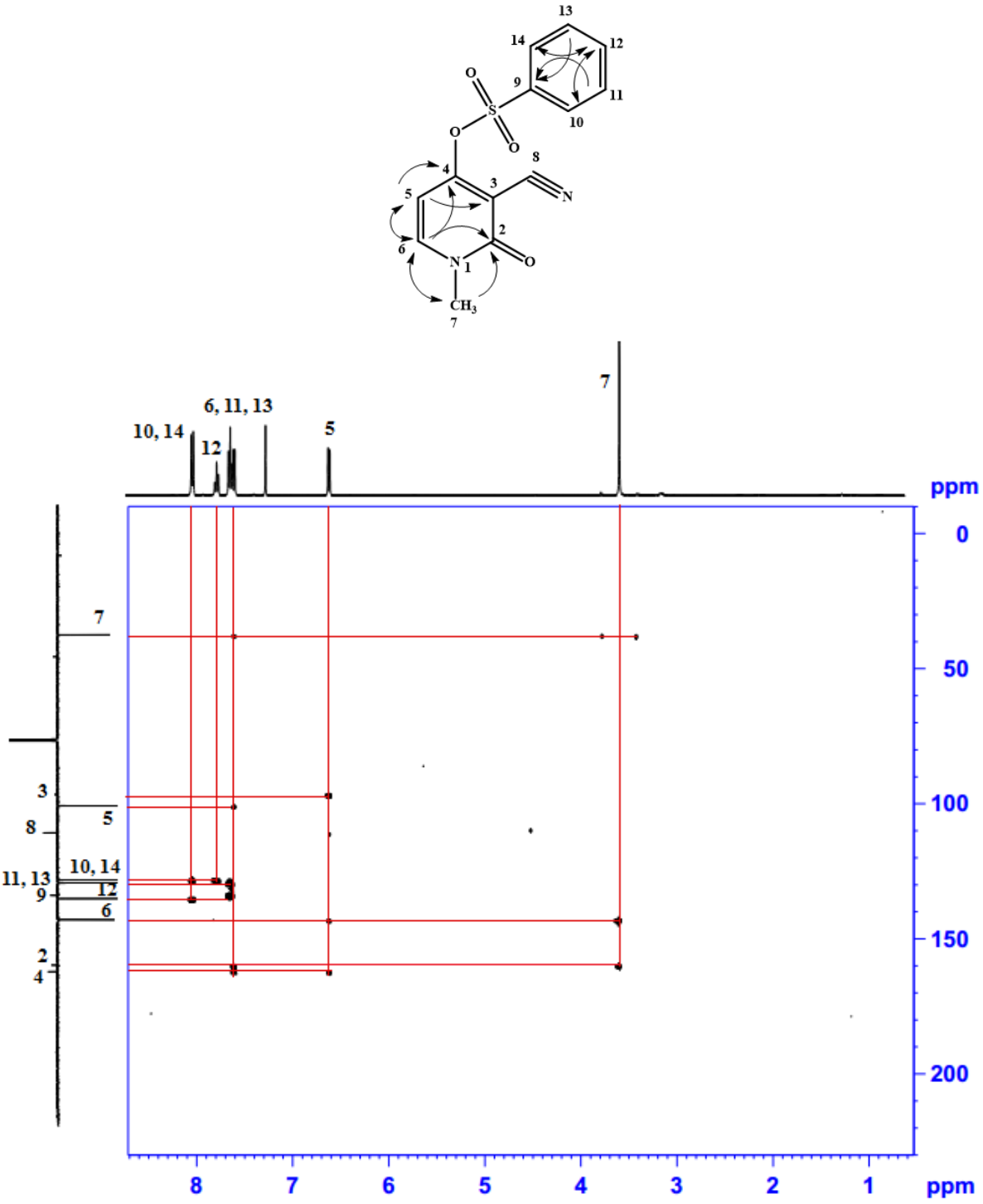

Figure S12. HMBC correlation spectrum of compound **7**.

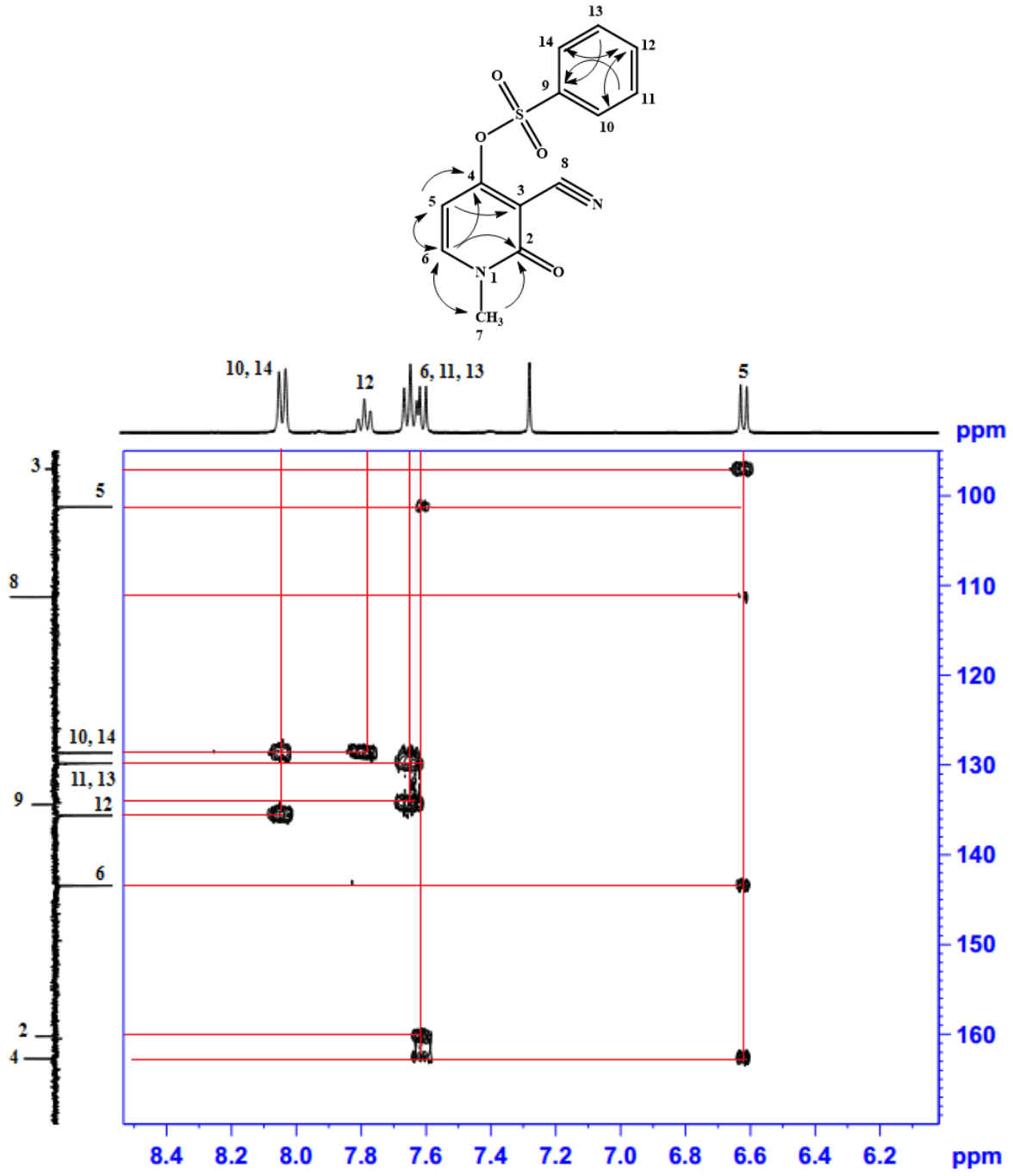

Figure S13. Selected HMBC correlation spectrum of compound **7** from δ_H 6-8 ppm, and from δ_C 100-170 ppm.

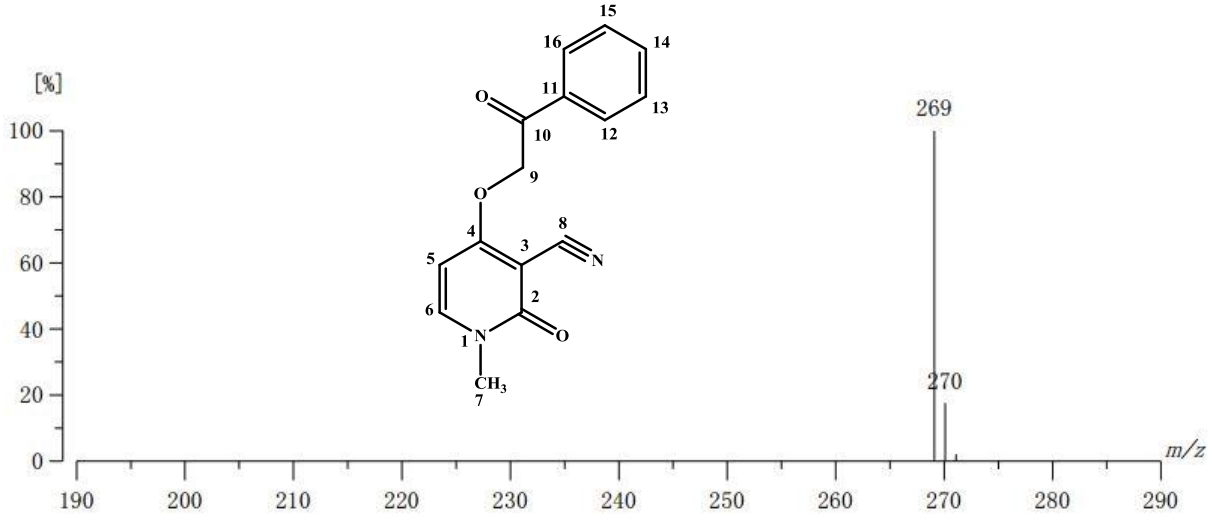

Figure S14. High resolution FAB$^+$ -MS spectra of compound **8**, showing $[M+H]^+$ ion peak at *m/z* 269.0924 (calcd. for $C_{15}H_{13}N_2O_3$, 269.0926).

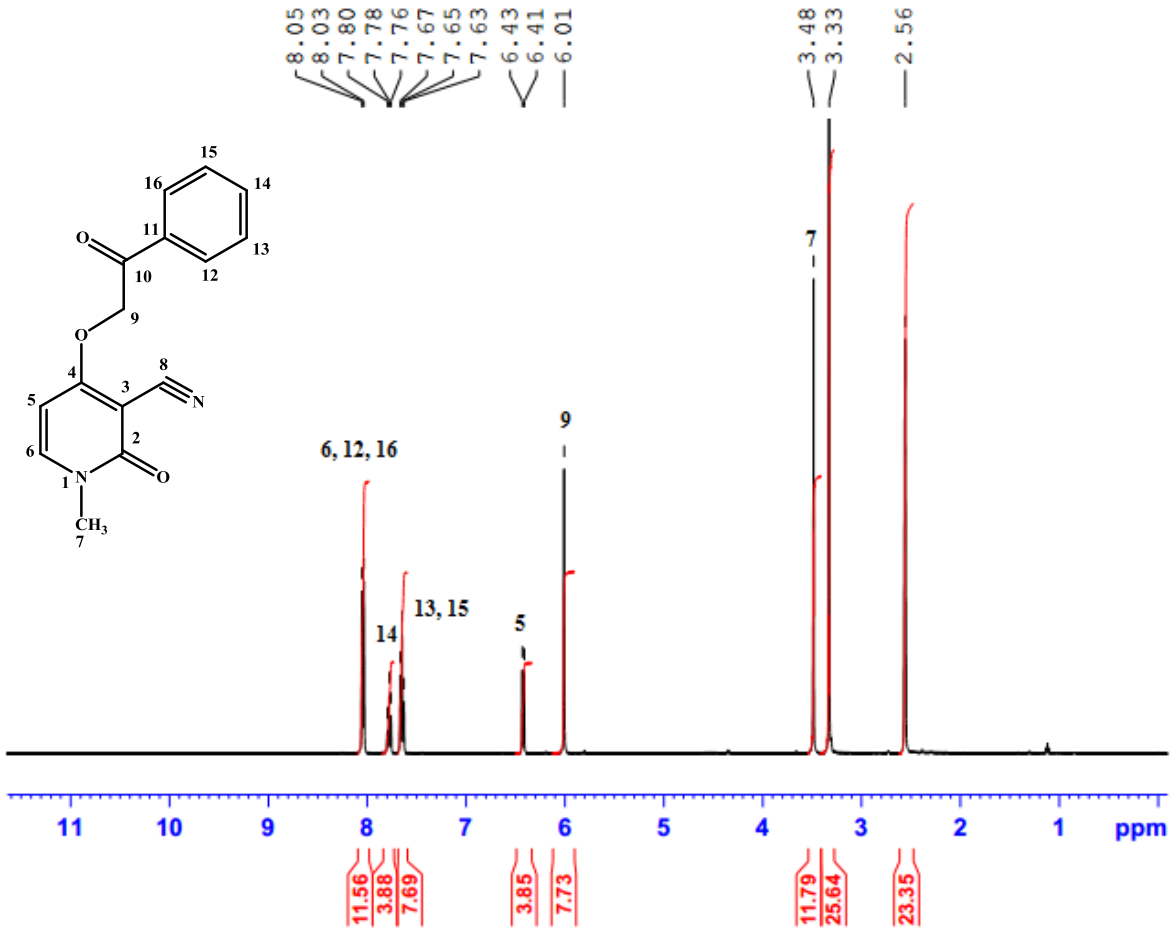

Figure S15. ^{1}H-NMR spectrum (400 MHz, $(CD_3)_2SO$) of compound **8**.

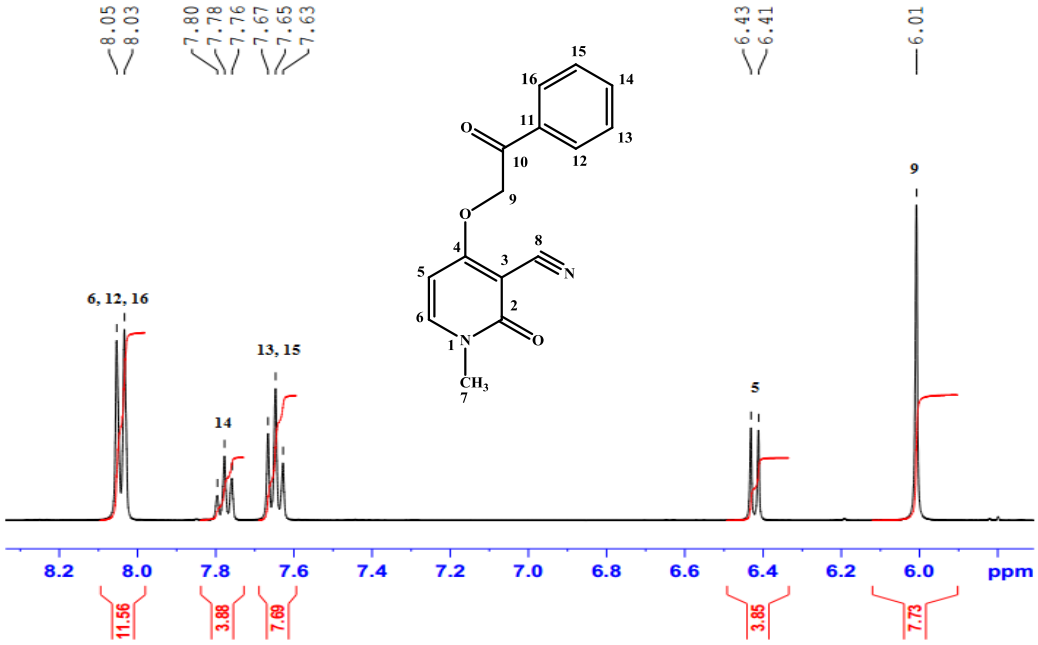

Figure S16. Expansion of ^{1}H-NMR spectrum (400 MHz, $(CD_3)_2SO$) of compound **8**.

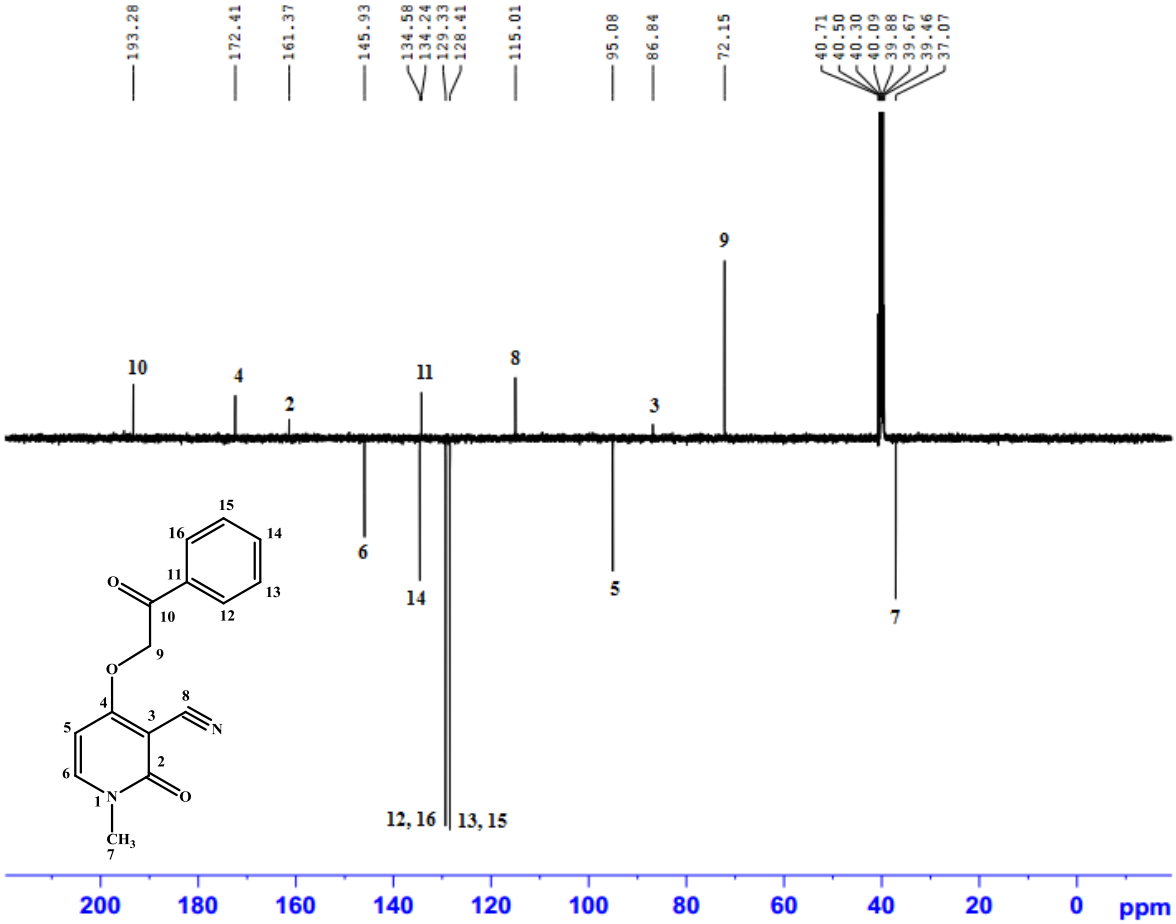

Figure S17. APT spectrum (100 MHz, $(CD_3)_2SO$) of compound **8**.

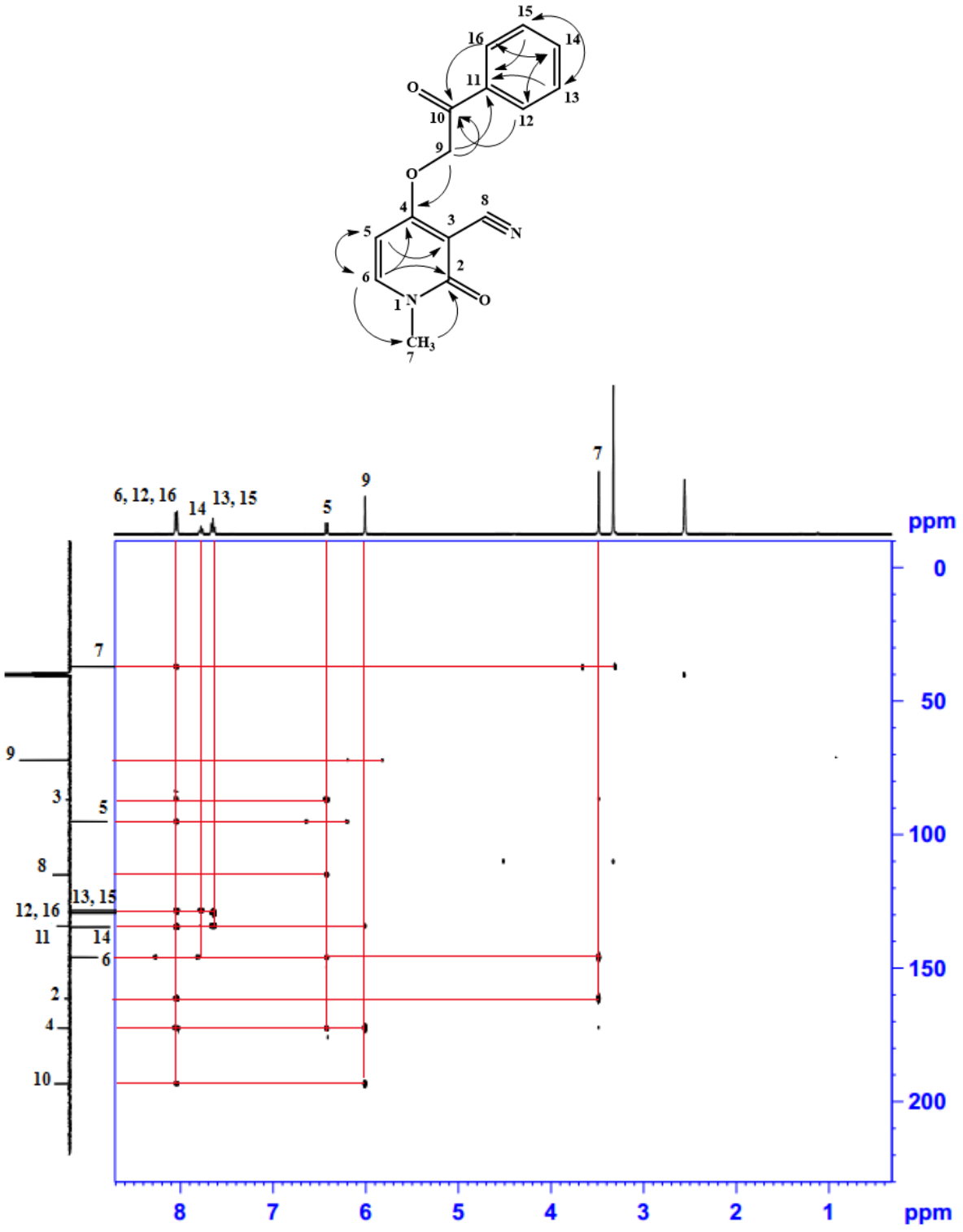

Figure S18. HMBC correlation spectrum of compound **8**.

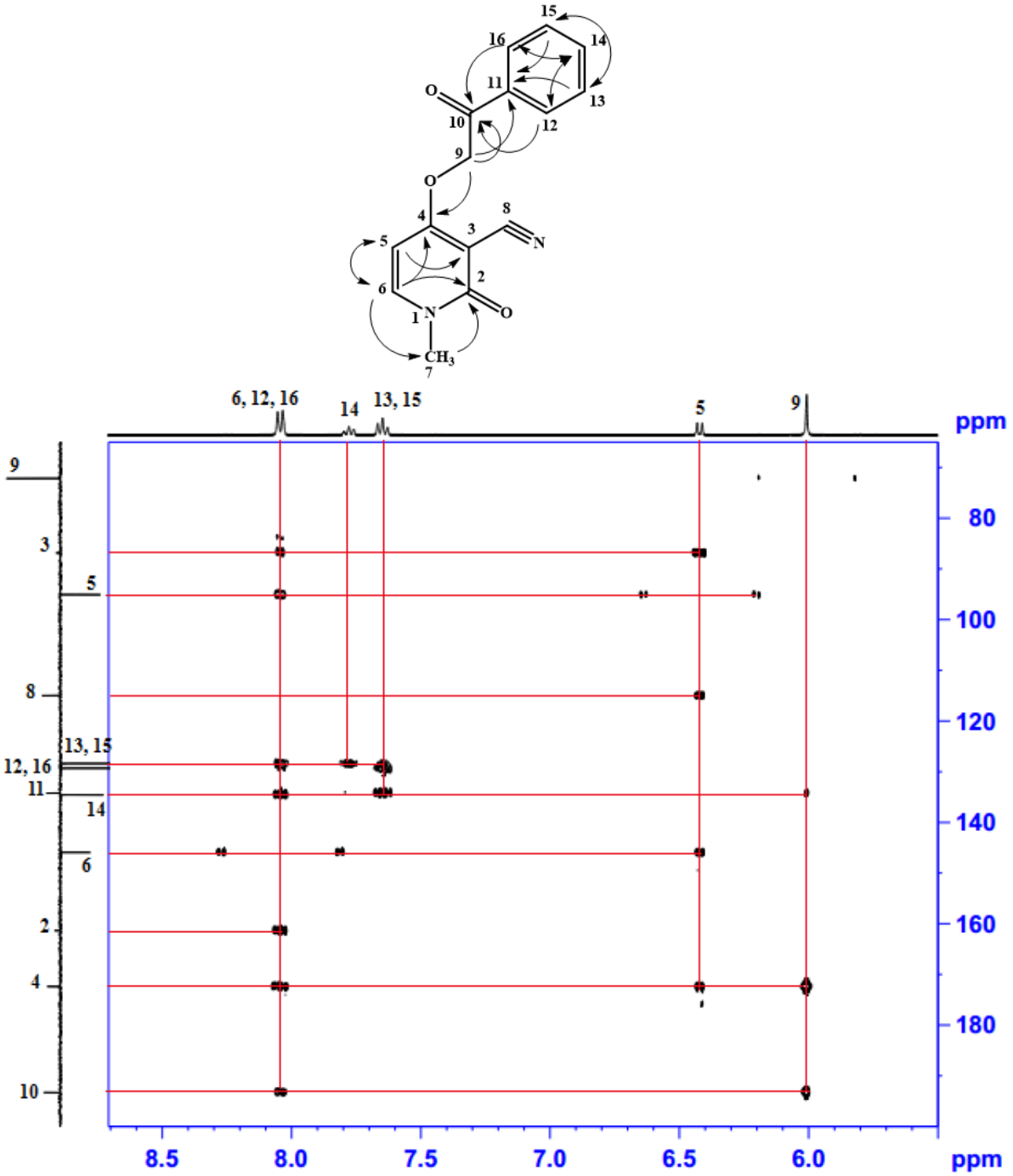

Figure S19. Selected HMBC correlation spectrum of compound **8** from δ_H 5-8.5 ppm, and from δ_C 70-190 ppm.

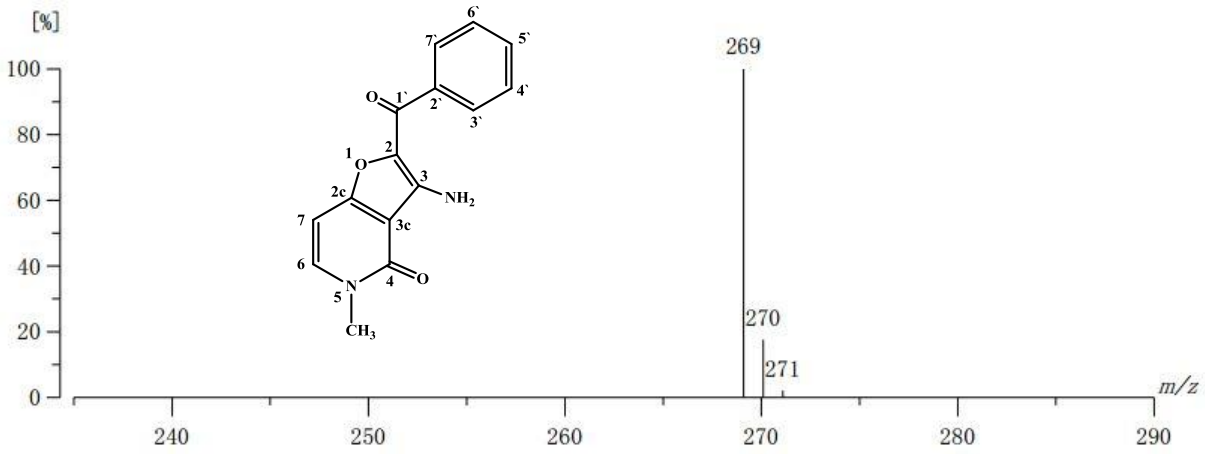

Figure S20. High resolution FAB$^+$ -MS spectra of compound **9**, showing $[M+H]^+$ ion peak at *m/z* 269.0926 (calcd. for $C_{15}H_{13}N_2O_3$, 269.0926).

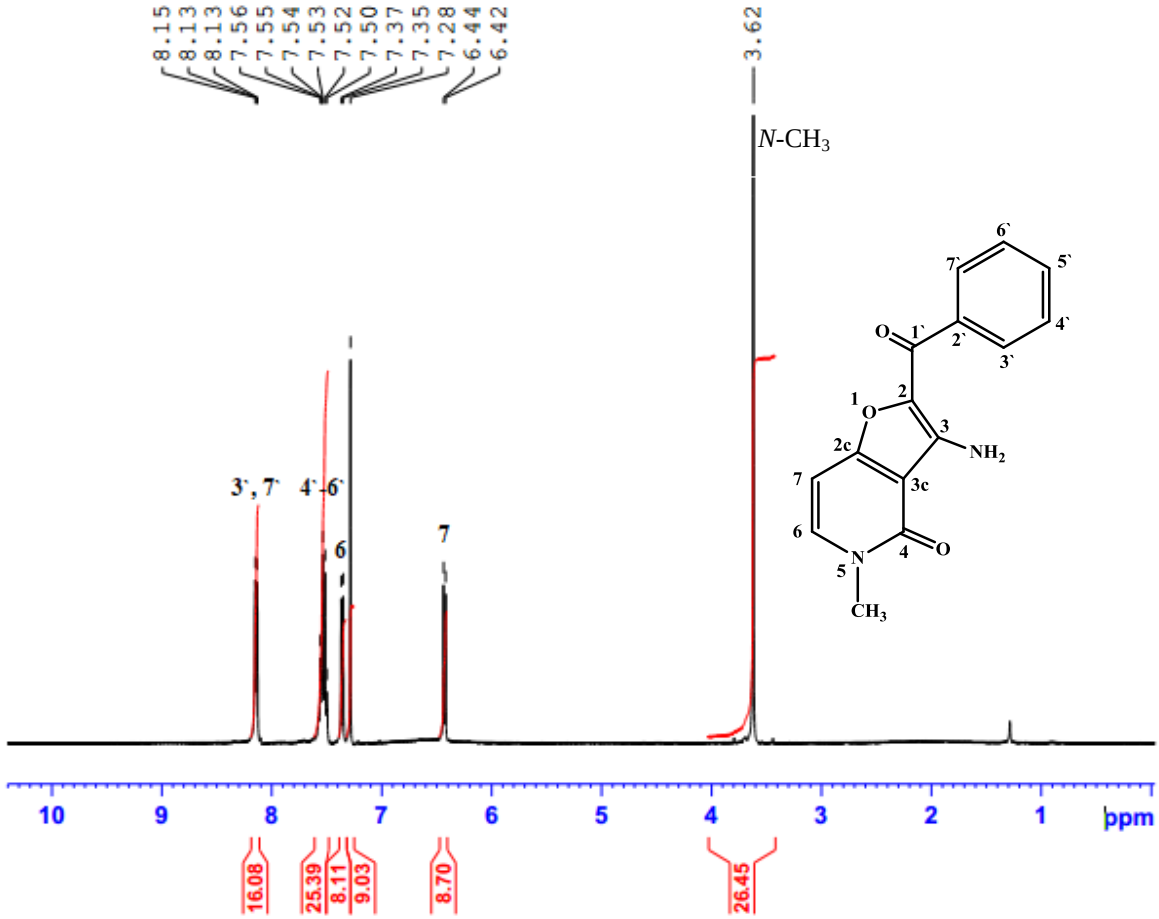

Figure S21. ^{1}H-NMR spectrum (400 MHz, $CDCl_3$) of compound **9**.

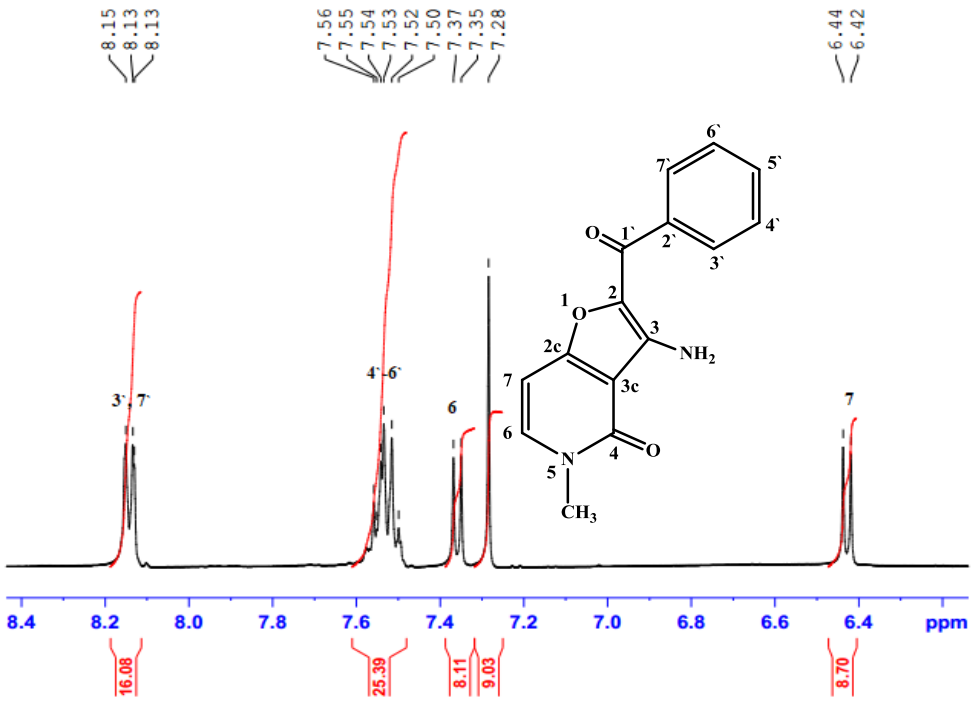

Figure S22. Expansion of ^{1}H-NMR spectrum (400 MHz, $CDCl_3$) of compound **9**.

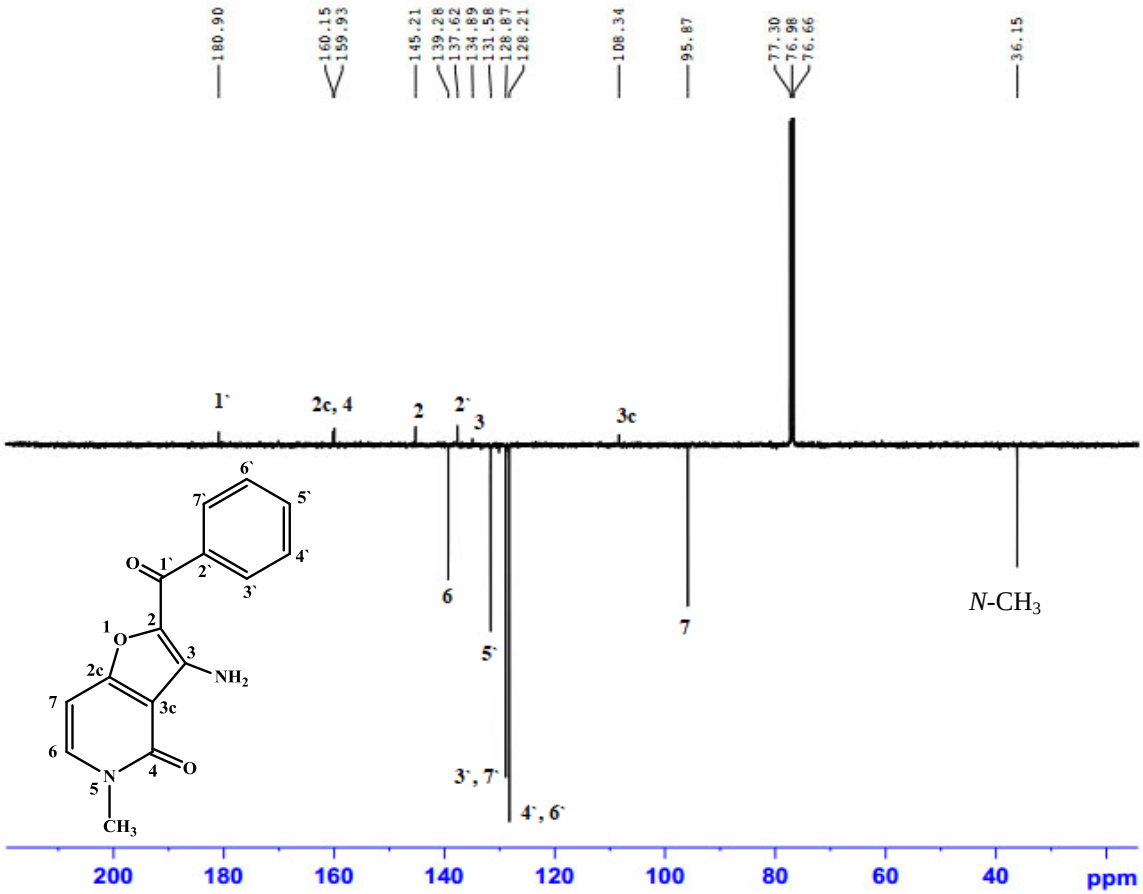

Figure S23. APT spectrum (100 MHz, $CDCl_3$) of compound **9**.

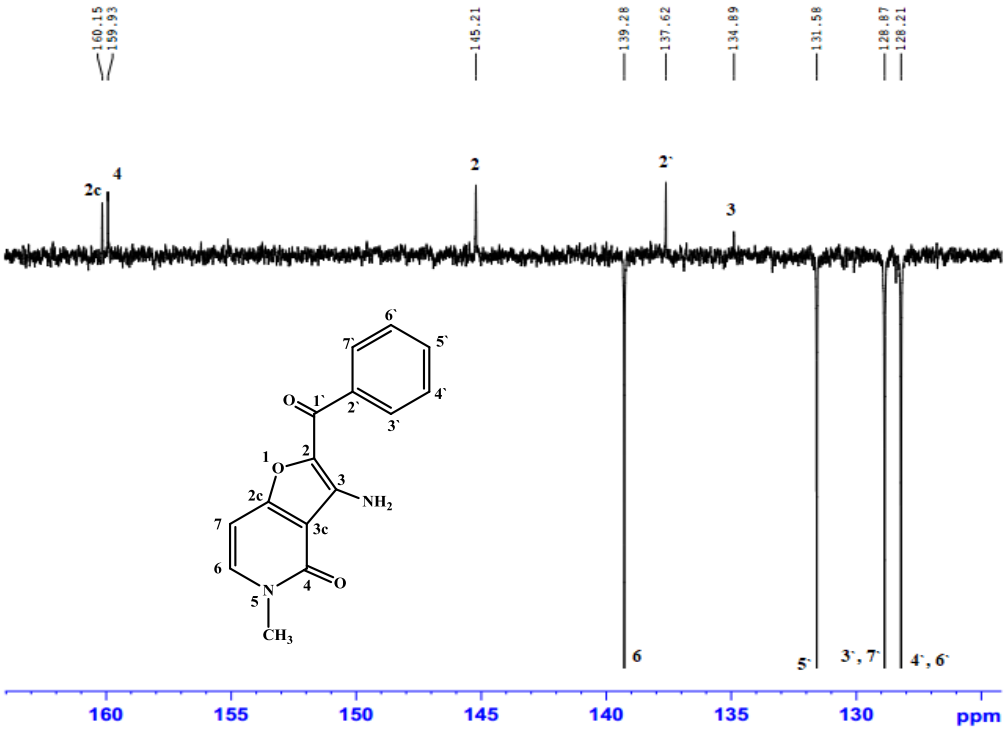

Figure S24. Expansion of APT spectrum (100 MHz, $CDCl_3$) of compound **9**.

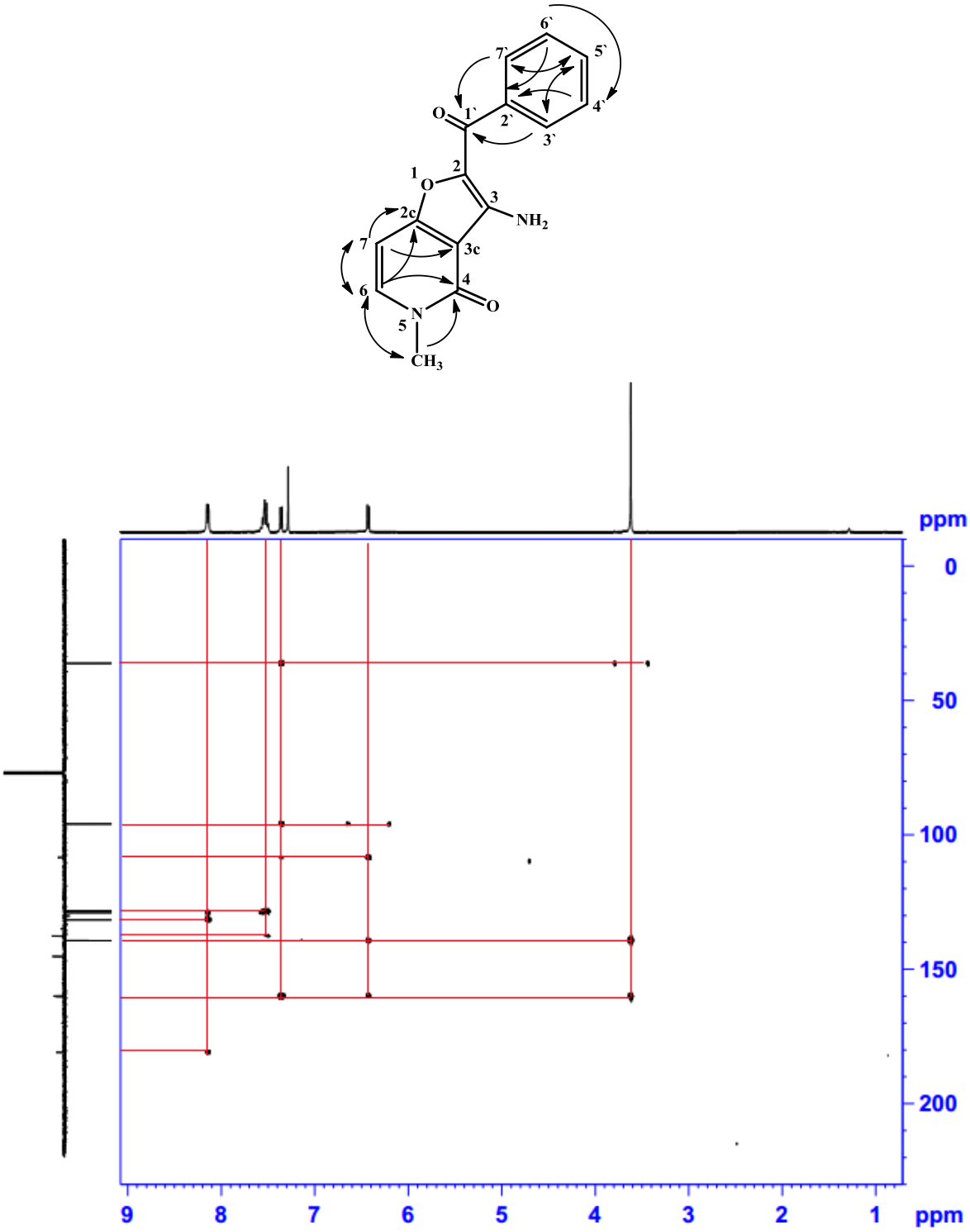

Figure S25. HMBC correlation spectrum of compound **9**.

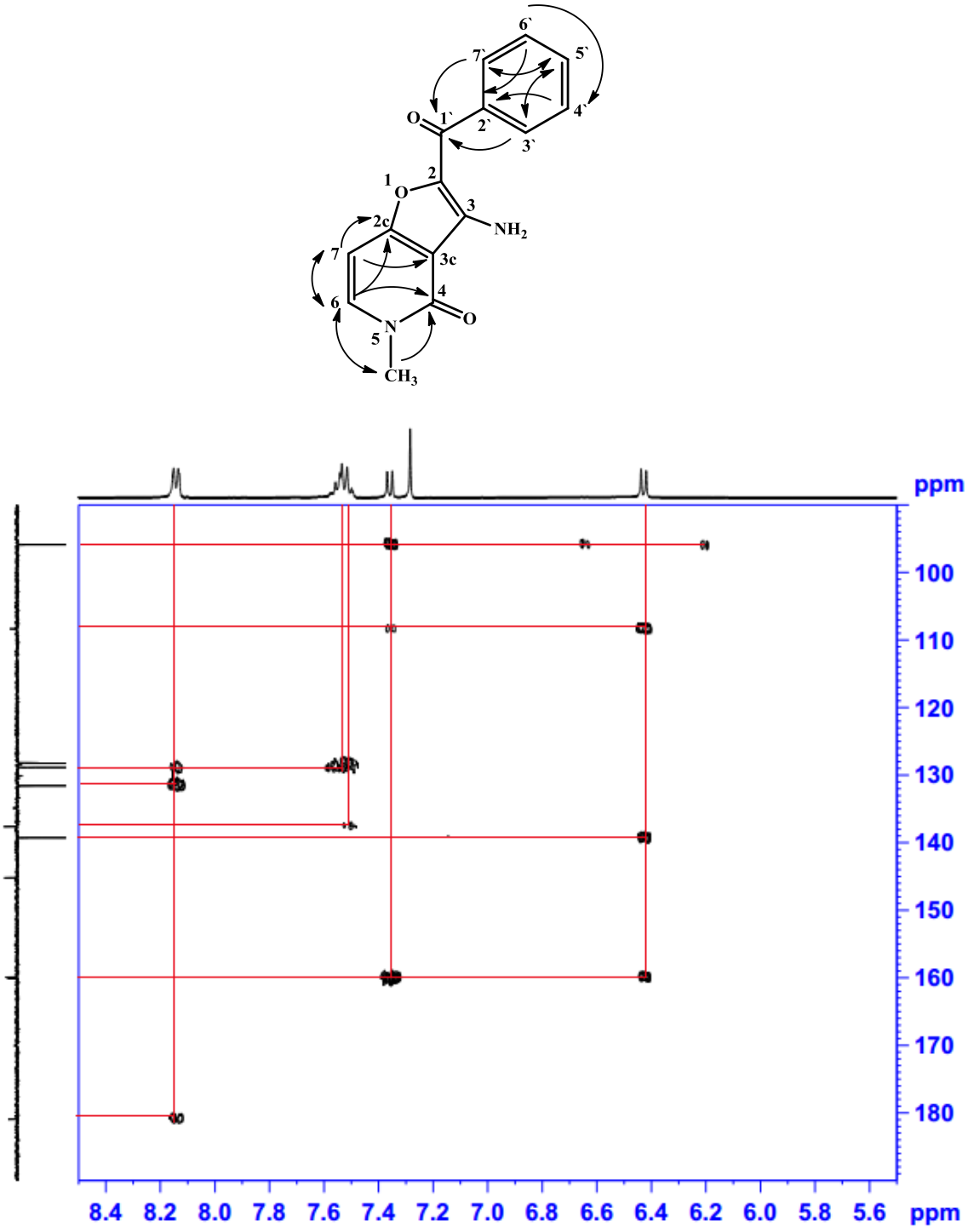

Figure S26. Selected HMBC correlation spectrum of compound **9** from δ_H 5.5-8.5 ppm, and from δ_C 90-190 ppm.

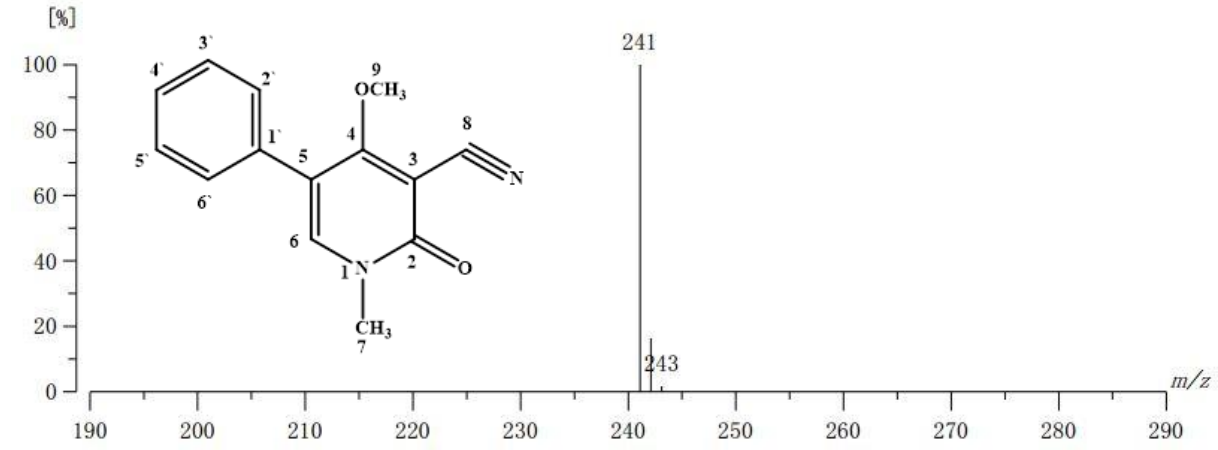

Figure S27. High resolution FAB$^+$ -MS spectra of compound **12**, showing $[M+H]^+$ ion peak at *m/z* 241.0975 (calcd. for $C_{14}H_{13}N_2O_2$, 241.0977).

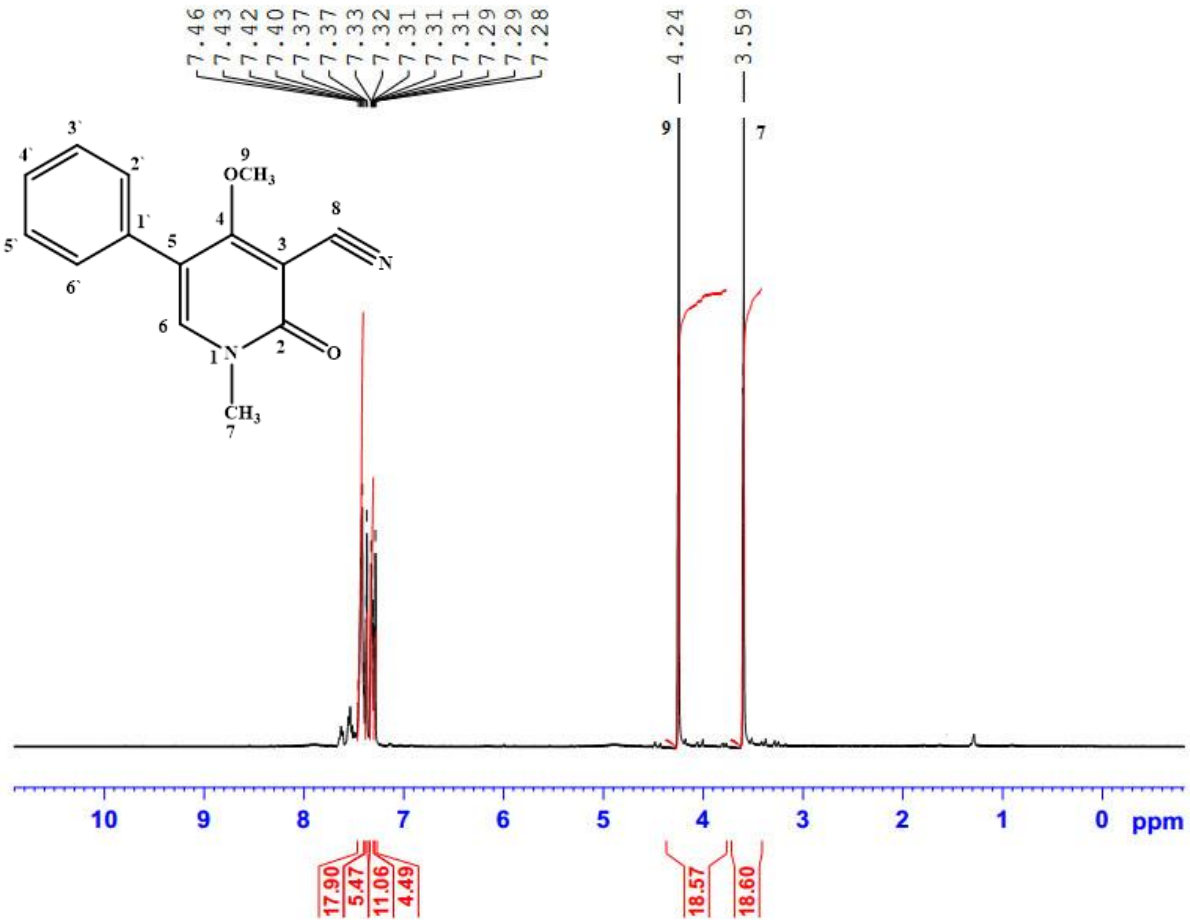

Figure S28. ^{1}H-NMR spectrum (400 MHz, $CDCl_3$) of compound **12**.

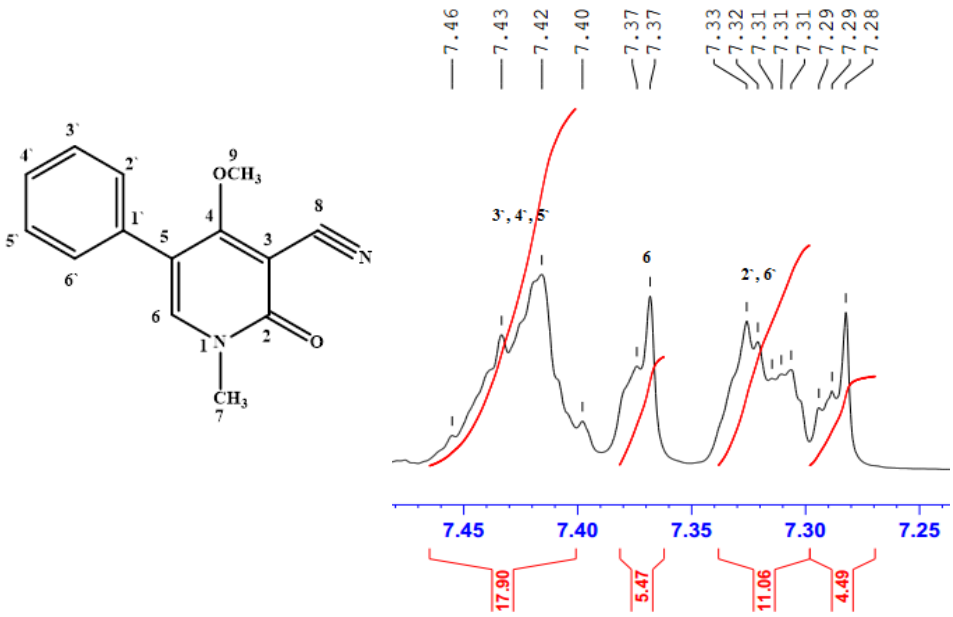

Figure S29. Expansion of ^{1}H-NMR spectrum (400 MHz, $CDCl_3$) of compound **12**.

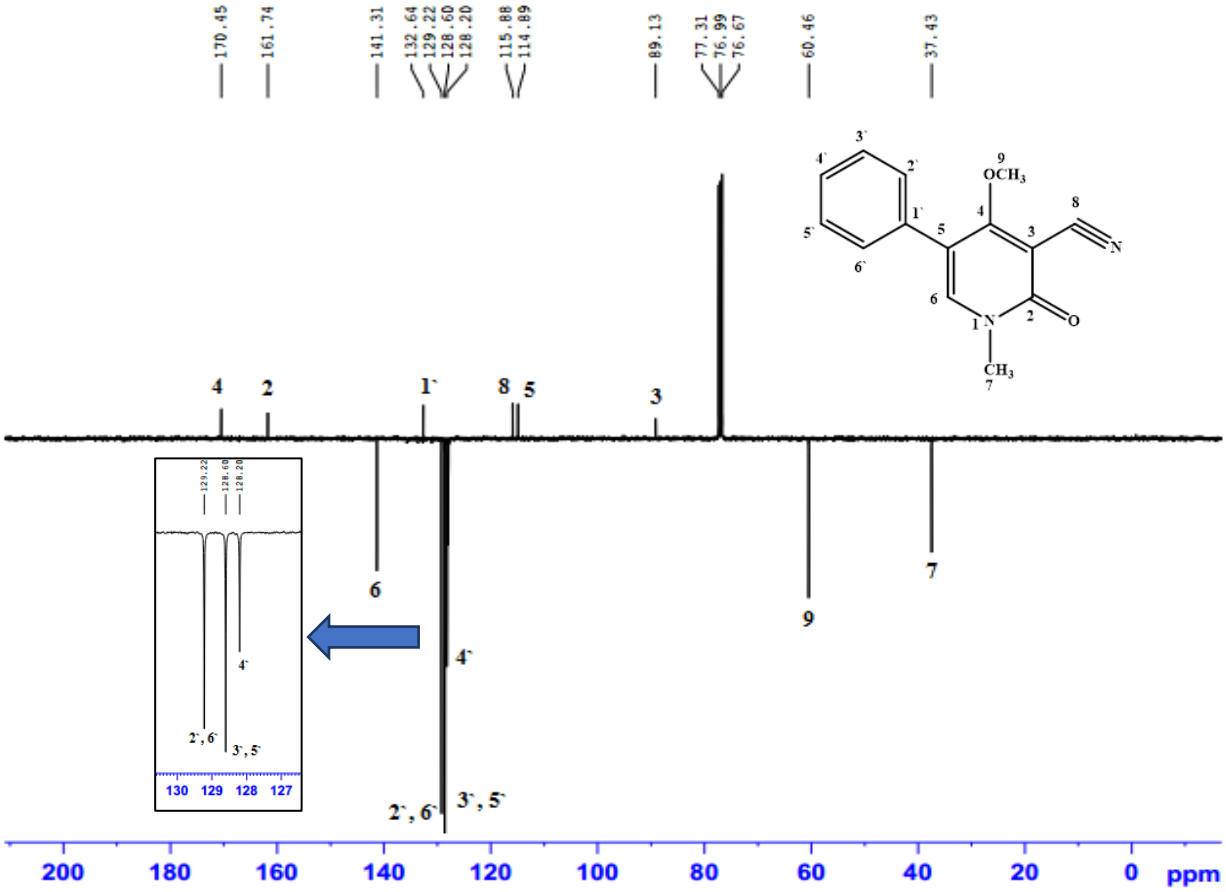

Figure S30. APT spectrum (100 MHz, $CDCl_3$) of compound **12**.

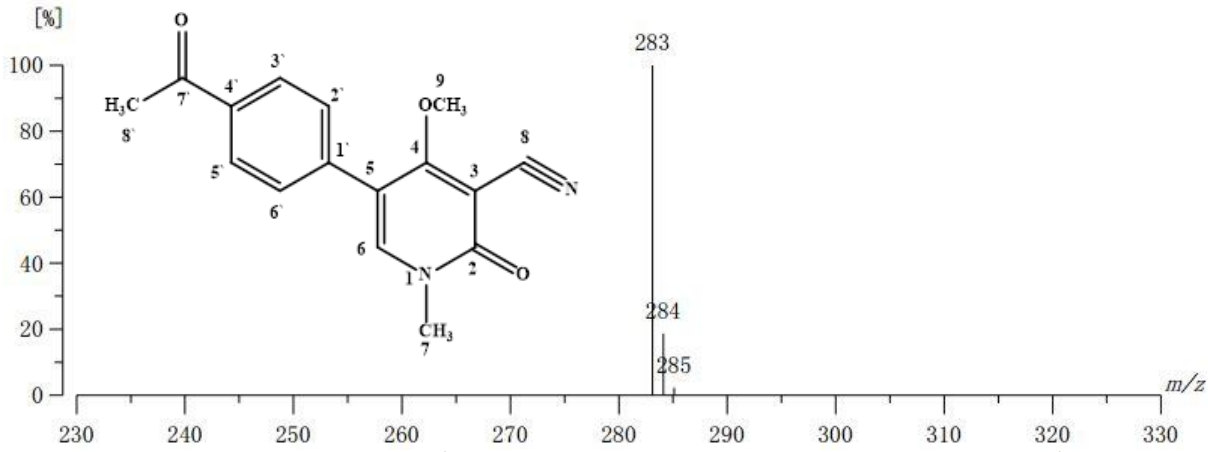

Figure S31. High resolution FAB$^+$ -MS spectra of compound **13**, showing $[M+H]^+$ ion peak at *m/z* 283.1084 (calcd. for $C_{16}H_{15}N_2O_3$, 283.1083).

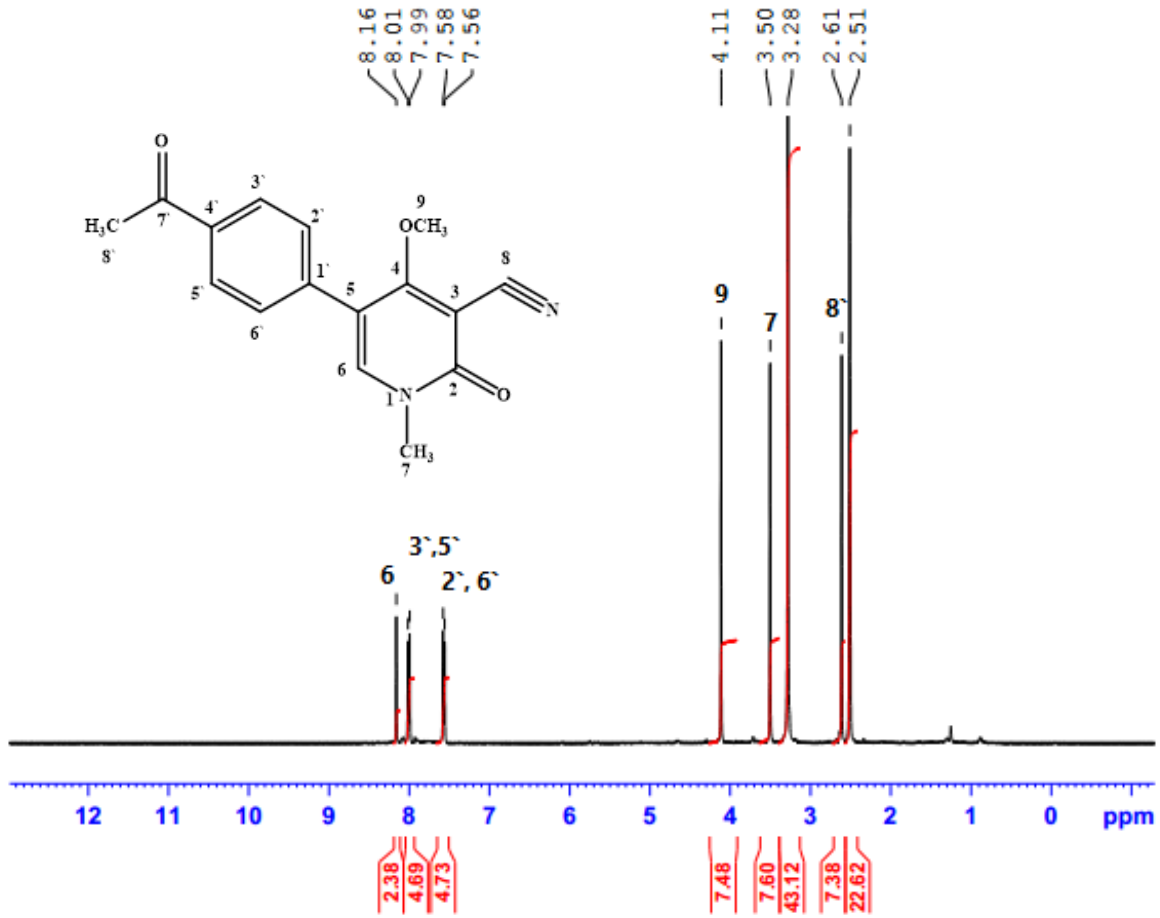

Figure S32. ^{1}H-NMR spectrum (400 MHz, $(CD_3)_2SO$) of compound **13**.

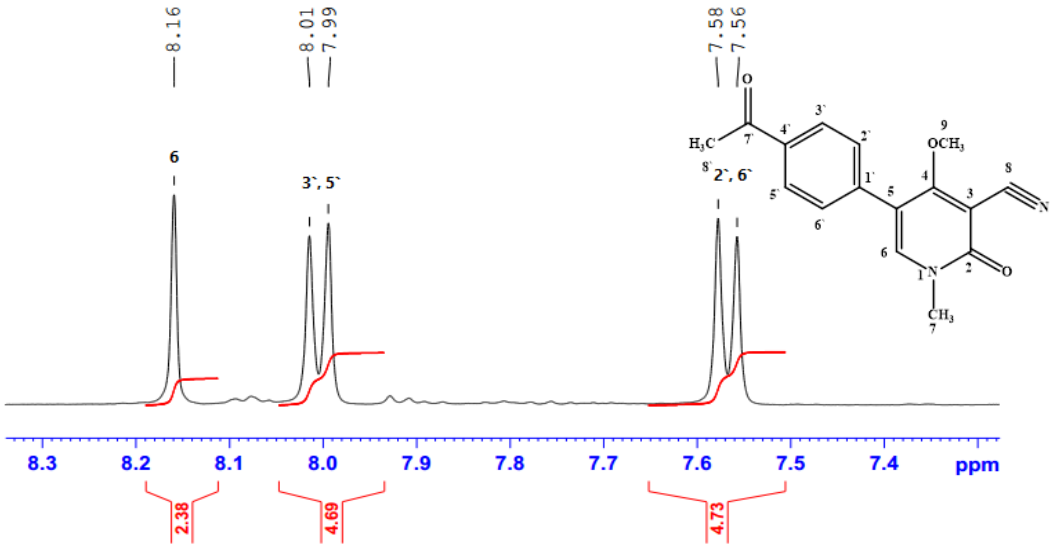

Figure S33. Expansion of ^{1}H-NMR spectrum (400 MHz, $(CD_3)_2SO$) of compound **13**.

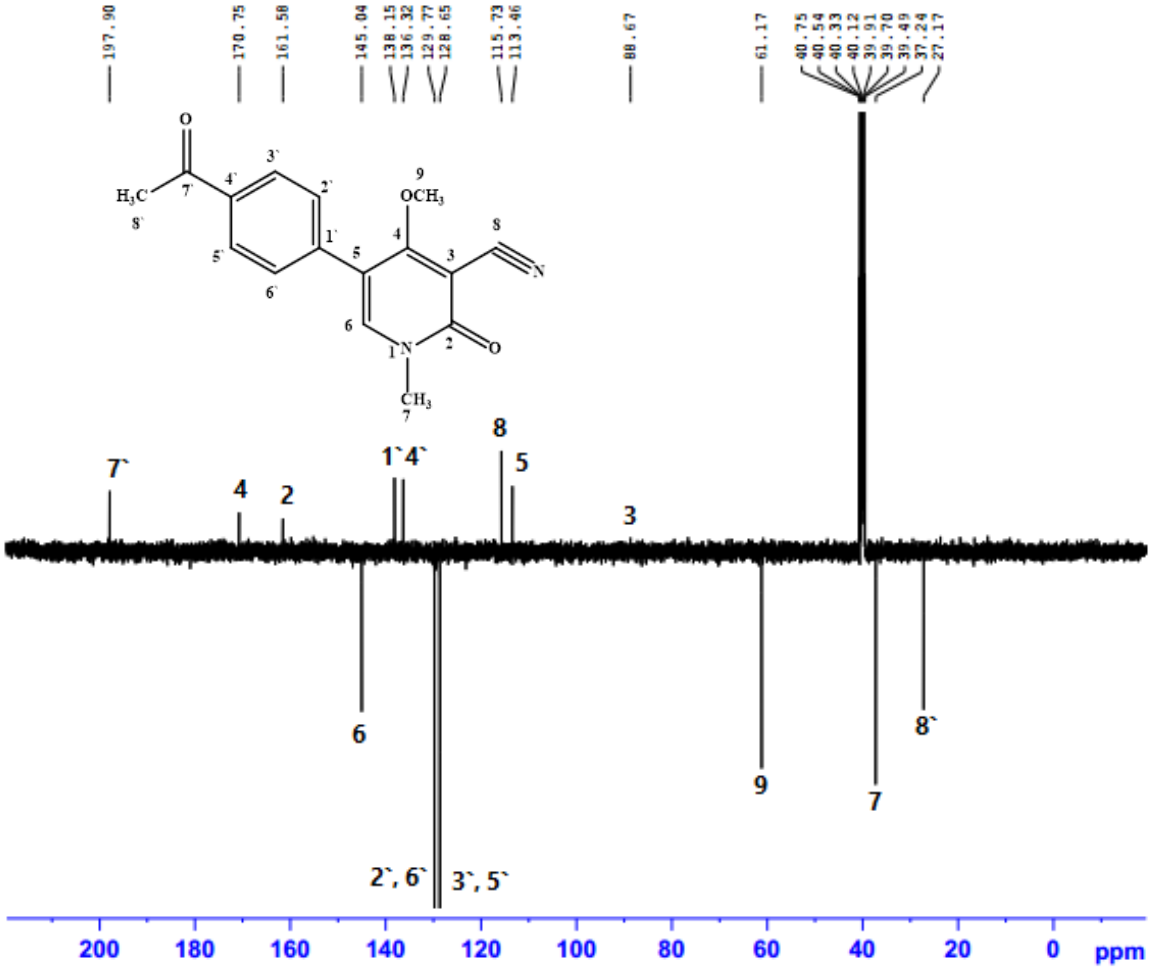

Figure S34. APT spectrum (100 MHz, $(CD_3)_2SO$) of compound **13**.

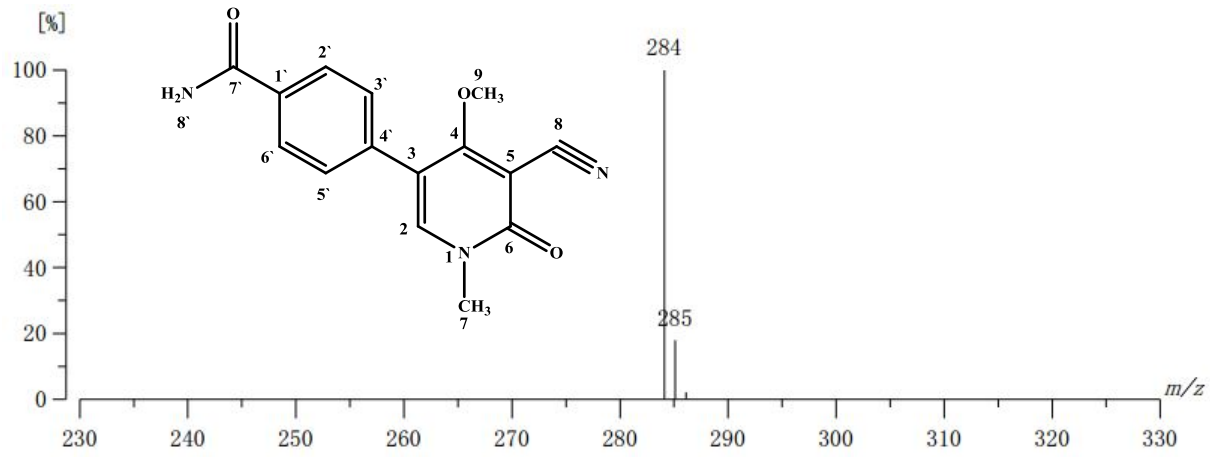

Figure S35. High resolution FAB^+ -MS spectra of compound **14**, showing $[M+H]^+$ ion peak at *m/z* 284.1034 (calcd. for $C_{15}H_{14}N_3O_3$, 284.1035).

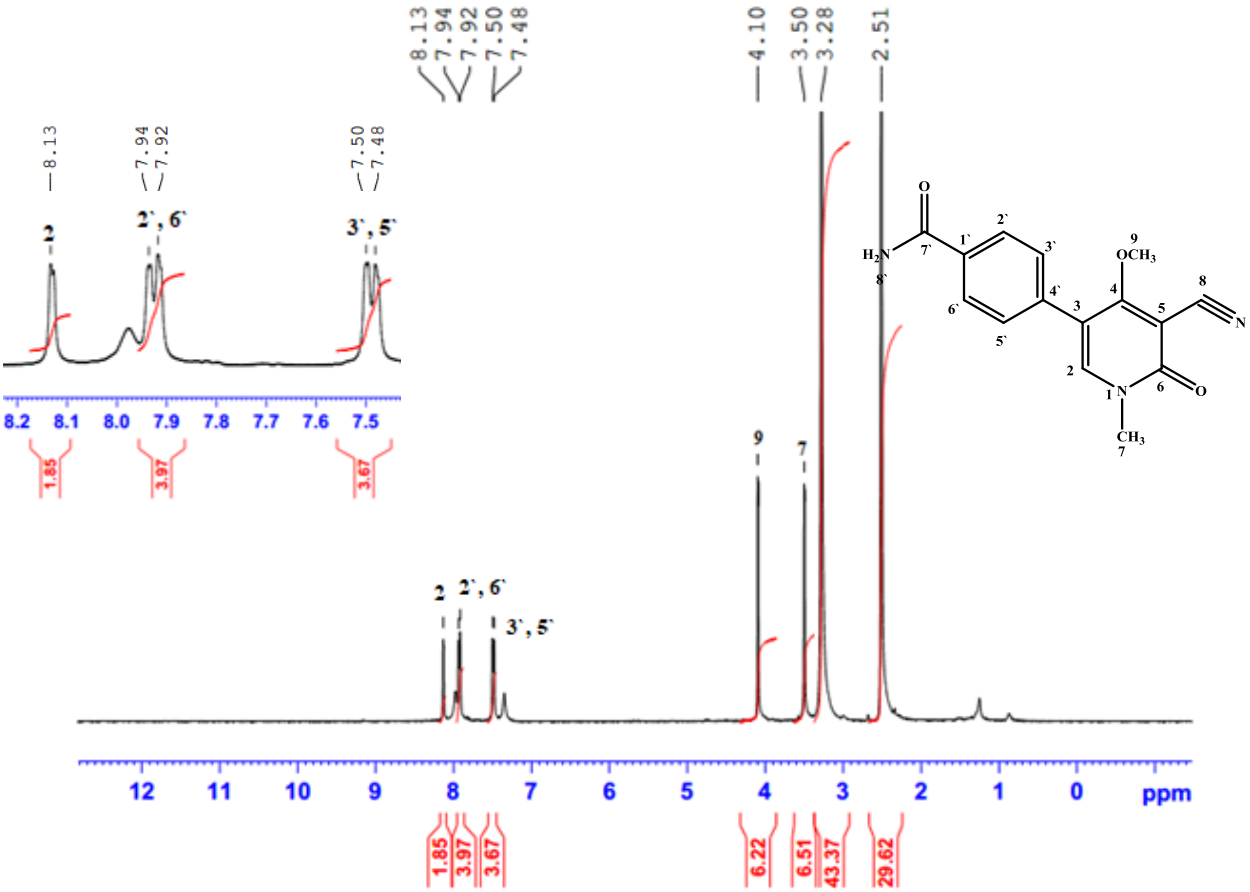

Figure S36. ^{1}H-NMR spectrum (400 MHz, $(CD_3)_2SO$) of compound **14**.

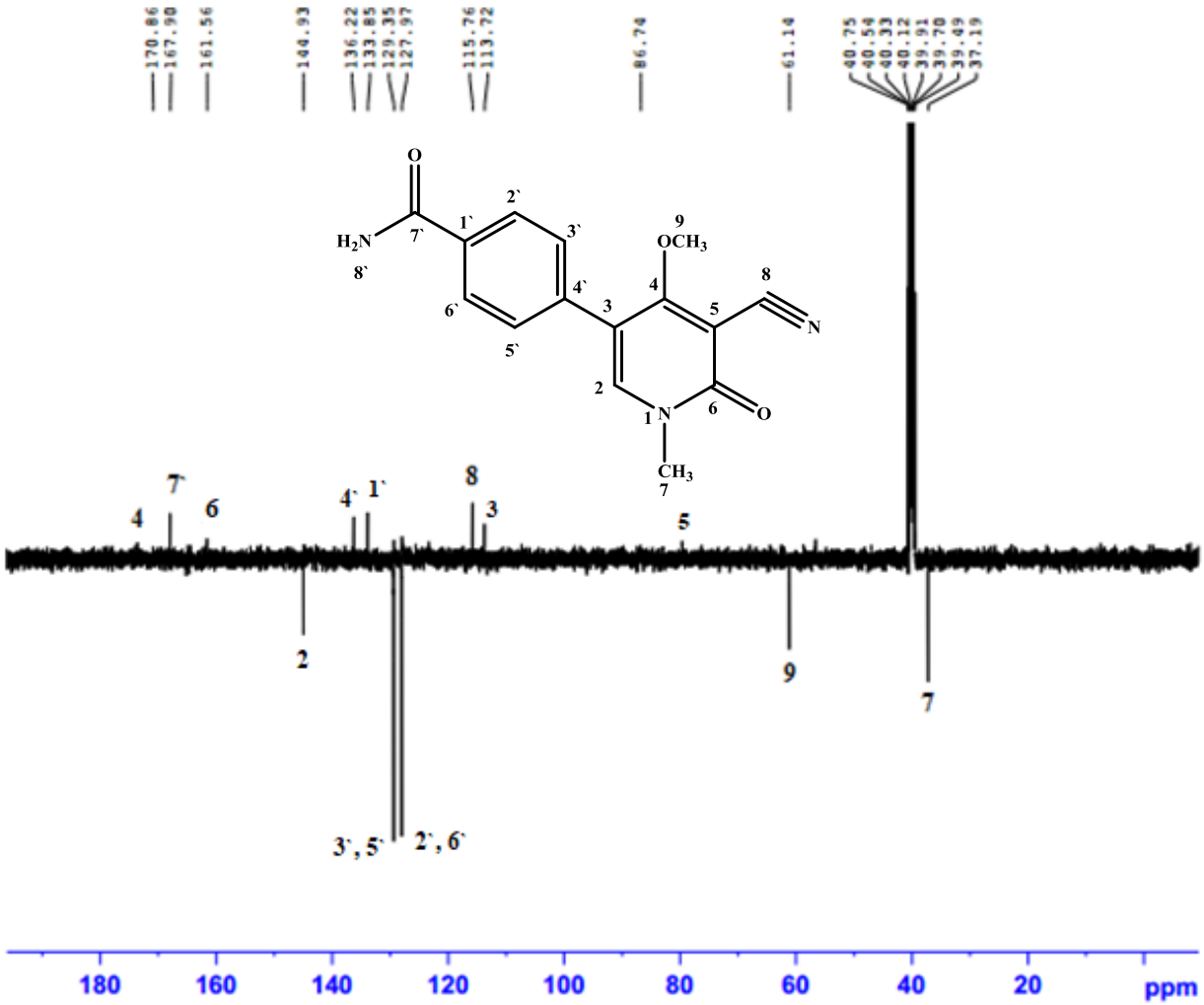

Figure S37. APT spectrum (100 MHz, $(CD_3)_2SO$) of compound **14**.

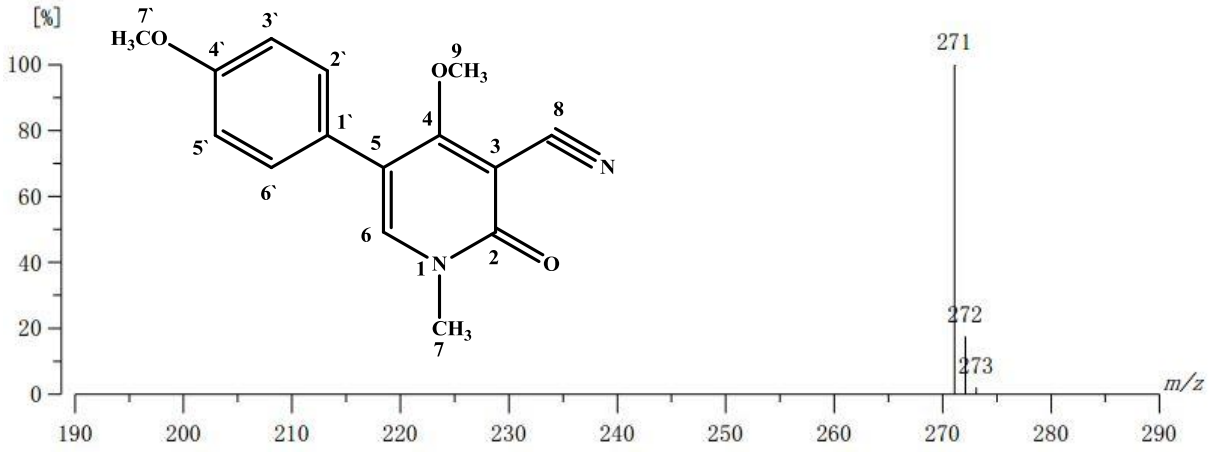

Figure S38. High resolution FAB^+ -MS spectra of compound **15**, showing $[M+H]^+$ ion peak at *m/z* 271.1082 (calcd. for $C_{15}H_{15}N_2O_3$, 271.1083).

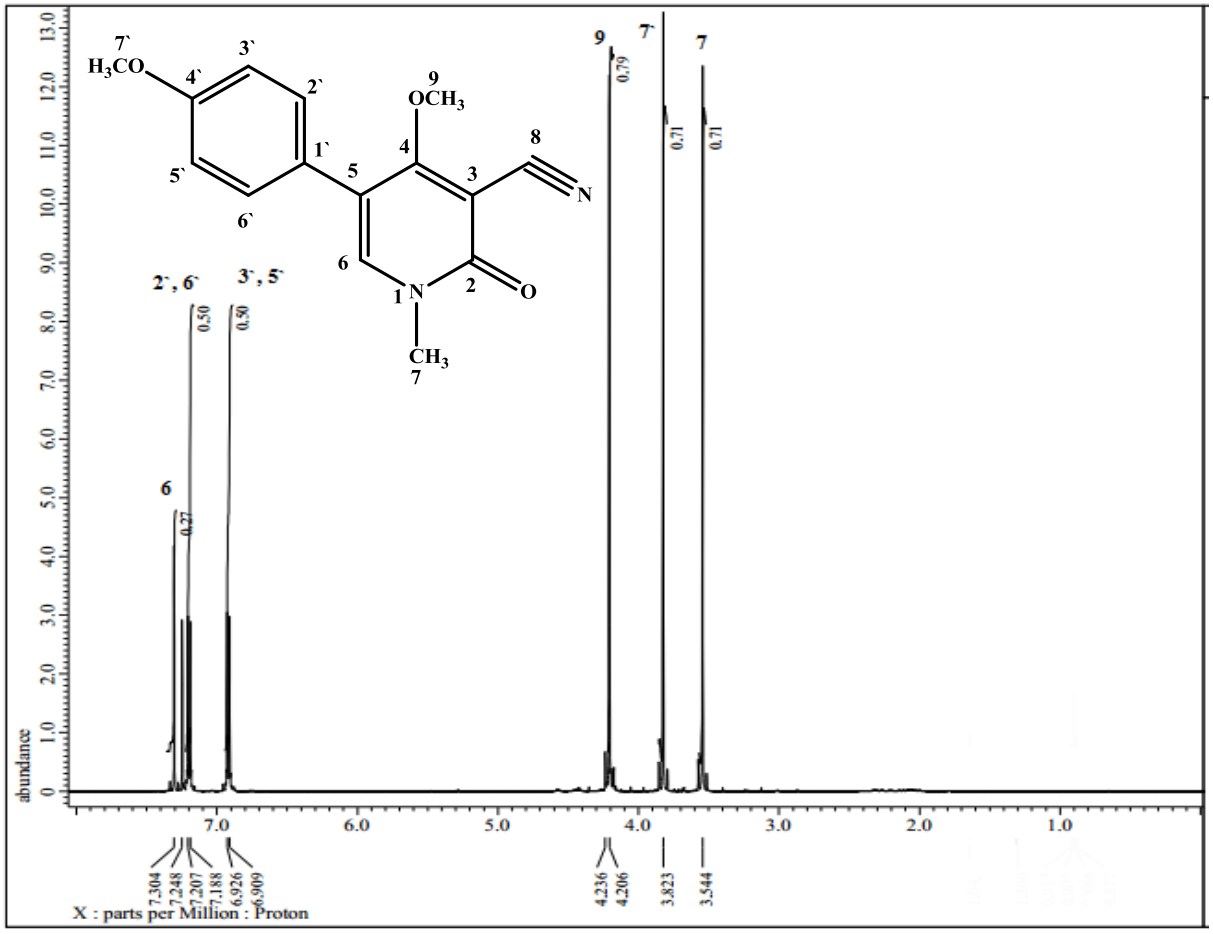

Figure S39. ^{1}H-NMR spectrum (500 MHz, $CDCl_3$) of compound **15**.

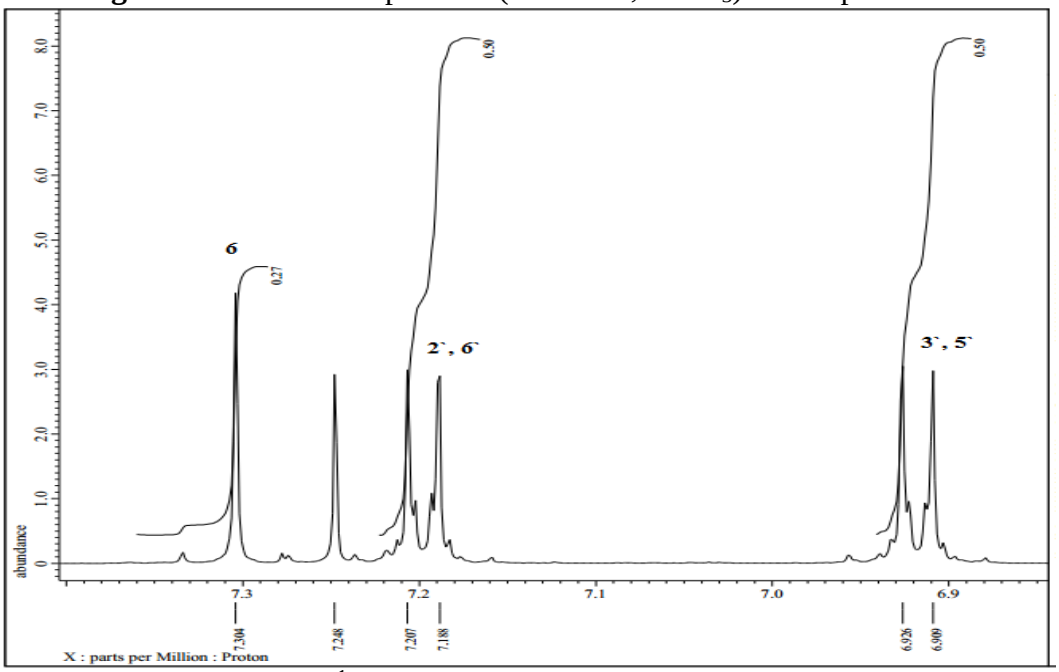

Figure S40. Expansion of ^{1}H-NMR spectrum (500 MHz, $CDCl_3$) of compound **15**.

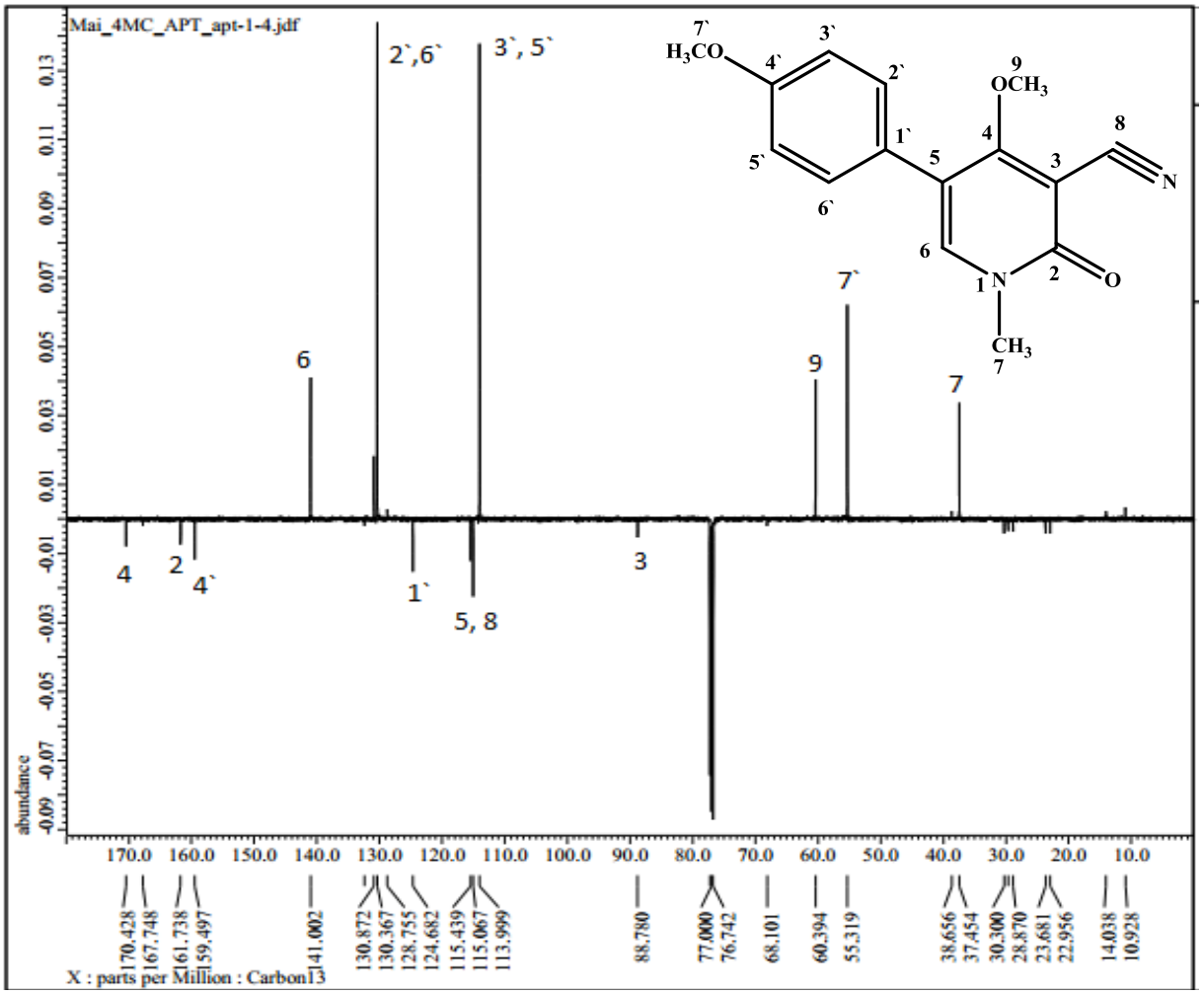

Figure S41. APT spectrum (125 MHz, $CDCl_3$) of compound **15**.

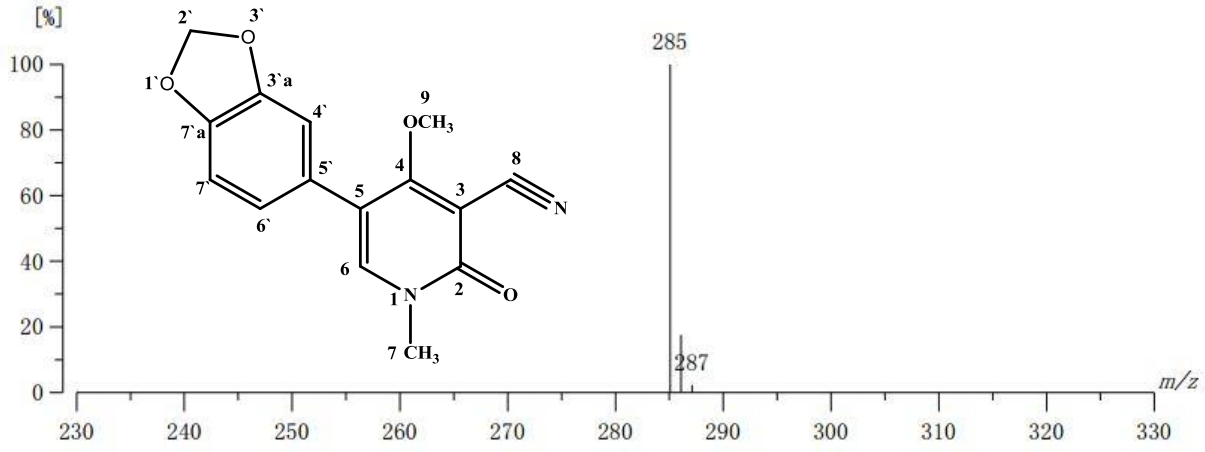

Figure S42. High resolution FAB^+ -MS spectra of compound **16**, showing $[M+H]^+$ ion peak at *m/z* 285.0875 (calcd. for $C_{15}H_{13}N_2O_4$, 285.0875).

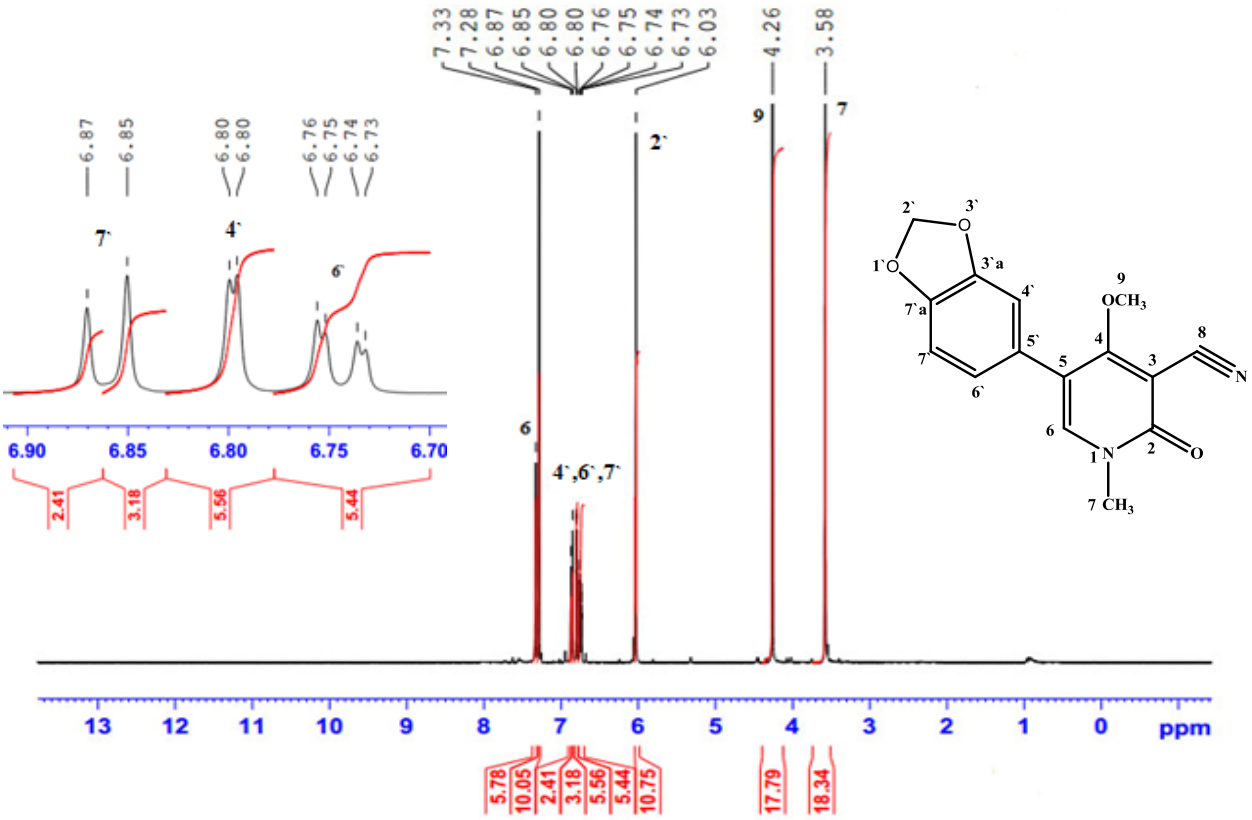

Figure S43. ^{1}H-NMR spectrum (400 MHz, $CDCl_3$) of compound **16**.

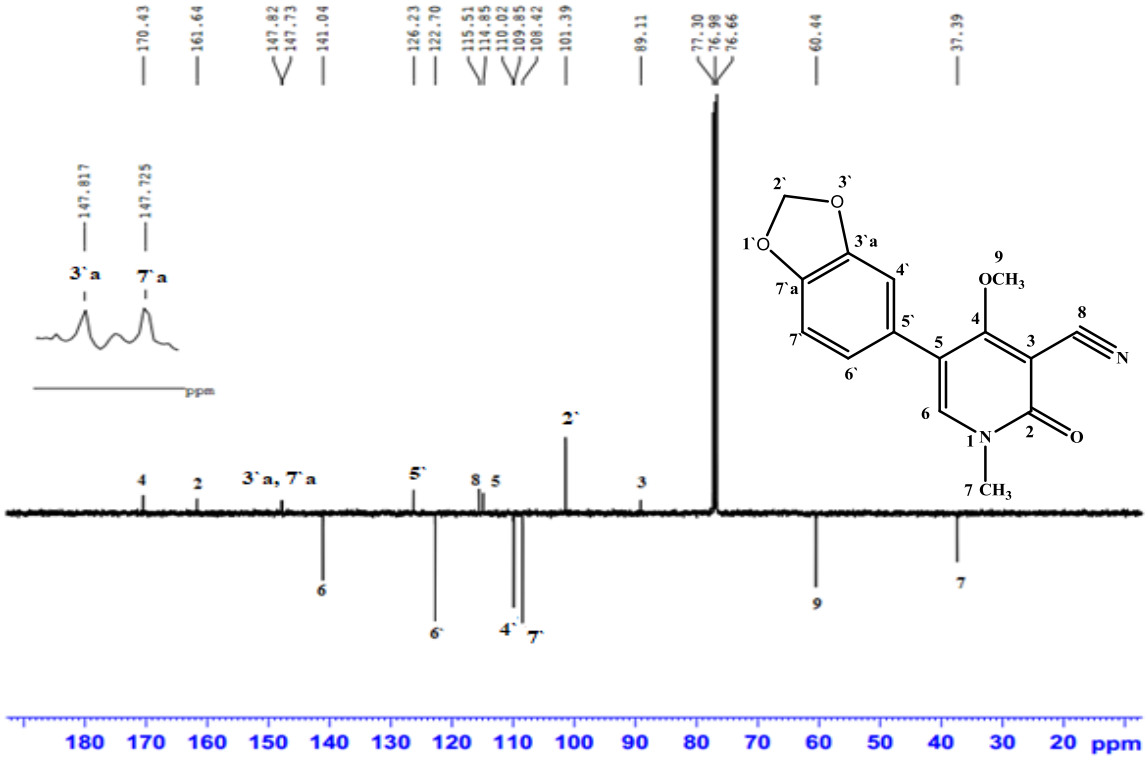

Figure S44. APT spectrum (100 MHz, $CDCl_3$) of compound **16**.

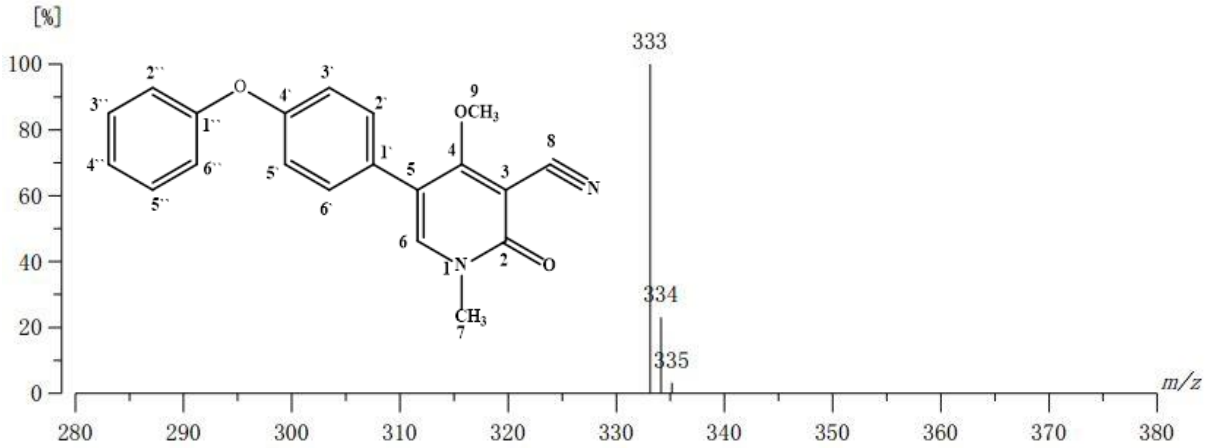

Figure S45. High resolution FAB$^+$ -MS spectra of compound **17**, showing $[M+H]^+$ ion peak at *m/z* 333.1240 (calcd. for $C_{20}H_{17}N_2O_3$, 333.1239).

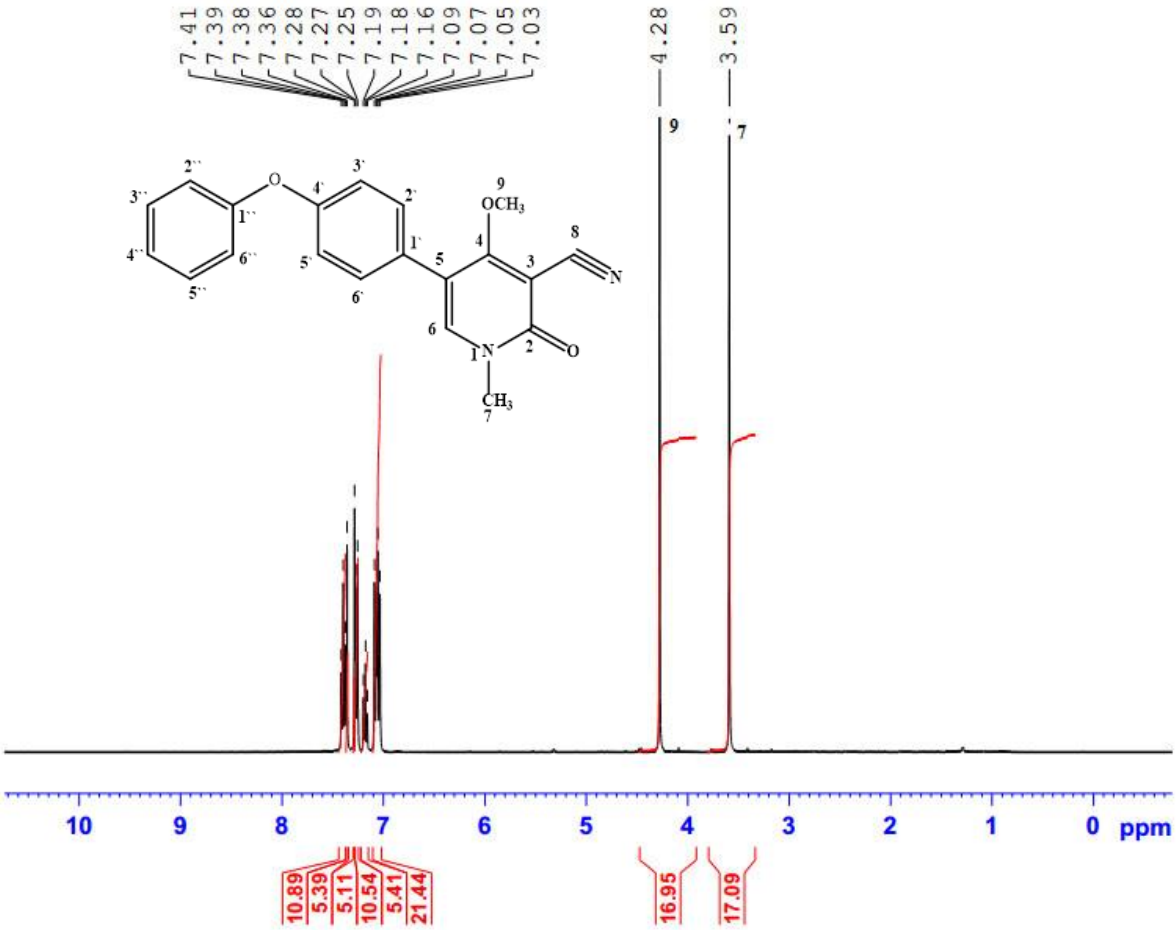

Figure S46. ^{1}H-NMR spectrum (400 MHz, $CDCl_3$) of compound **17**.

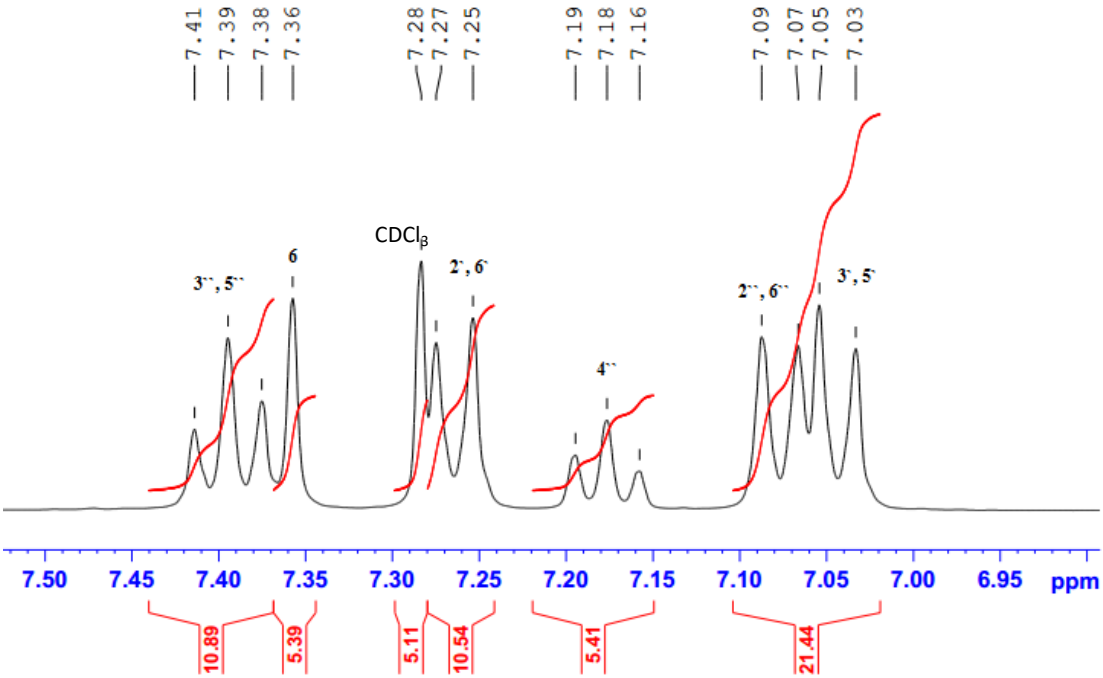

Figure S47. Expansion of ^{1}H-NMR spectrum (400 MHz, $CDCl_3$) of compound **17**.

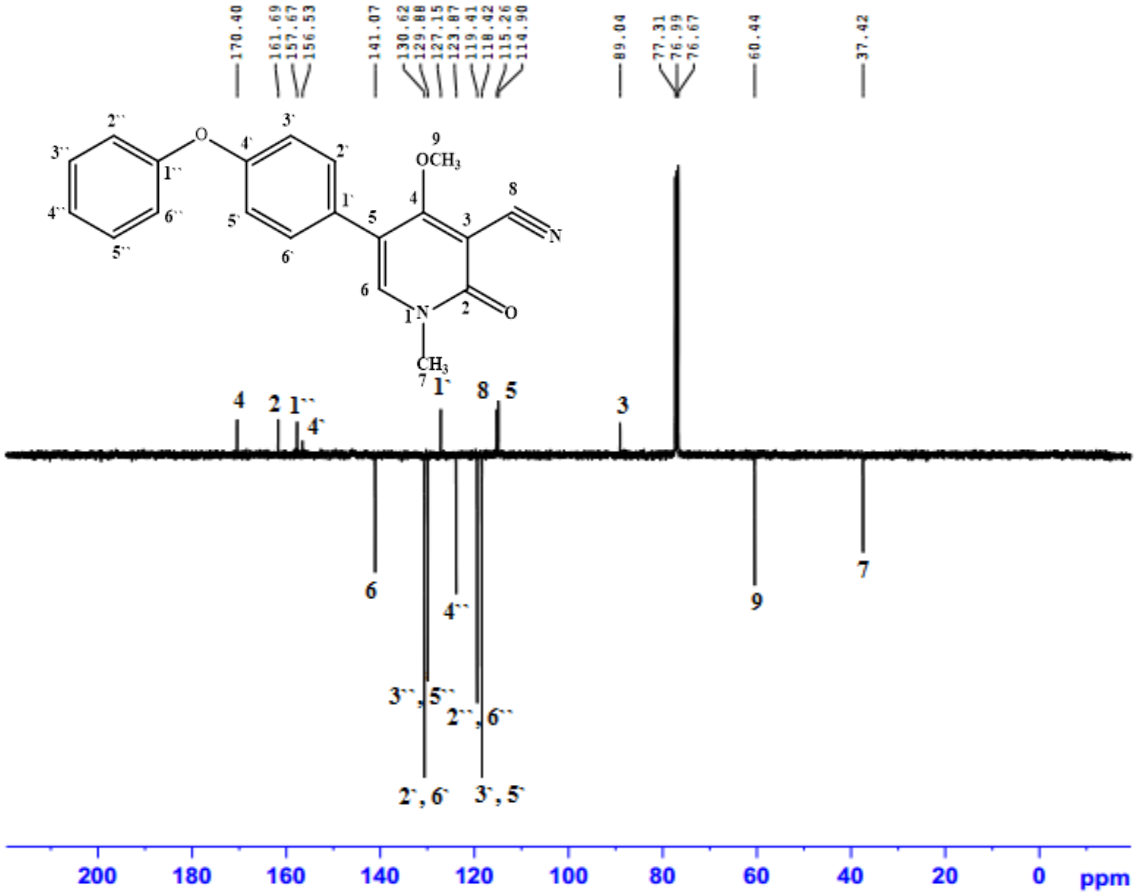

Figure S48. APT spectrum (100 MHz, $CDCl_3$) of compound **17**.

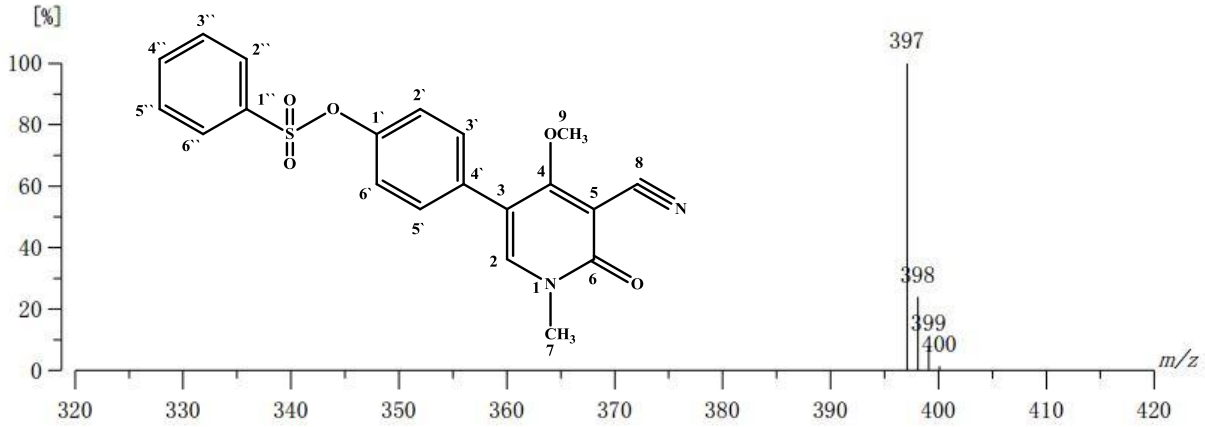

Figure S49. High resolution FAB$^+$ -MS spectra of compound **18**, showing $[M+H]^+$ ion peak at *m/z* 397.0858 (calcd. for $C_{20}H_{17}N_2O_5S$, 397.0858).

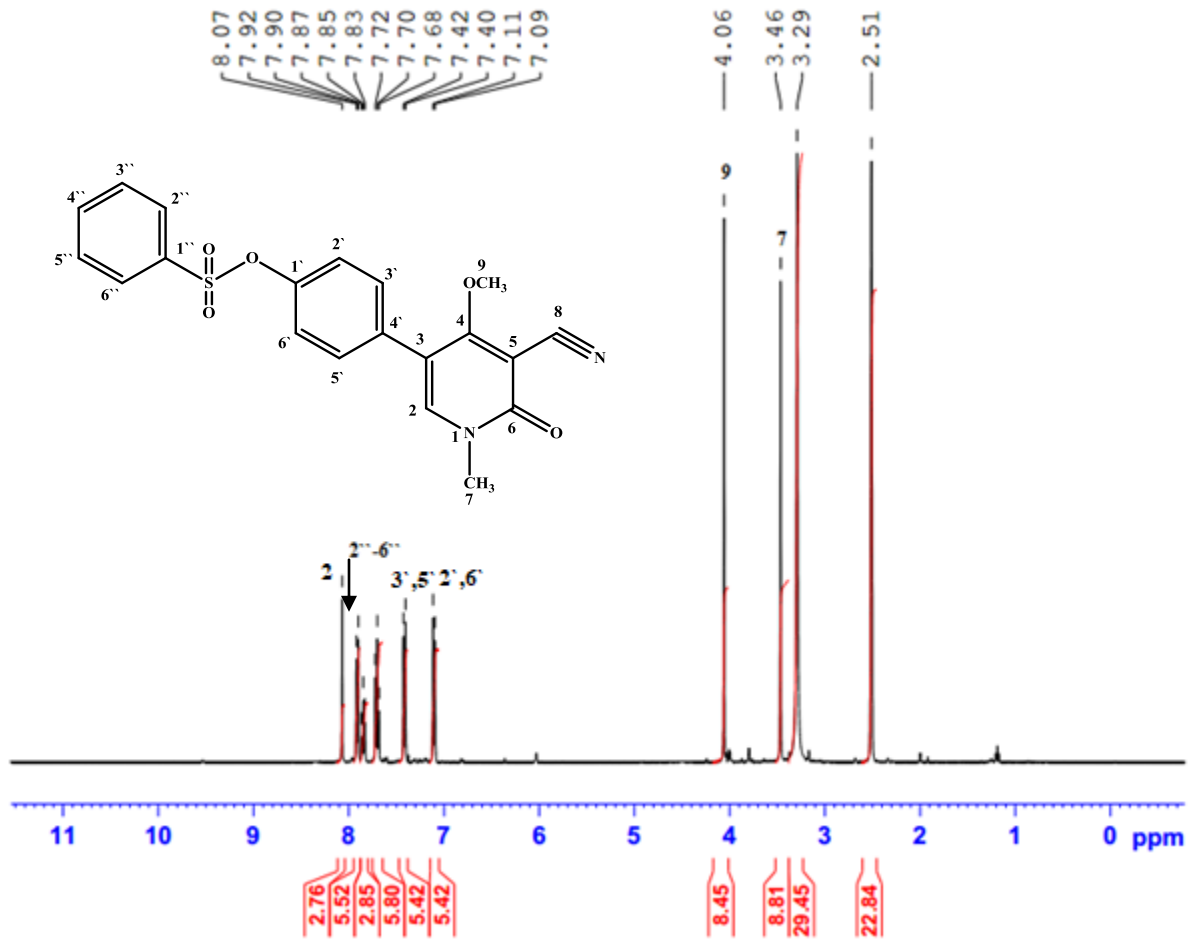

Figure S50. ^{1}H-NMR spectrum (400 MHz, $(CD_3)_2SO$) of compound **18**.

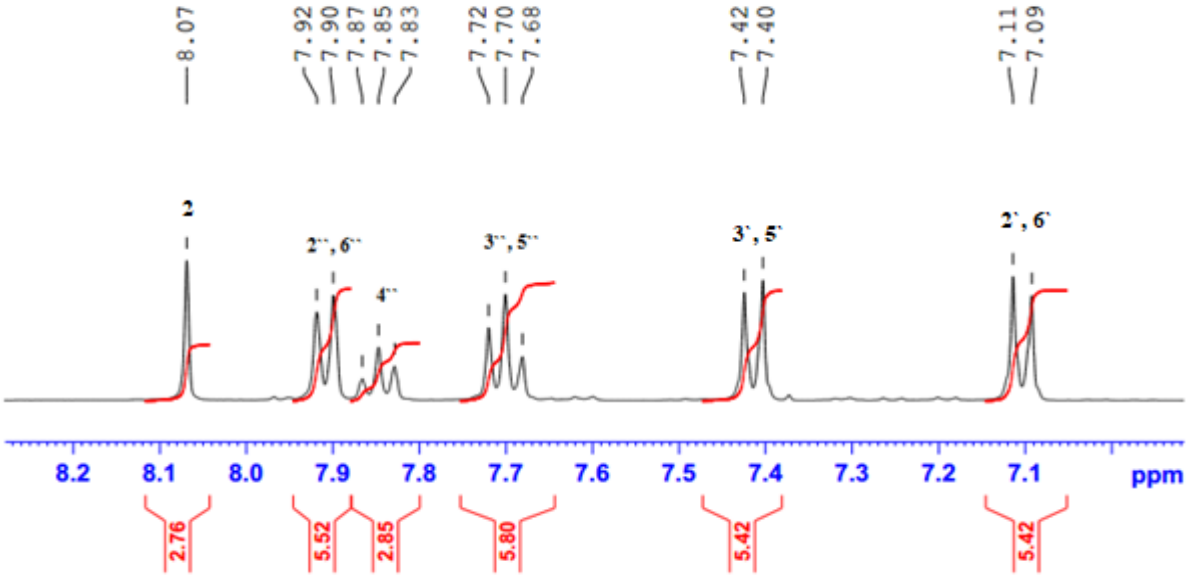

Figure S51. Expansion of ^{1}H-NMR spectrum (400 MHz, $(CD_3)_2SO$) of compound **18**.

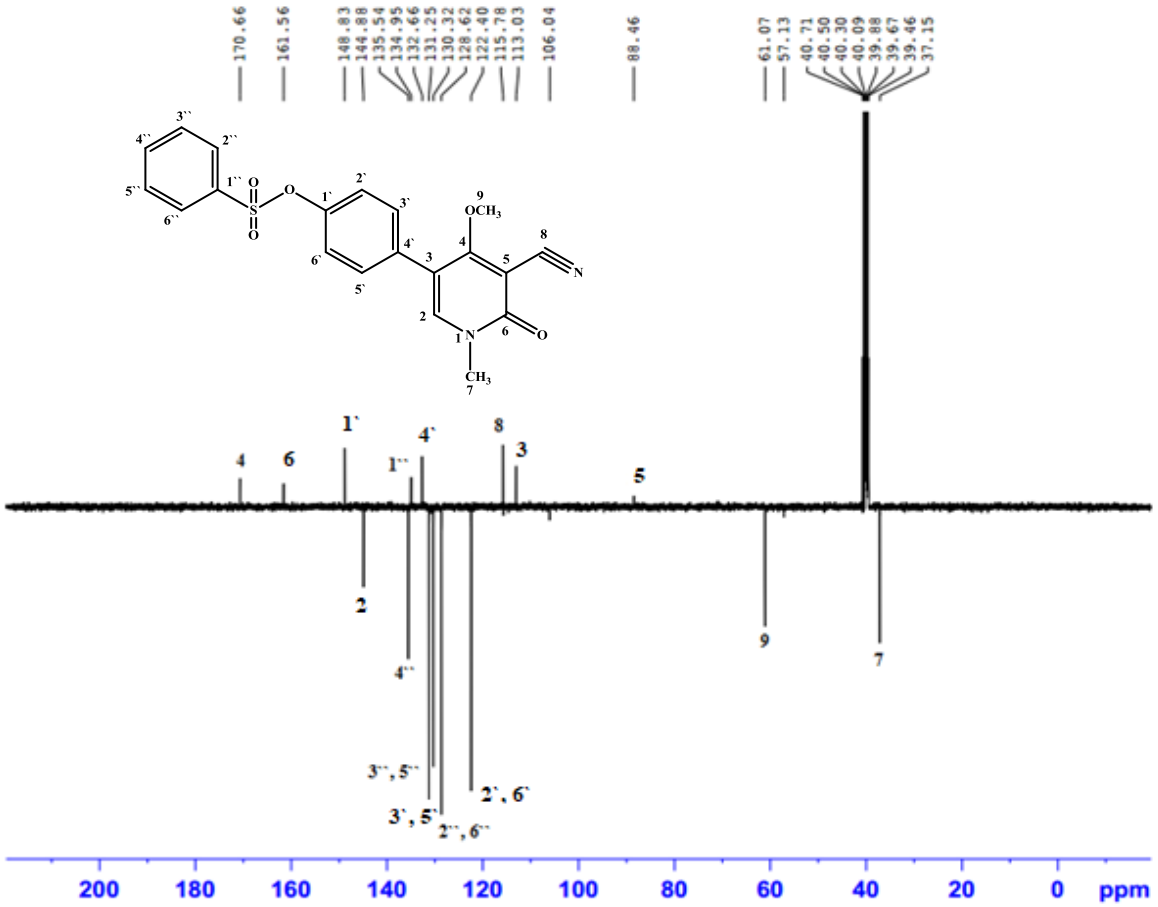

Figure S52. APT spectrum (100 MHz, $(CD_3)_2SO$) of compound **18**.

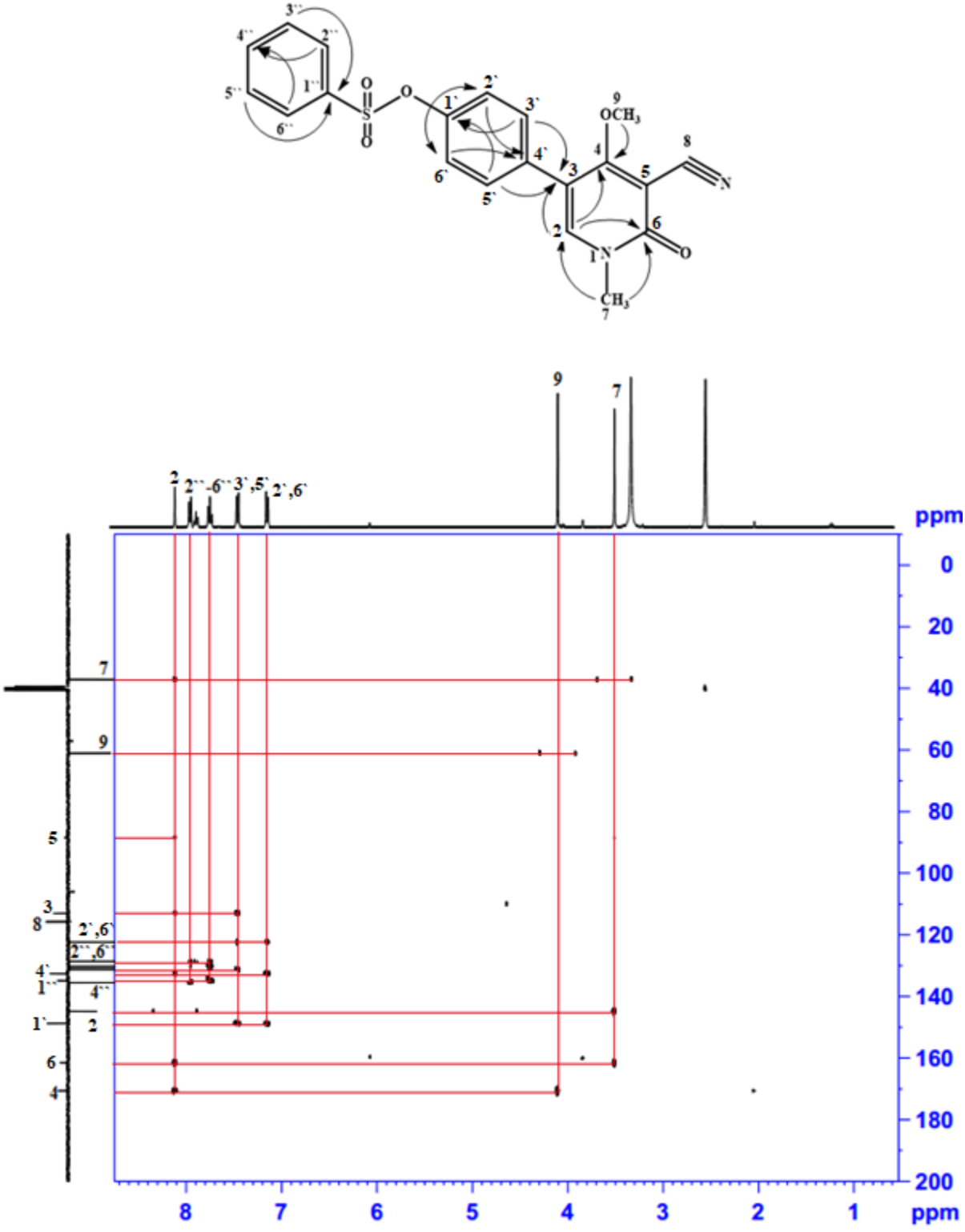

Figure S53. HMBC correlation spectrum of compound **18**.

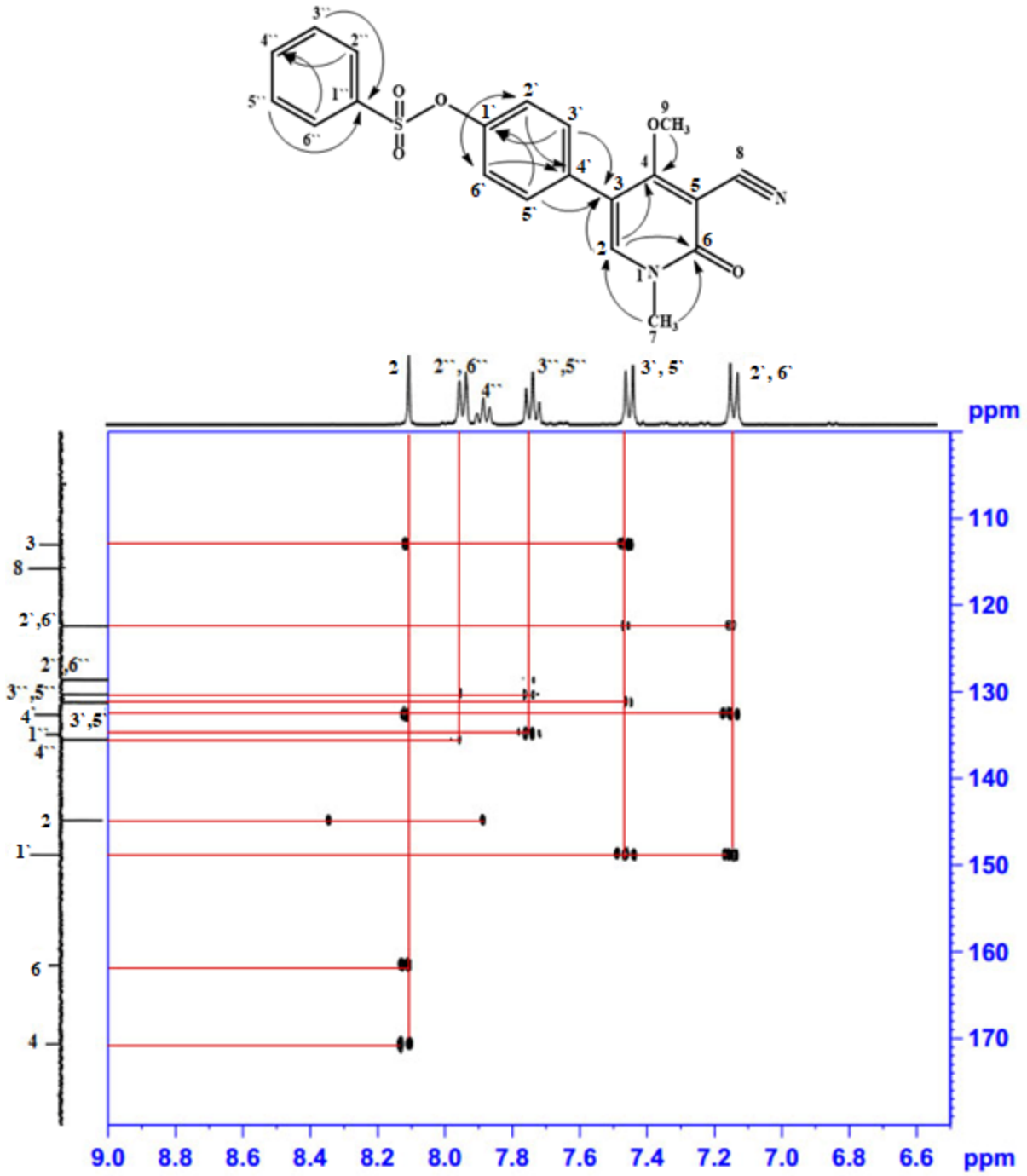

Figure S54. Selected HMBC correlation spectrum of compound **18** from δ_H 6.5-9 ppm, and from δ_C 100-180 ppm.

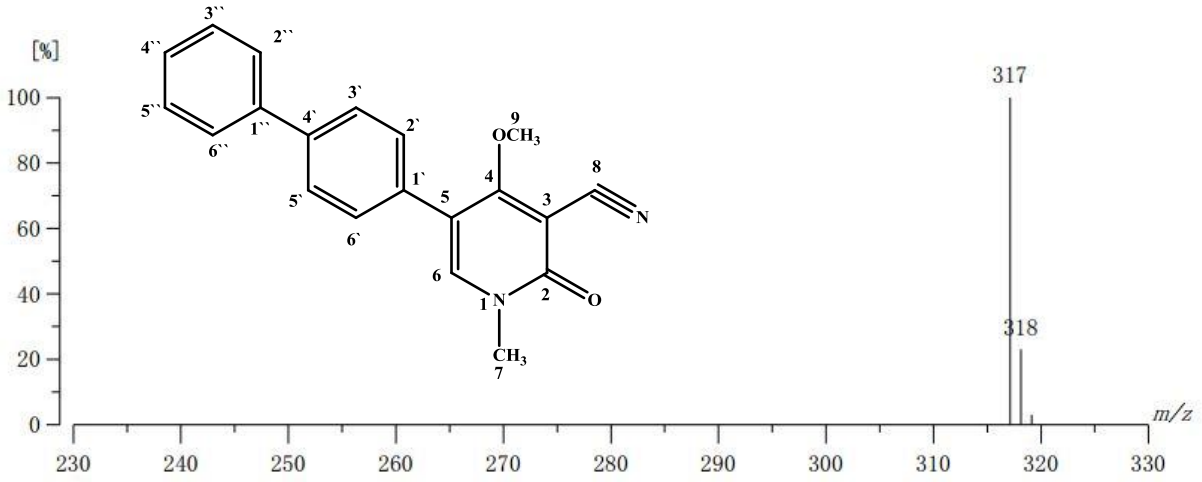

Figure S55. High resolution FAB$^+$ -MS spectra of compound **19**, showing $[M+H]^+$ ion peak at *m/z* 317.1290 (calcd. for $C_{20}H_{17}N_2O_2$, 317.1290).

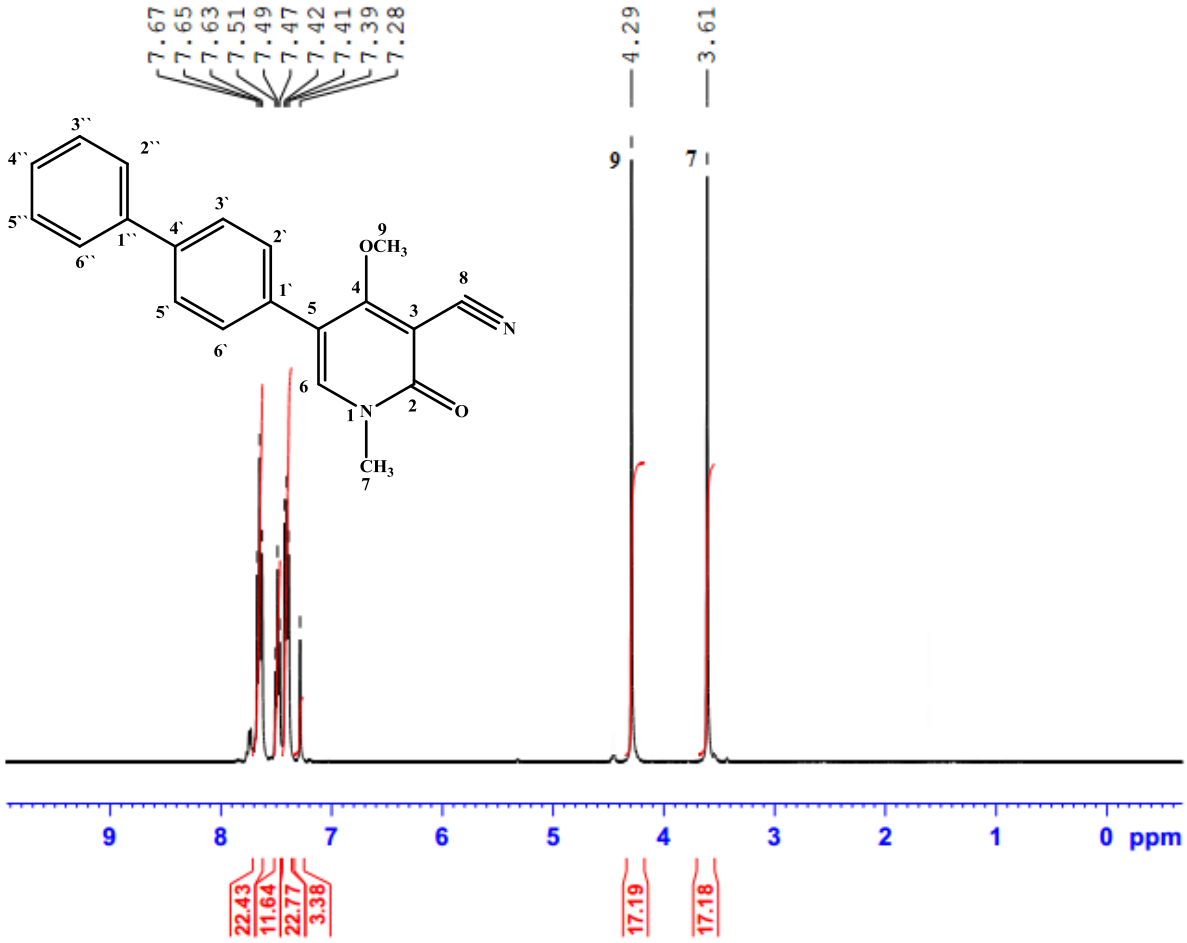

Figure S56. ^{1}H-NMR spectrum (400 MHz, $CDCl_3$) of compound **19**.

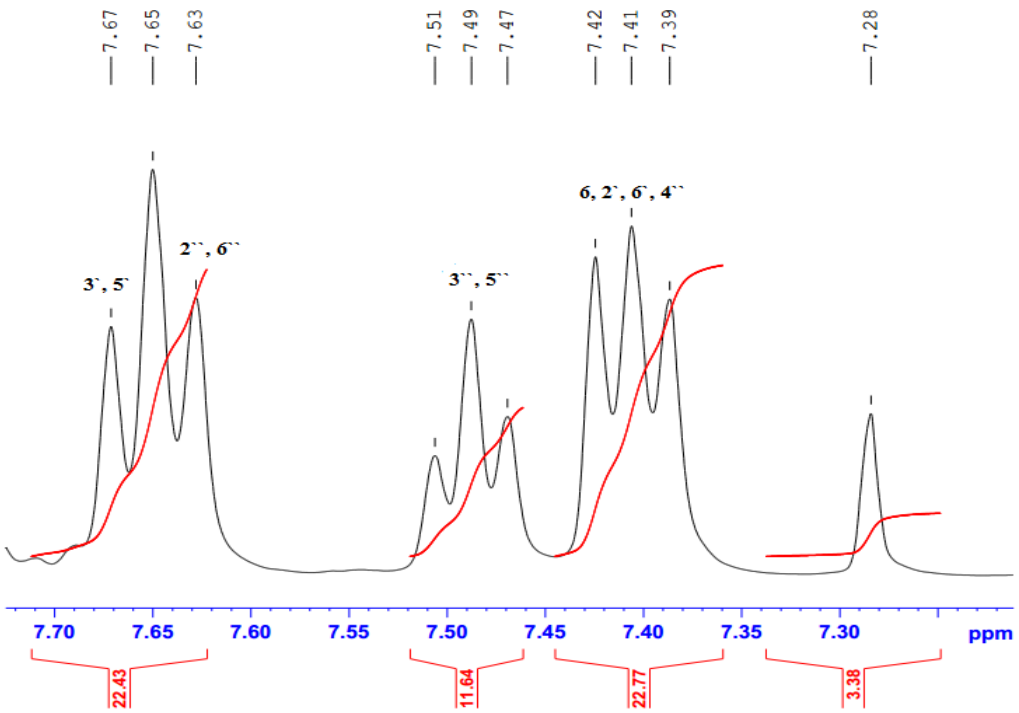

Figure S57. Expansion ^{1}H-NMR spectrum (400 MHz, $CDCl_3$) of compound **19**.

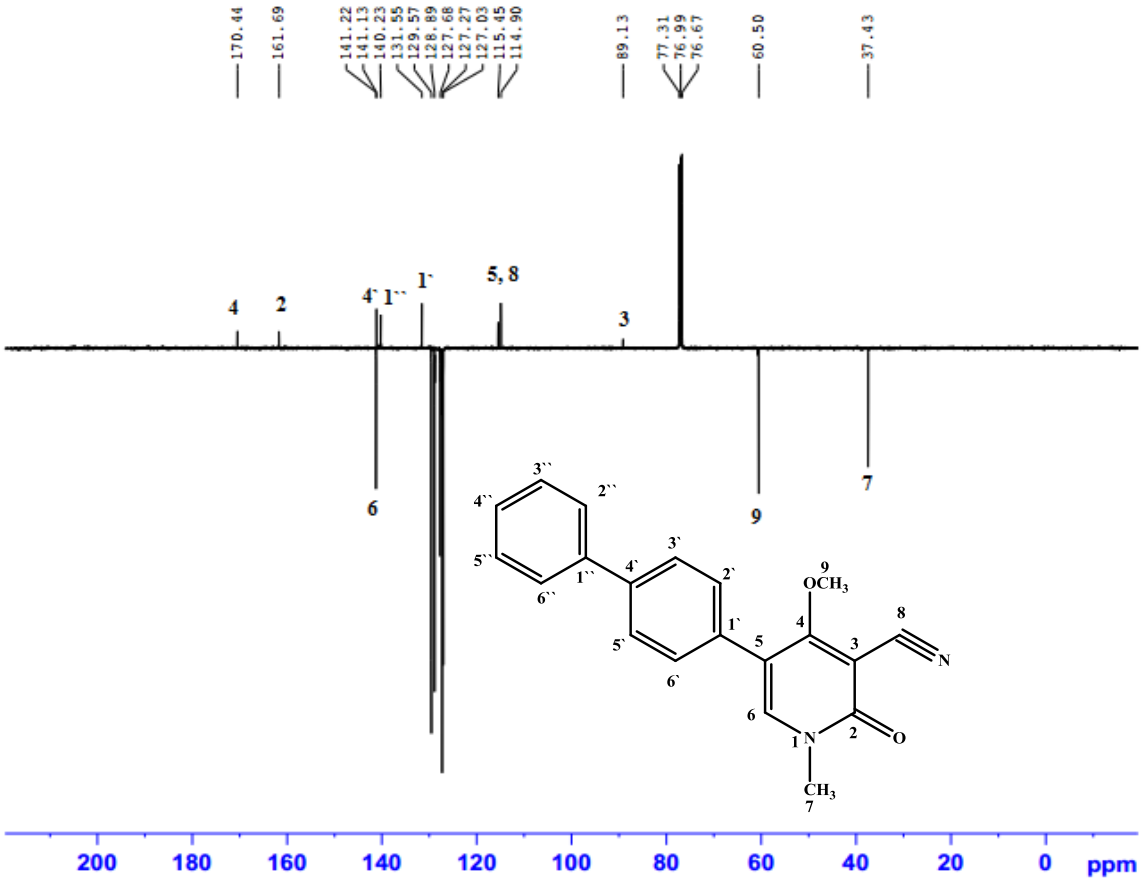

Figure S58. APT spectrum (100 MHz, $CDCl_3$) of compound **19**.

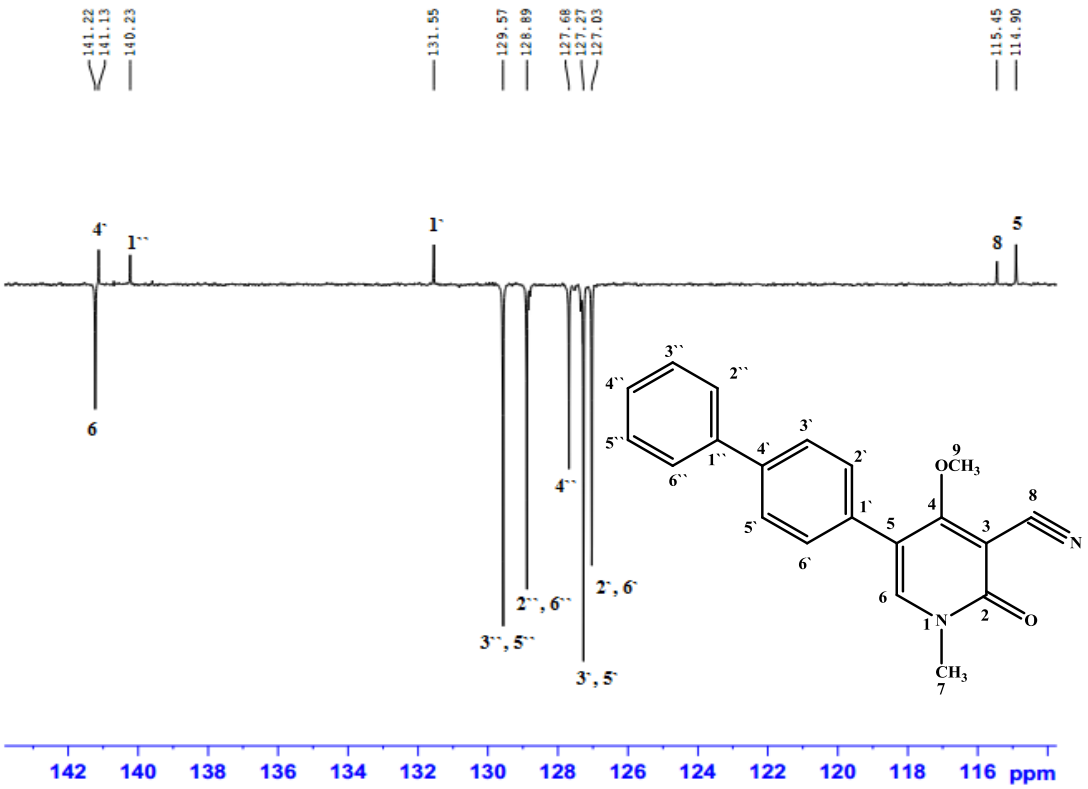

Figure S59. Expansion of APT spectrum (100 MHz, $CDCl_3$) of compound **19**.

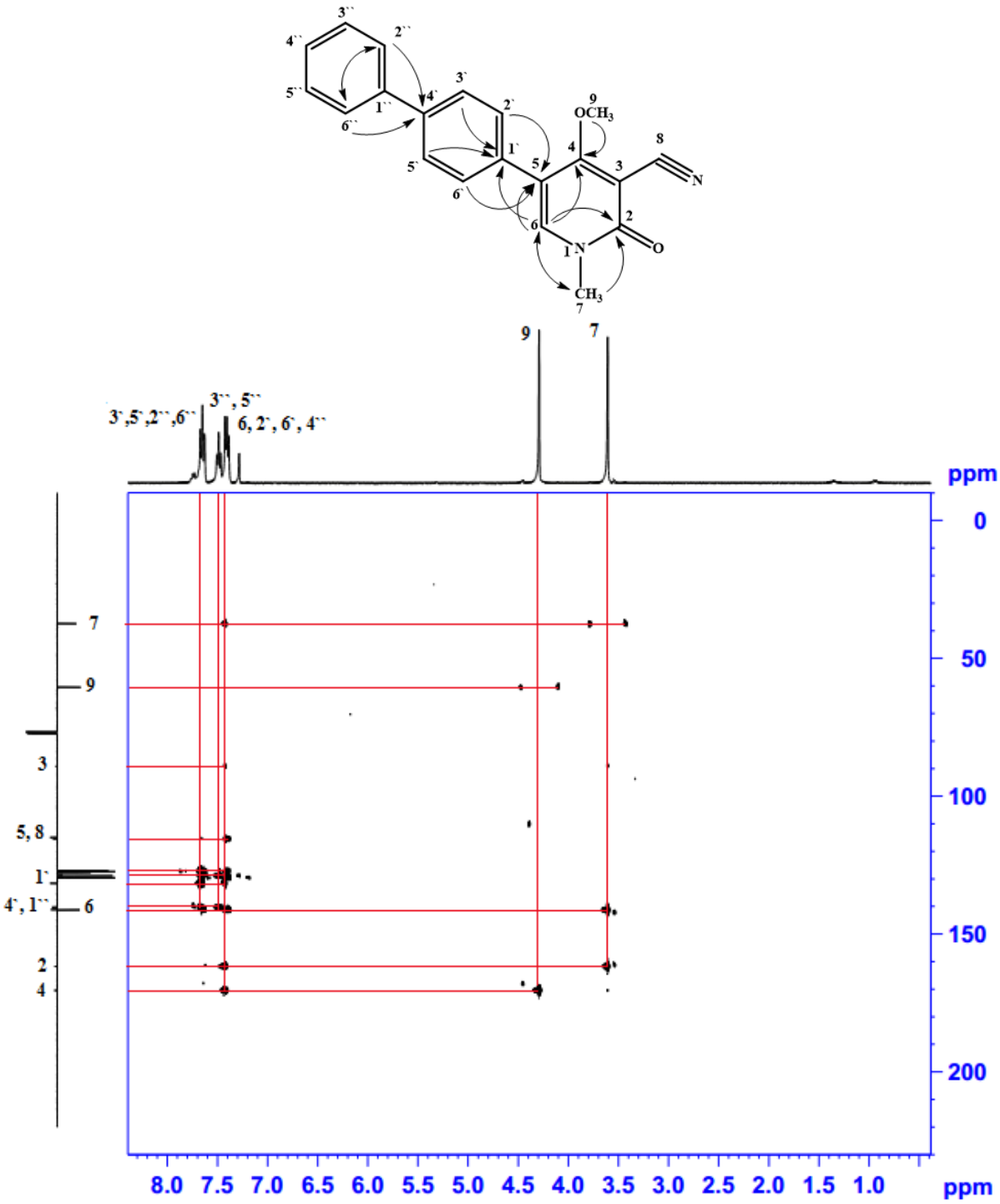

Figure S60. HMBC correlation spectrum of compound **19**.

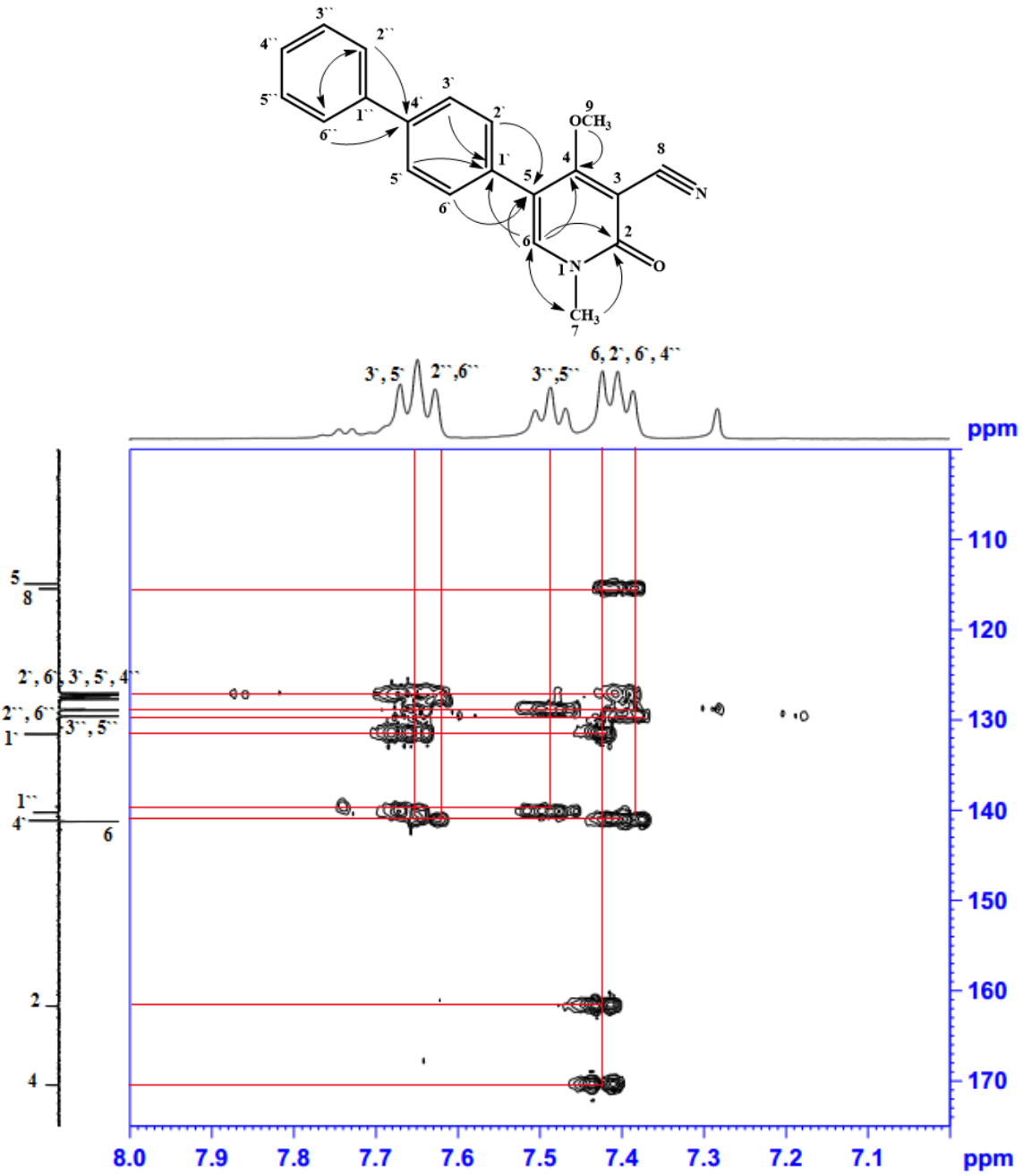

Figure S61. Selected HMBC correlation spectrum of compound **19** from δ_H 5-10 ppm, and from δ_C 120-170 ppm.

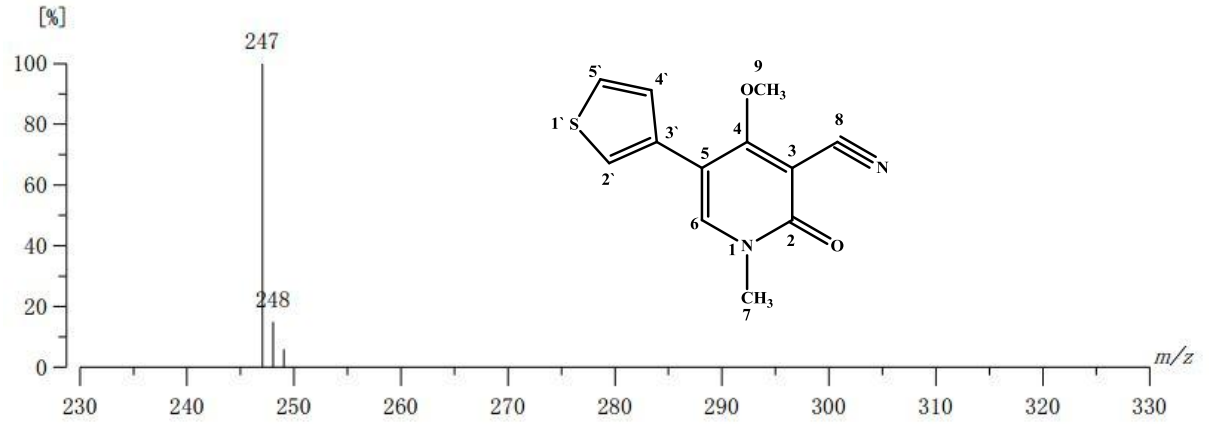

Figure S62. High resolution FAB$^+$-MS spectra of compound **20**, showing $[M+H]^+$ ion peak at *m/z* 247.0541 (calcd. for $C_{12}H_{11}N_2O_2S$, 247.0541).

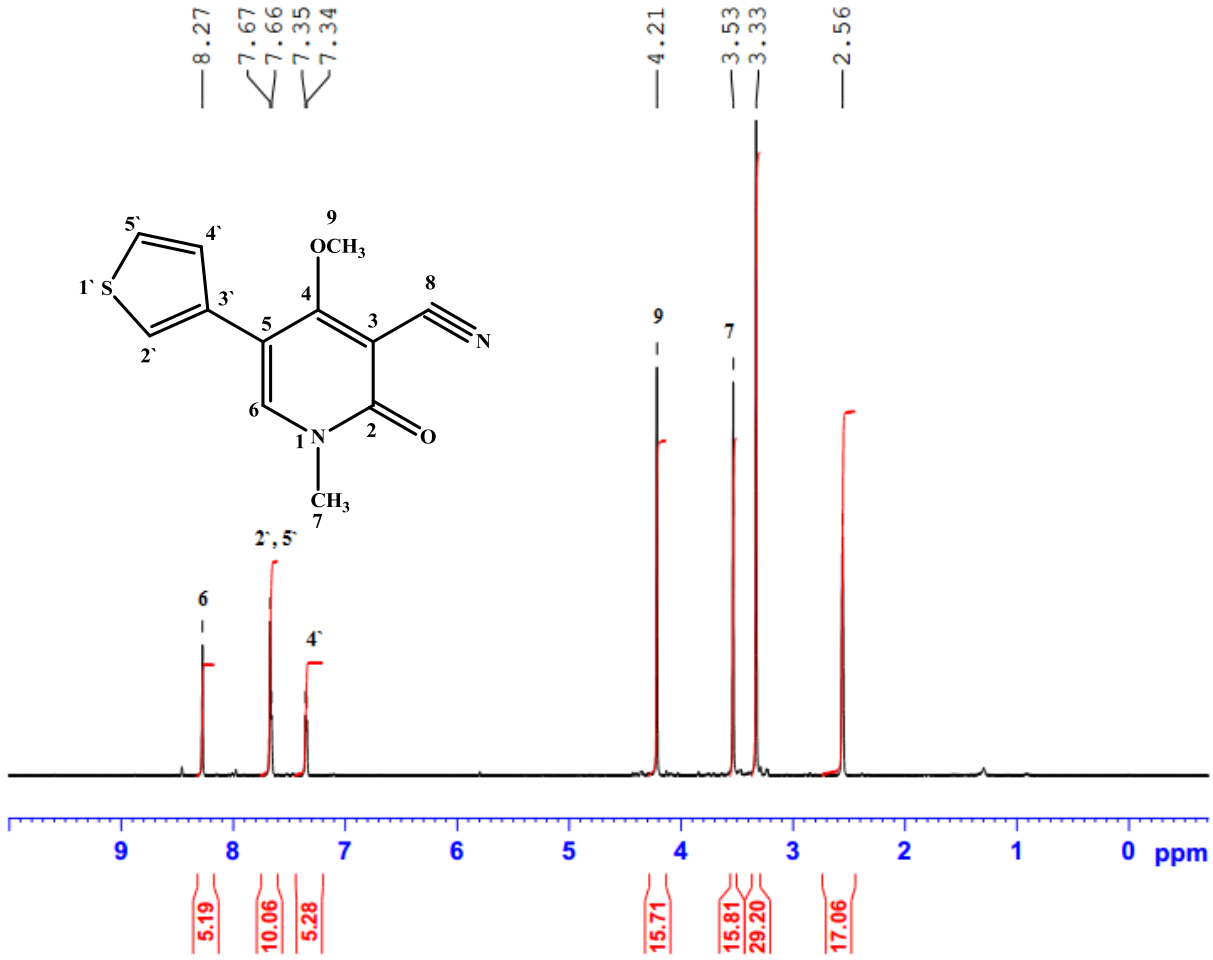

Figure S63. ^{1}H-NMR spectrum (400 MHz, $(CD_3)_2SO$) of compound **20**.

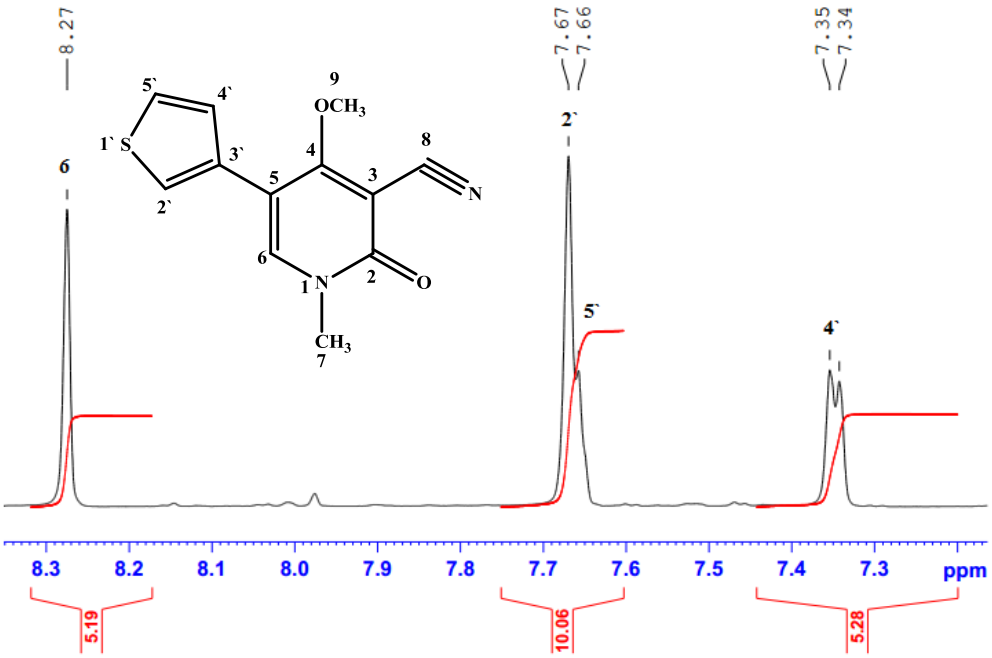

Figure S64. Expansion of ^{1}H-NMR spectrum (400 MHz, $(CD_3)_2SO$) of compound **20**.

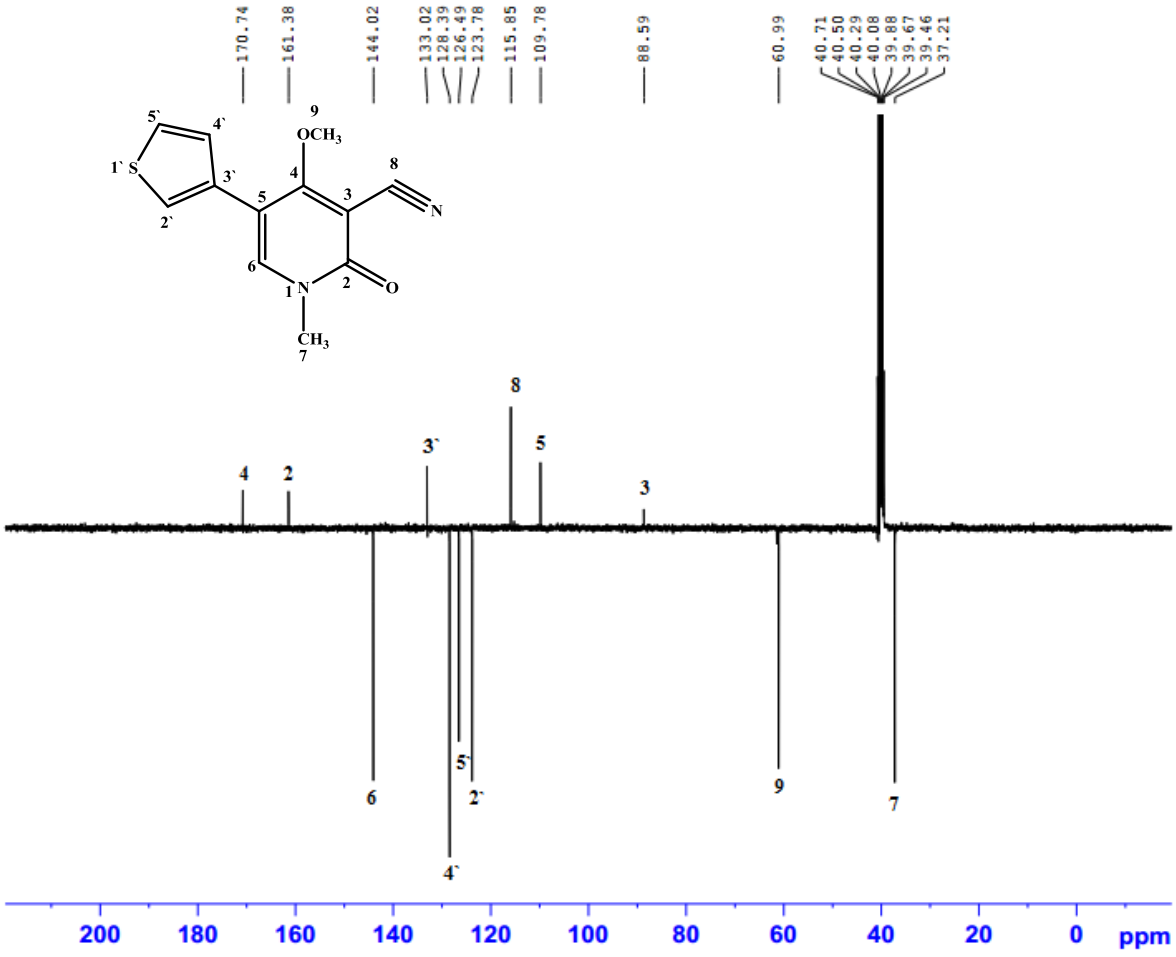

Figure S65. APT spectrum (100 MHz, $(CD_3)_2SO$) of compound **20**.

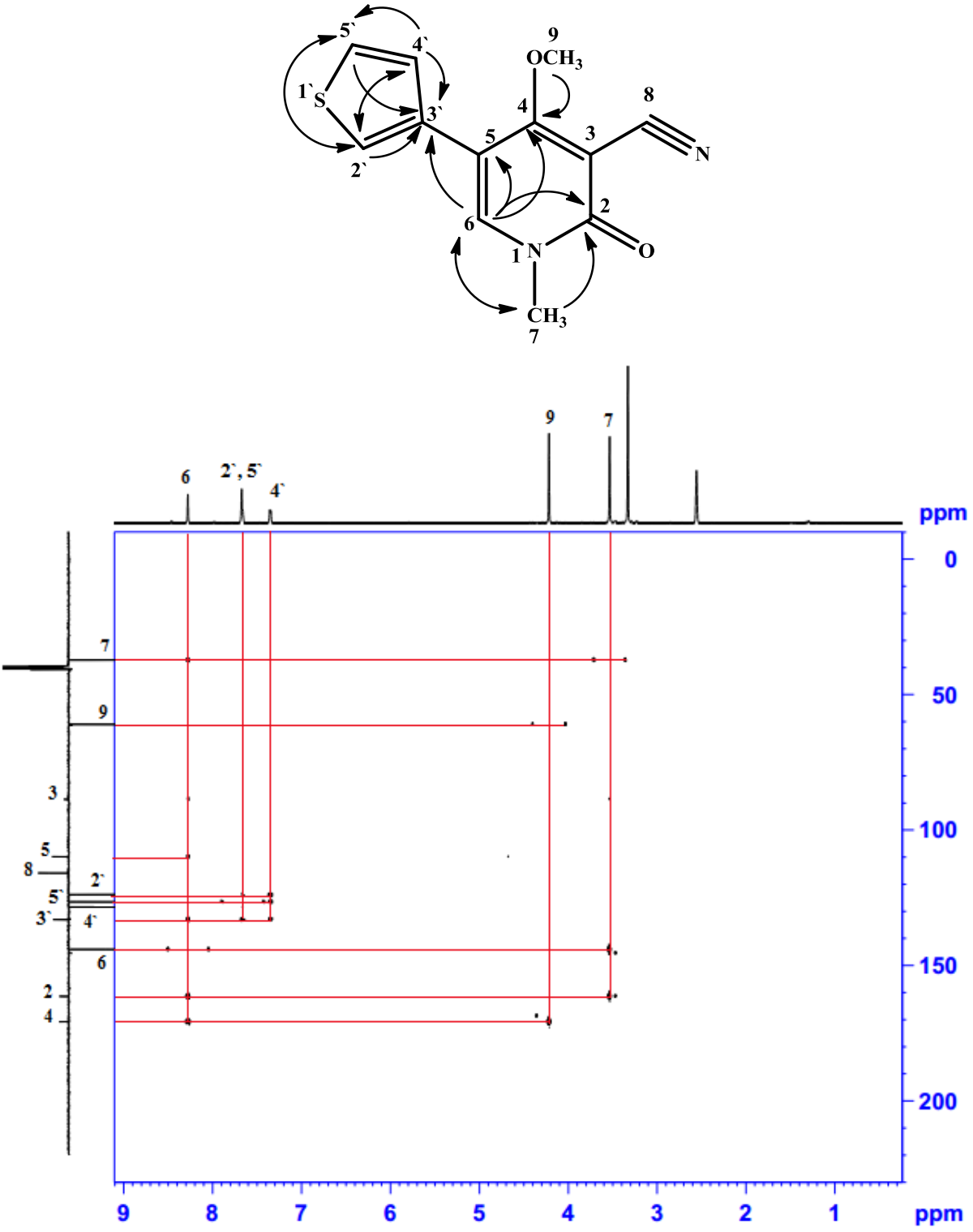

Figure S66. HMBC correlation spectrum of compound **20**.

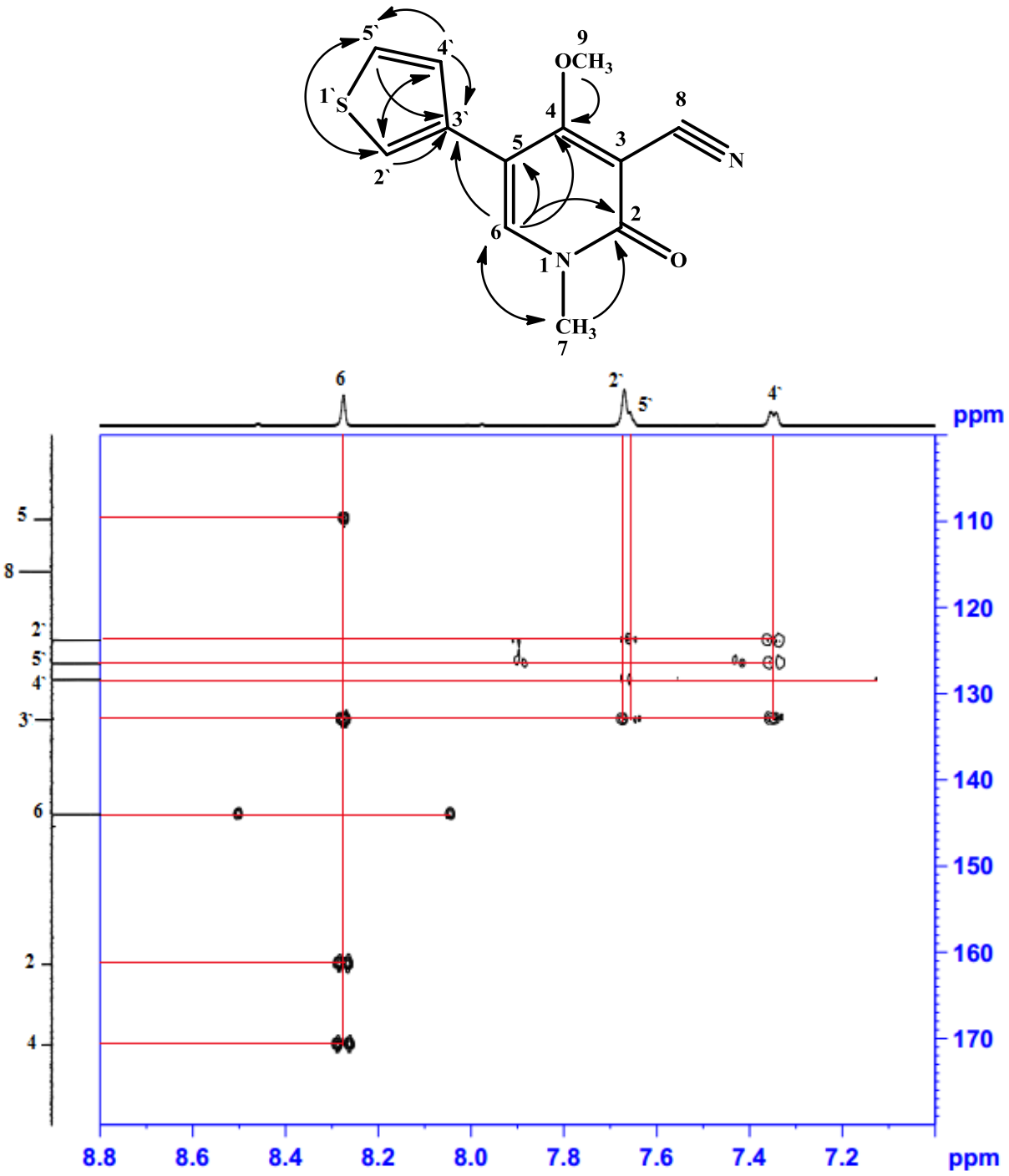

Figure S67. Selected HMBC correlation spectrum of compound **20** from δ_H 7-8.8 ppm, and from δ_C 90-180 ppm.

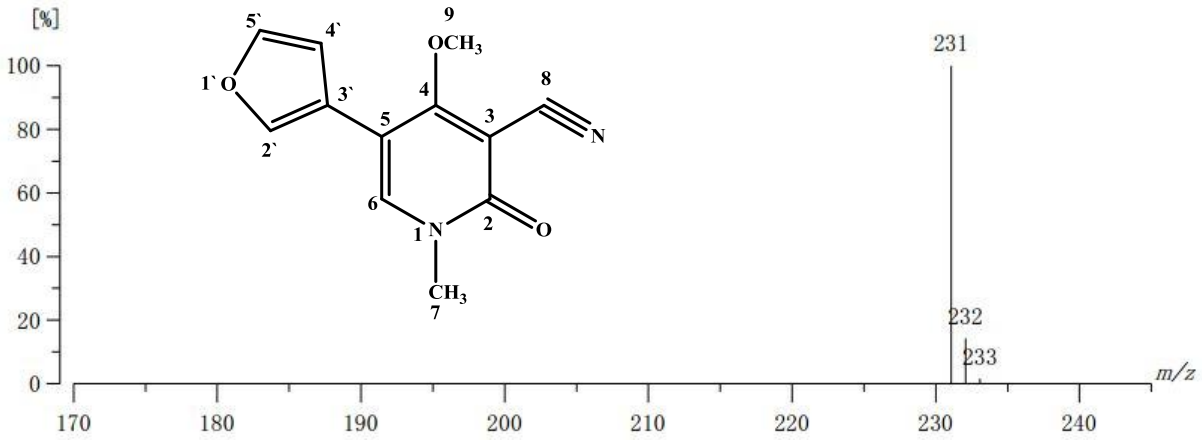

Figure S68. High resolution FAB$^+$ -MS spectra of compound **21**, showing $[M+H]^+$ ion peak at *m/z* 231.0773 (calcd. for $C_{12}H_{11}N_2O_3$, 231.0770).

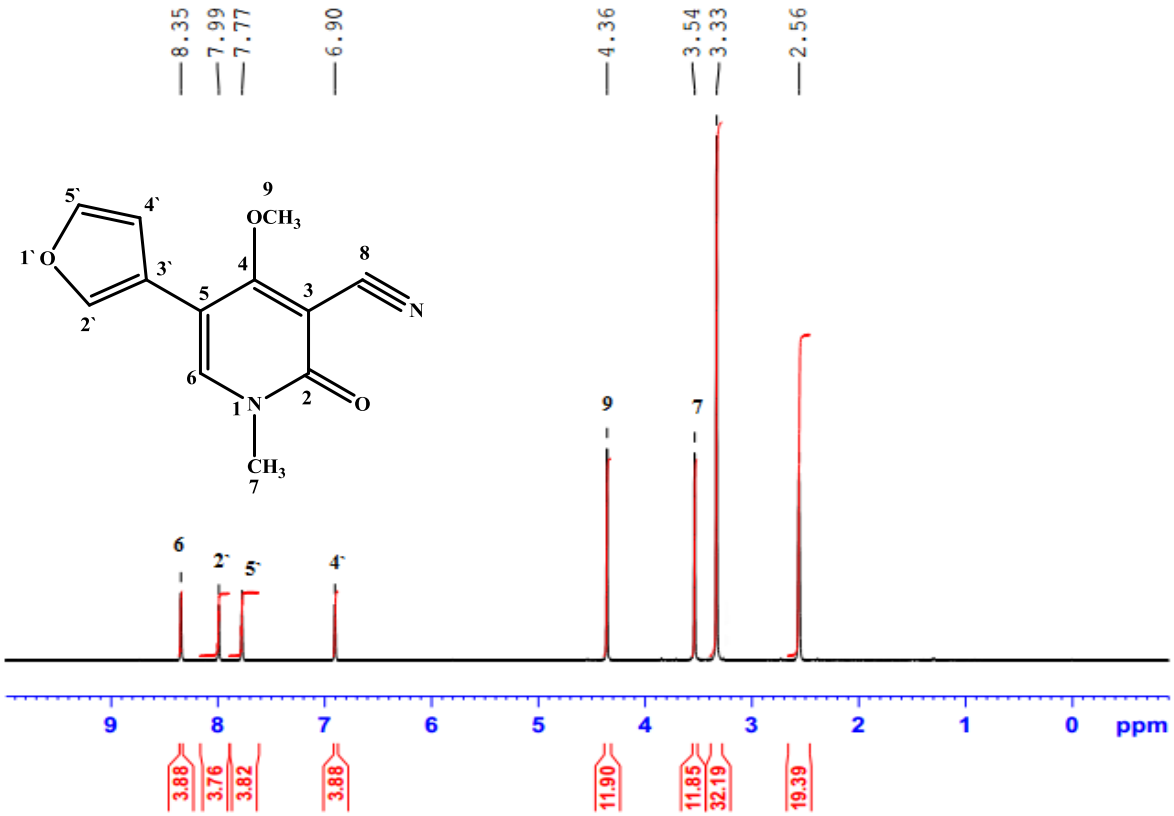

Figure S69. ^{1}H-NMR spectrum (400 MHz, $(CD_3)_2SO$) of compound **21**.

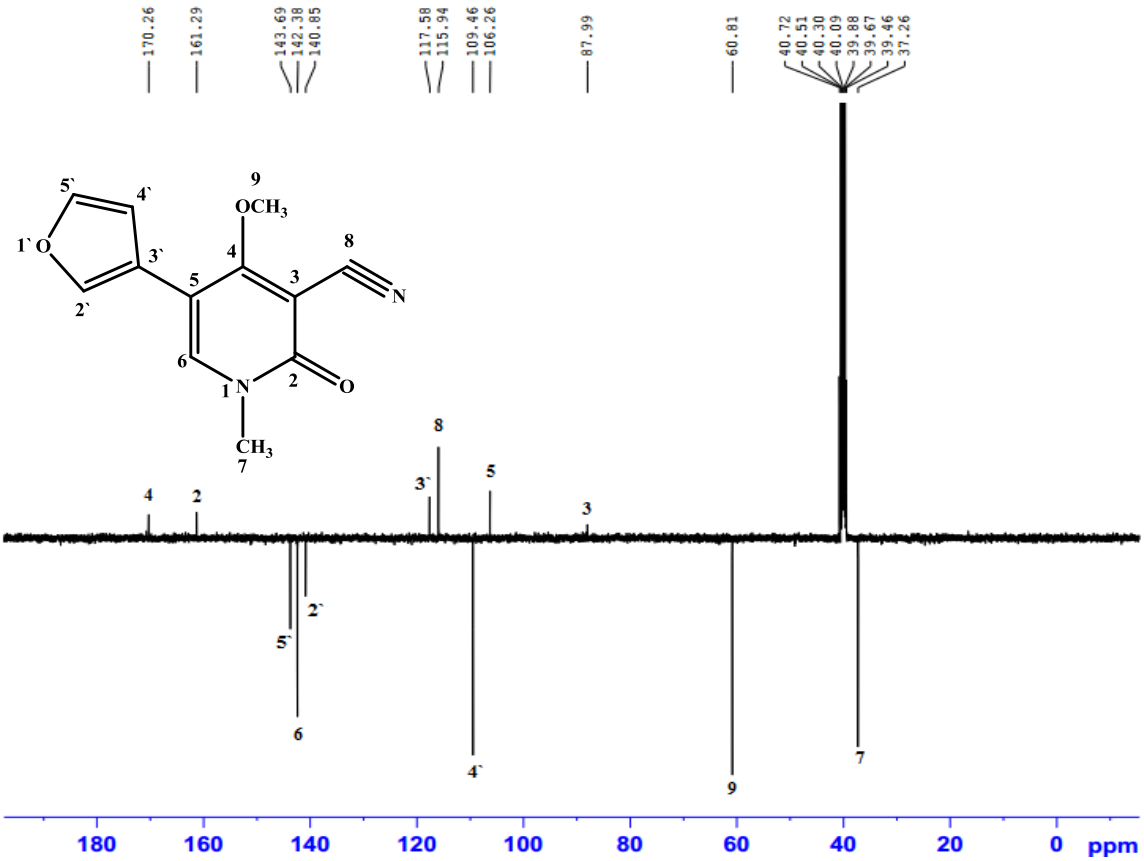

Figure S70. APT spectrum (100 MHz, $(CD_3)_2SO$) of compound **21**.

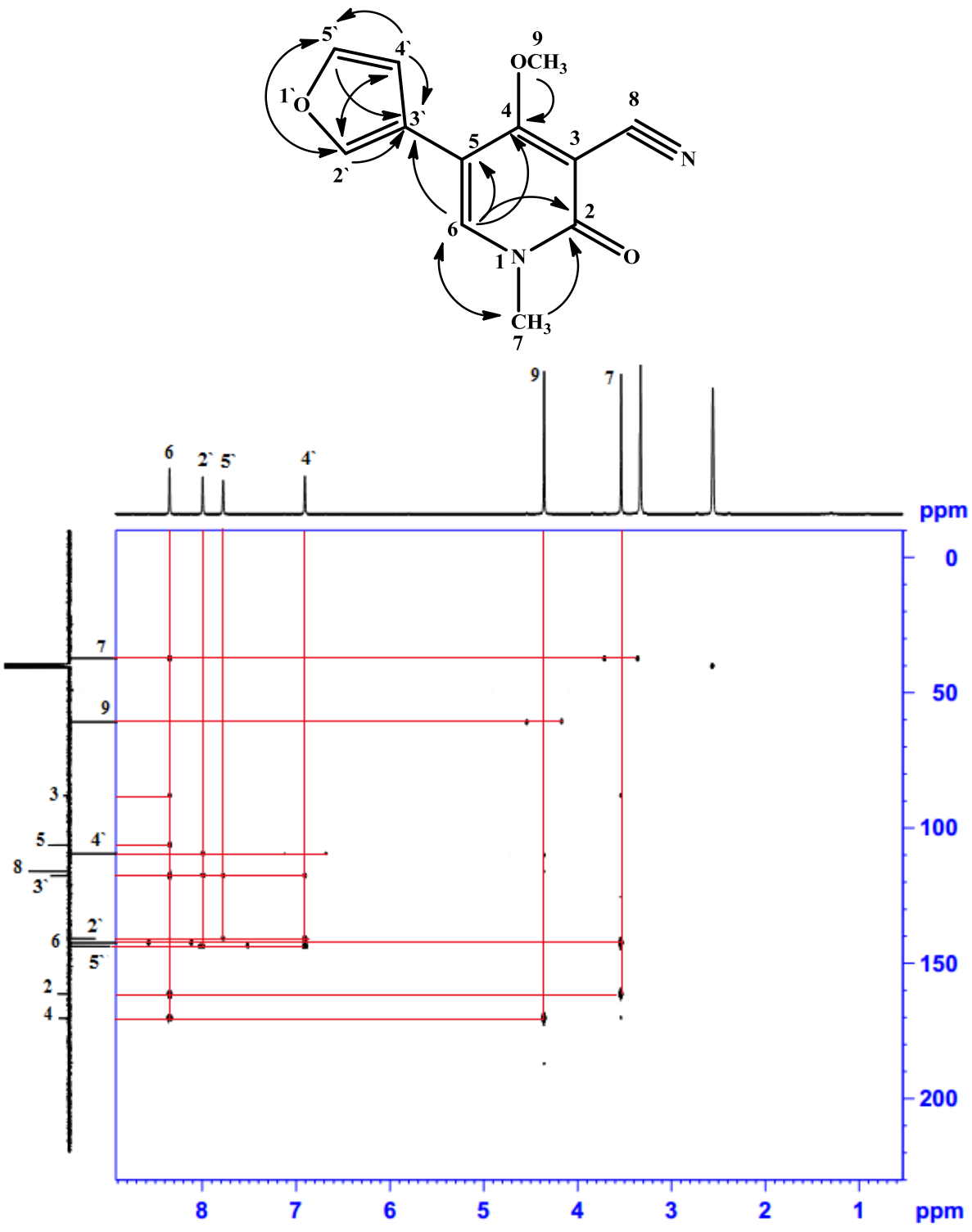

Figure S71. HMBC correlation spectrum of compound **21**.

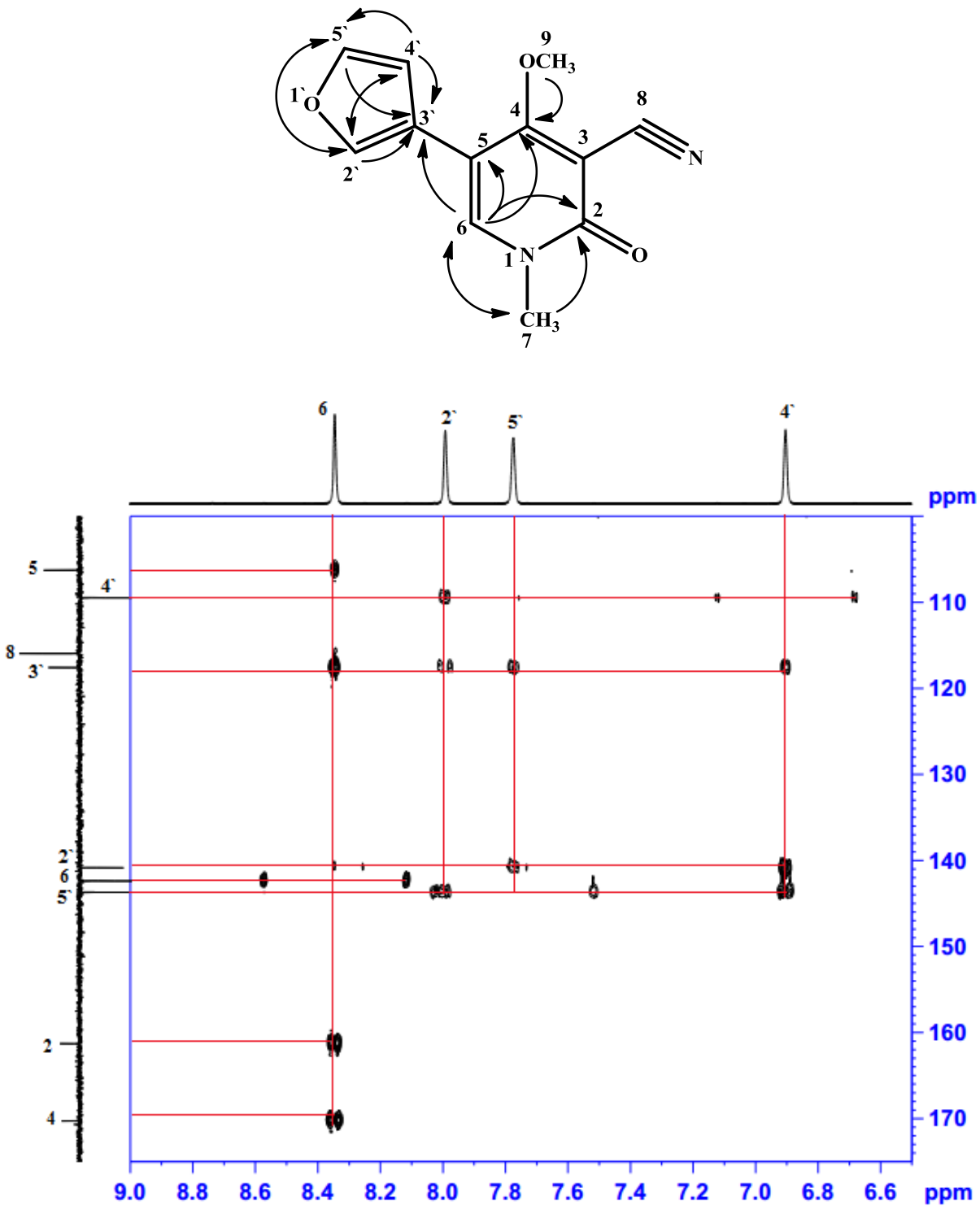

Figure S72. Selected HMBC correlation spectrum of compound **21** from δ_H 6.5-9 ppm, and from δ_C 90-180 ppm.

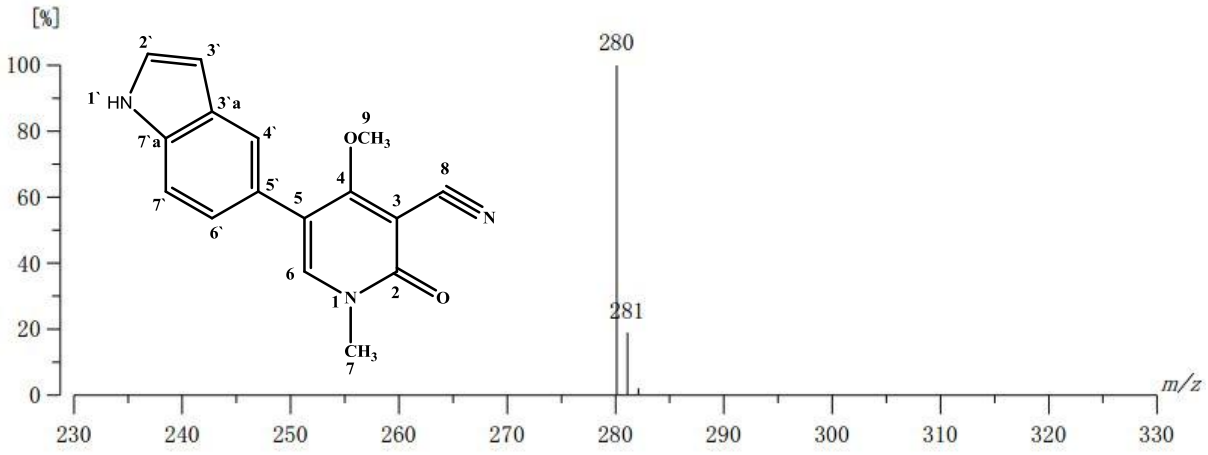

Figure S73. High resolution FAB$^+$-MS spectra of compound **22**, showing $[M+H]^+$ ion peak at *m/z* 280.1086 (calcd. for $C_{16}H_{14}N_3O_2$, 280.1086).

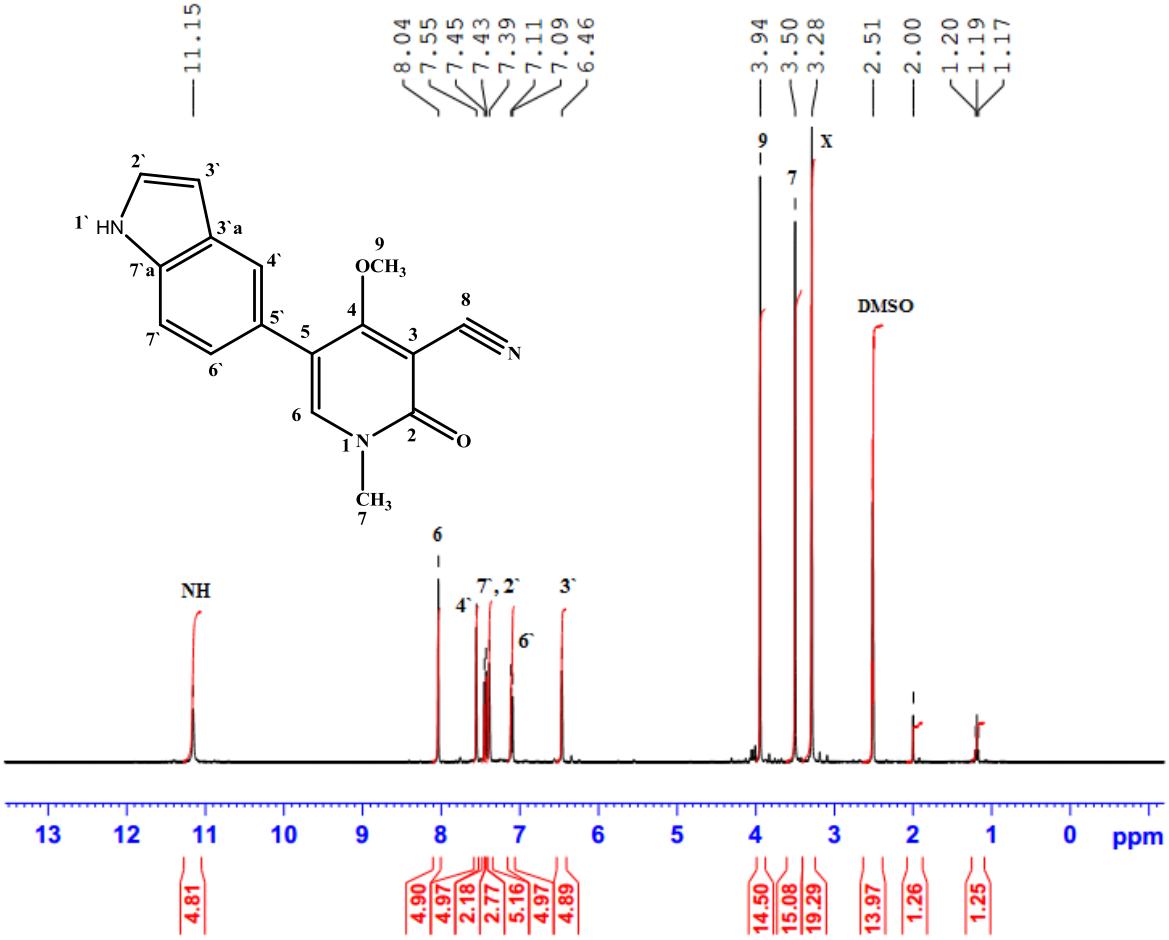

Figure S74. ^{1}H-NMR spectrum (400 MHz, $(CD_3)_2SO$) of compound **22**.

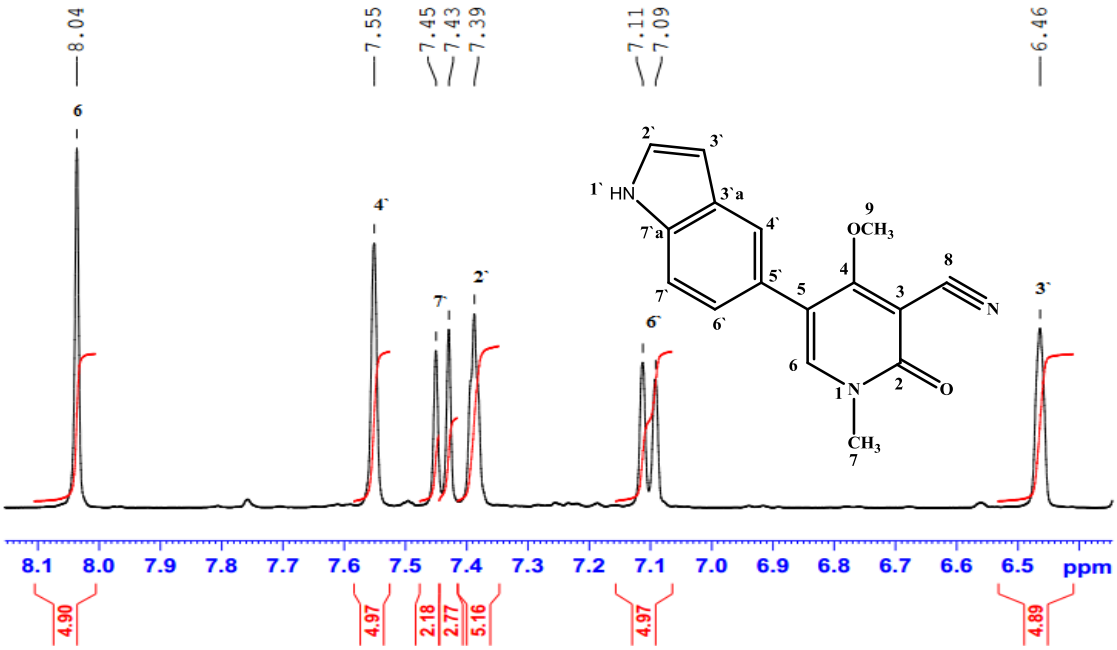

Figure S75. Expansion of ^{1}H-NMR spectrum (400 MHz, $(CD_3)_2SO$) of compound **22**.

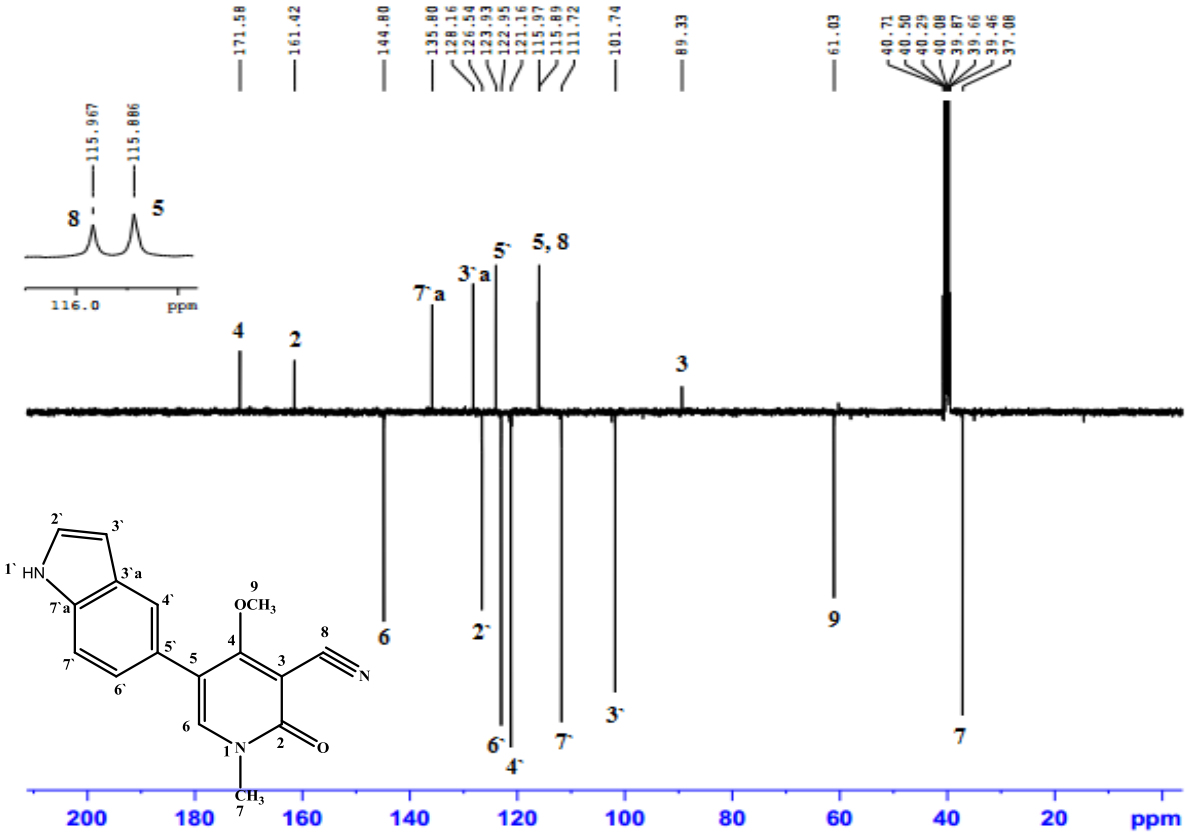

Figure S76. APT spectrum (100 MHz, $(CD_3)_2SO$) of compound **22**.

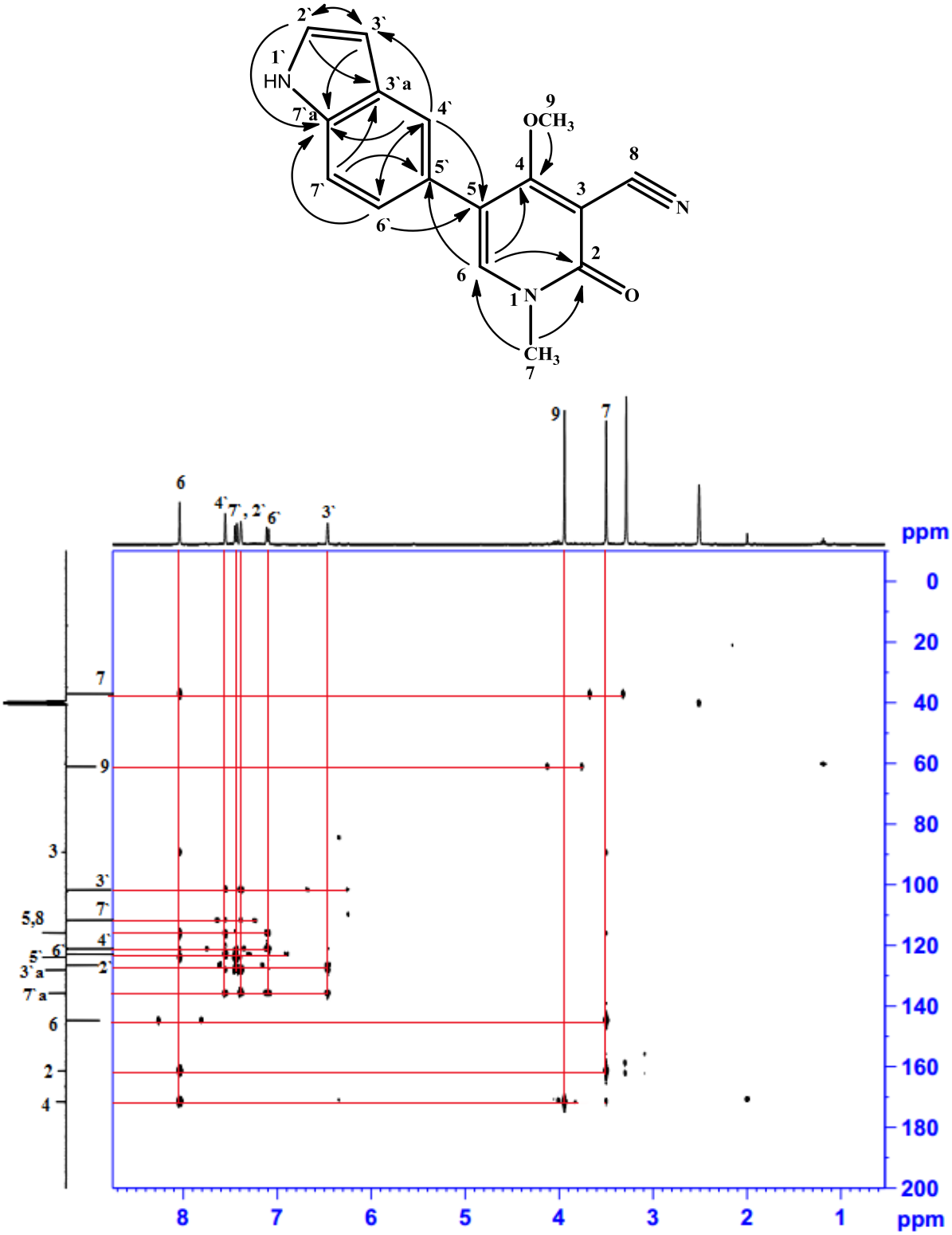

Figure S77. HMBC correlation spectrum of compound **22**.

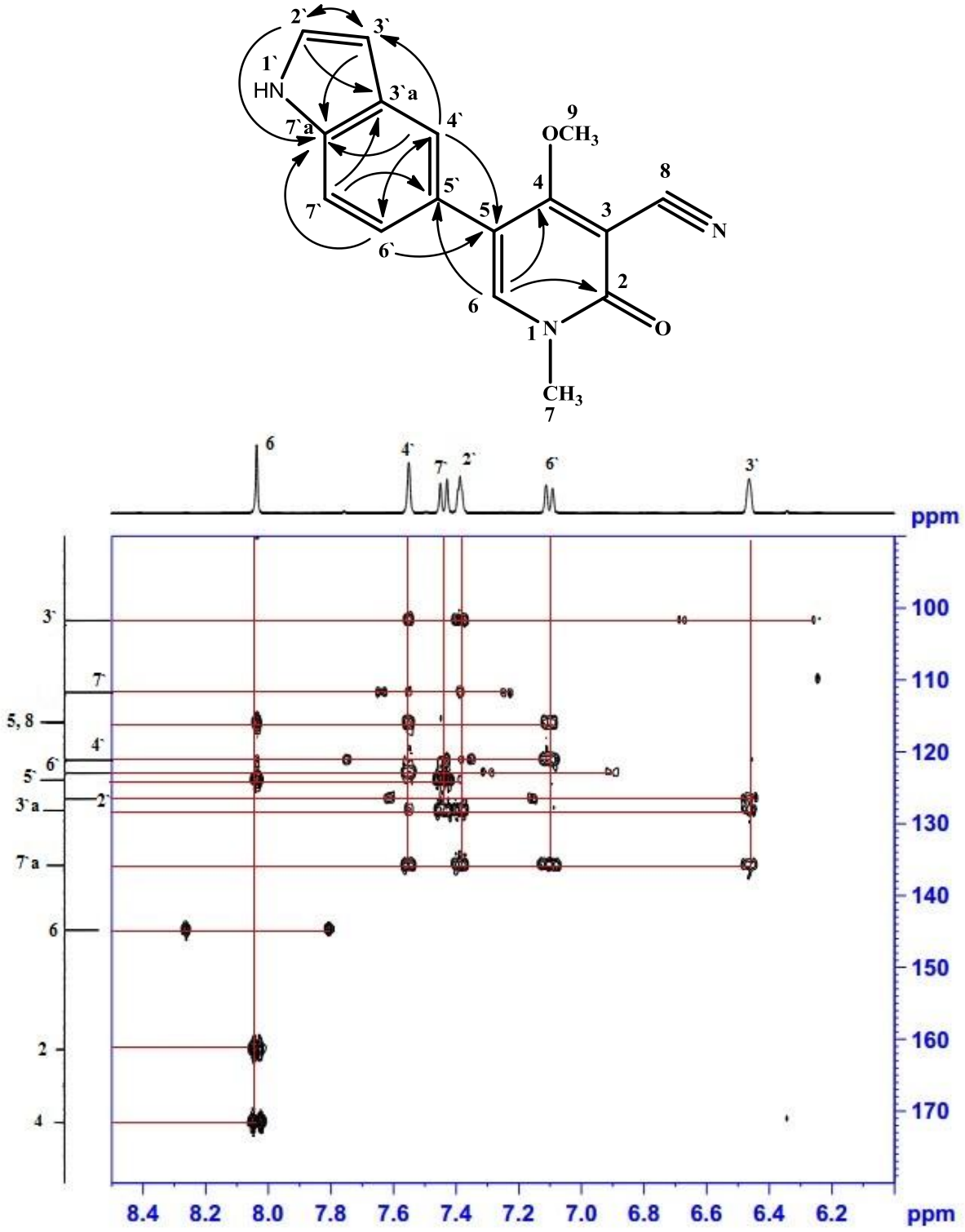

Figure S78. Selected HMBC correlation spectrum of compound **22** from δ_H 6-8.5 ppm, and from δ_C 90-180 ppm.

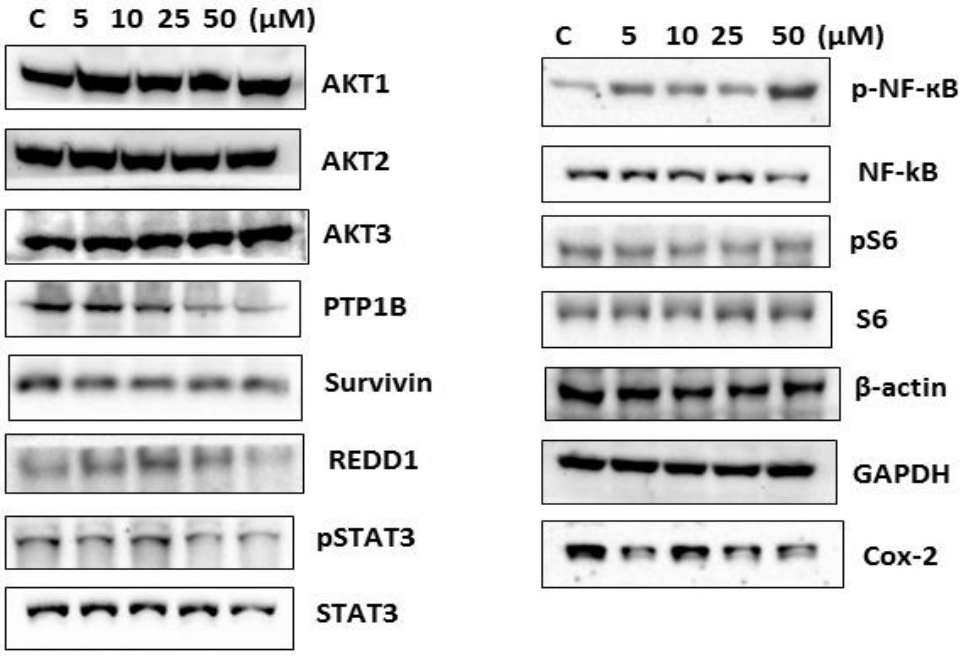

Figure S79. Western blot analysis of Akt1, Akt2, Akt3, PTP1B, Survivin, REDD1, p-STAT3, STAT3, pNF-κB, NF-κB, pS6, S6, β-actin, GAPDH and COX-2 proteins in the cytosolic extract of SAS cells treated with compound 19. The blots for β-actin and GAPDH are representative images of all β-actin and GAPDH blots.

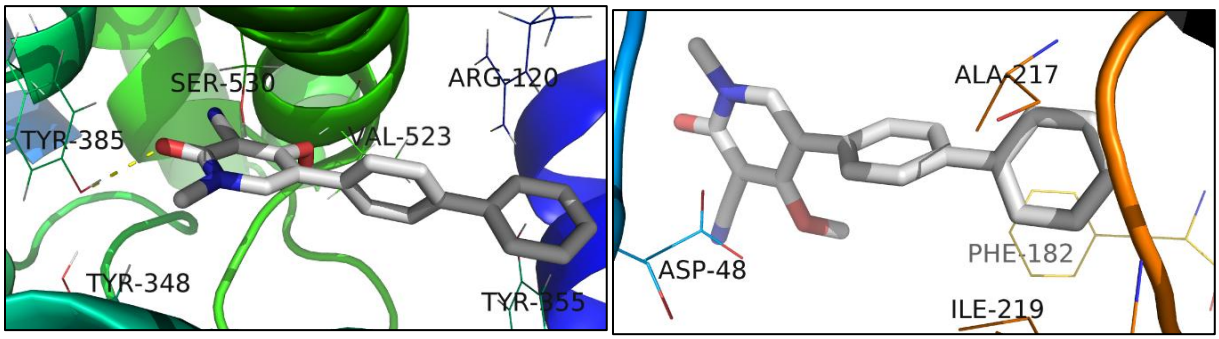

Figure S80. Molecular model of compound 19 binding with; A) PTP1B; B) COX-2 active sites, obtained by AutoDock Vina in PyRx 0.8.

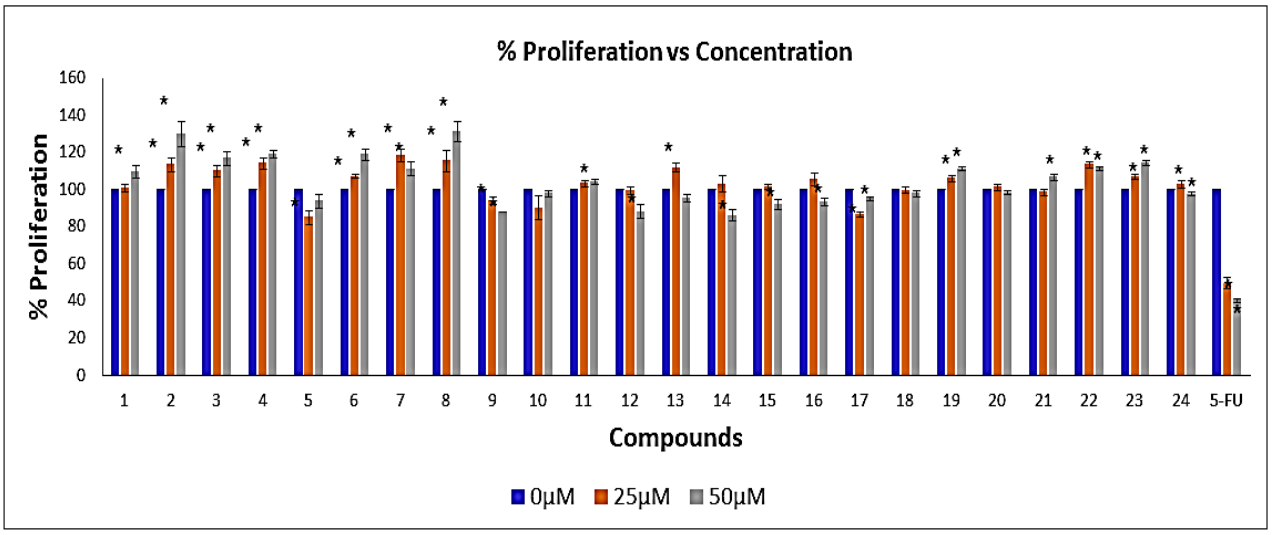

Figure S81. Bar graph shows the effect of ricinine derivatives and standard chemotherapeutic agent 5-FU on the proliferation of normal epithelial cells (L132 cells). L132 cells were seeded in 96 well culture plates at a density of 2000 cells/100µl/well and treated with 0, 25 and 50 µM of compounds 1-24 and 5-FU for 72 hr. The rate of proliferation was estimated by MTT assay. Values are presented as mean ±SE of the experiment performed in sextuplicate (*= $P<0.05$ vs. control (0µM).

References

El-Naggar MH, Elgaml A, Abdel Bar FM, Badria FA. 2019. Antimicrobial and antiquorum-sensing activity of Ricinus communis extracts and ricinine derivatives. Natural product research. Jun;33:1556-1562. Epub 2018/01/16.

Trott O, Olson AJ. 2010. AutoDock Vina: improving the speed and accuracy of docking with a new scoring function, efficient optimization, and multithreading. J Comput Chem.31:455-461.